

UNIVERSITY OF SOUTHAMPTON

Phenomenology of the minimal $B - L$
Model: the Higgs sector at the Large
Hadron Collider and future Linear
Colliders

by

Giovanni Marco Pruna

A thesis submitted in partial fulfillment for the
degree of Doctor of Philosophy

in the

Faculty of Physical and Applied Sciences
School of Physics and Astronomy

October 2018

UNIVERSITY OF SOUTHAMPTON

Abstract

Faculty of Physical and Applied Sciences
School of Physics and Astronomy

Doctor of Philosophy

by [Giovanni Marco Pruna](#)

This Thesis is devoted to the study of the phenomenology of the Higgs sector of the minimal $B - L$ extension of the Standard Model at present and future colliders. Firstly, the motivations that call for the minimal $B - L$ extension are summarised. In addition, the model is analysed in its salient parts. Moreover, a detailed review of the phenomenological allowed Higgs sector parameter space is given. Finally, a complete survey of the distinctive Higgs boson signatures of the model at both the Large Hadron Collider and the future linear colliders is presented.

Contents

Abstract	i
List of Figures	iv
List of Tables	vi
Declaration of Authorship	vii
Acknowledgements	ix
1 Introduction	1
1.1 The Standard Model	1
1.2 A bottom-up approach: the minimal $B - L$ model	3
1.3 Experimental frameworks: present and future colliders	4
1.3.1 The LHC	4
1.3.2 Future linear collider prototypes	5
1.4 Organisation of the work	6
2 The minimal $B - L$ model	7
2.1 The Lagrangian and the parameterisation	8
2.1.1 The Yang-Mills sector	8
2.1.2 The fermion sector	9
2.1.3 The scalar sector	10
2.1.4 The Yukawa term	10
2.2 Spontaneous $SU(2)_L \times U(1)_Y \times U(1)_{B-L}$ breaking	11
2.2.1 The scalar mass spectrum	12
2.2.2 The gauge mass spectrum	13
2.3 The Feynman-gauge and the ghost Lagrangian	15
2.3.1 The Feynman gauge	15
2.3.2 The Fadeev-Popov Lagrangian	16
2.4 See-saw mechanism and neutrino masses	18
2.5 Counting of parameters	20
3 The Higgs sector parameter space	21
3.1 Experimental constraints on the Higgs boson sector	22

3.1.1	High-precision data and constraints on the Higgs sector	22
3.1.2	Direct searches and constraints on the Higgs sector	23
3.1.3	Other experimental constraints	24
3.2	Theoretical constraints on the Higgs boson sector	25
3.2.1	Perturbative unitarity	25
3.2.2	Triviality and vacuum stability bounds	34
3.2.3	Unitarity and triviality constraints on g'_1	39
3.2.4	The fine-tuning constraint	44
4	Higgs phenomenology at colliders	47
4.1	Parameter space and implementation of the model in CalcHEP	47
4.2	Branching ratios and total widths	49
4.3	Higgs bosons at the LHC	54
4.3.1	The LHC scheduled working plan	54
4.3.2	Standard production mechanisms	54
4.3.3	Non-standard production mechanisms	56
4.3.4	Event Rates	59
4.4	Higgs bosons at future linear colliders	63
4.4.1	The future linear collider running proposals	64
4.4.2	Standard single-Higgs production mechanisms	64
4.4.3	Non-standard single-Higgs production mechanisms	66
4.4.4	Single scalar production in association with a pair of vector bosons	72
4.4.5	Double scalar production mechanisms	74
5	Conclusions	81
A	The scalar potential	85
B	The minimal $B - L$ Feynman rules	89
	Bibliography	103

List of Figures

3.1	Experimental constraints on the Higgs boson sector - Direct searches and constraints on the Higgs sector	24
3.2	Theoretical constraints on the Higgs boson sector - Perturbative unitarity (1)	30
3.3	Theoretical constraints on the Higgs boson sector - Perturbative unitarity (2)	33
3.4	Theoretical constraints on the Higgs boson sector - Triviality and vacuum stability (1)	37
3.5	Theoretical constraints on the Higgs boson sector - Triviality and vacuum stability (2)	38
3.6	Theoretical constraints on the Higgs boson sector - Unitarity and triviality constraints on g'_1	43
4.1	Branching ratios and total widths (1)	50
4.2	Branching ratios and total widths (2)	51
4.3	Branching ratios and total widths (3)	52
4.4	Higgs at LHC - Standard production mechanisms	55
4.5	Higgs at LHC - Non-standard production mechanisms (1)	57
4.6	Higgs at LHC - Non-standard production mechanisms (2)	58
4.7	Higgs at LHC - Event rates (1)	60
4.8	Higgs at LHC - Event rates (2)	61
4.9	Higgs at LHC - Event rates (3)	62
4.10	Higgs at LHC - Event rates (4)	63
4.11	Higgs at future linear colliders - Standard single-Higgs production mechanisms	65
4.12	Higgs at future linear colliders - Non-standard single-Higgs production mechanisms (1)	67
4.13	Higgs at future linear colliders - Non-standard single-Higgs production mechanisms (2)	68
4.14	Higgs at future linear colliders - Non-standard single-Higgs production mechanisms (3)	70
4.15	Higgs at future linear colliders - Non-standard single-Higgs production mechanisms (4)	71
4.16	Higgs at future linear colliders - Single scalar production in association to a pair of vector bosons (1)	73
4.17	Higgs at future linear colliders - Single scalar production in association to a pair of vector bosons (2)	74
4.18	Higgs at future linear colliders - Double scalar production mechanisms (1)	75
4.19	Higgs at future linear colliders - Double scalar production mechanisms (2)	76

- 4.20 Higgs at future linear colliders - Double scalar production mechanisms (3) [78](#)
- 4.21 Higgs at future linear colliders - Double scalar production mechanisms (4) [79](#)

List of Tables

3.1	Theoretical constraints on the Higgs boson sector - Perturbative unitarity (1)	28
3.2	Theoretical constraints on the Higgs boson sector - Perturbative unitarity (2)	32
3.3	Theoretical constraints on the Higgs boson sector - Unitarity and triviality constraints on g'_1	44
4.1	Higgs at future linear colliders - Future linear collider prototypes	64

Declaration of Authorship

I, Giovanni Marco Pruna, declare that this thesis titled, “Phenomenology of the minimal $B-L$ Model: the Higgs sector at the Large Hadron Collider and future Linear Colliders” and the work presented in it are my own. I confirm that:

- This work was done wholly or mainly while in candidature for a research degree at this University.
- Where any part of this thesis has previously been submitted for a degree or any other qualification at this University or any other institution, this has been clearly stated.
- Where I have consulted the published work of others, this is always clearly attributed.
- Where I have quoted from the work of others, the source is always given. With the exception of such quotations, this thesis is entirely my own work.
- I have acknowledged all main sources of help.
- Where the thesis is based on work done by myself jointly with others, I have made clear exactly what was done by others and what I have contributed myself.

Signed:

Date:

“Se non è vero, è molto ben trovato.”
(“If it is not true, it is very well invented.”)

Giordano Bruno (1548-1600),
burnt at the stake as a heretic by the Catholic Church.

Acknowledgements

With the oversight of my supervisor Professor Stefano Moretti, editorial advice has been sought. No changes of intellectual content were made as a result of this advice. For this and all the scientific and human support that I have received in the last years, I owe my deepest gratitude to him.

Then, I would like to thank Dr. Lorenzo Basso for sharing with me these years of (both domestic and scientific!) difficulties and challenges. He provided his support in many occasions, and this Thesis would not have been possible without his help.

Moreover, I will be always grateful to Dr. Alexander S. Belyaev, Professor Ulrich Ellwanger, Professor Per Osland, Professor Jonathan Flynn.

This PhD has been partially supported by the NExT Institute.

Questo PhD è stato finanziato dal progetto “Master and Back” della Regione Autonoma della Sardegna, pertanto un ringraziamento speciale va a Renato Soru senza il quale tale risorsa sarebbe senza dubbio mancata.

Luciano, Silvana, Francesca, e poi Daniele, Sara, Jacopo, Gabriella, Tonino, Carlo.

A voi.

Mi traboccano dal cuore alcune parole, che si attaccano ad una carta che forse nessuno leggerà, come le vostre vite.

Tu, cara nonna, che vestita di nero sin da giovane hai cresciuto tre bambine, e la prima e la più bella era mia madre.

Tu, che ti sei consumata fino a che, quel giorno, mi chiedesti di aiutarti a sollevare quel letto enorme, grandissimo, molto più grande di me che avevo solo sette anni.

Non riuscivi nemmeno a stare in piedi senza tremare, dalla vita di merda che hai fatto.

Tu, caro nonno, che sei dovuto scappare di casa, e andare a scavare nelle orribili miniere iglesienti sin da quando eri bambino, per sposarti e dare alla luce cinque bambini, ed il terzo e più bello era mio padre.

Tu che hai sputato i polmoni silicotici, ti sei consumato una spalla, al punto che quando avevi già ottant'anni suonati piangevi per non riuscire nemmeno a sollevare la mano destra per farti la barba.

Quando l'Alzheimer ti ha portato via, ho provato a convincermi che il motivo del tuo sorriso era il Segreto più grande, lo stesso che mi ruba le notti.

Voi, che non l'avete fatto per arricchire i signorotti del Nord, con quei ridicoli e falsi accenti e le teste vuote come cocomeri rotti al sole, che non hanno mai imparato nulla da Noi e men che mai sono stati in grado di insegnarci alcunché (“gente di nulla”).

Voi, che l'avete fatto per dare un futuro ai vostri figli, che a loro volta l'hanno fatto affinché quel futuro lo ereditassi io, e per fare in modo che lo possa lasciare in eredità ai miei figli.

A voi, che mi avete insegnato come nessun titolo di studio possa mai garantire “quel tanto” che rende l'uomo degno di appartenere alla sua specie, è dedicata questa tesi.

Vi penso sempre.

Chapter 1

Introduction

1.1 The Standard Model

Currently, the Standard Model (SM) of the electroweak (EW) and strong interactions of elementary particles represents one of the highest achievements of human kind in understanding the fundamental laws of Nature.

The EW theory is based on the gauge symmetry group $SU(2)_L \times U(1)_Y$ of lefthanded isospin and hypercharge. The Quantum Chromo-Dynamics (QCD)¹, instead, is based on the symmetry group $SU(3)_C$. These two theories provide a beautifully consistent picture of the particle physics phenomena observed up to now.

The gauge symmetry groups of the SM give rise to a quantum field theory that is perturbative at sufficiently high energies and renormalisable. For a complete review of the model in its deepest theoretical and phenomenological implications, see [1, 2].

Starting from this framework, it is widely accepted that each SM particle (in particular, each massive gauge boson) obtains mass by means of the so-called Higgs mechanism, i.e., the mechanism of spontaneous EW symmetry breaking ($EWSB$) realised by adding a theoretically consistent Higgs field: the minimal² choice is represented by the introduction of a $SU(2)$ doublet of complex scalar fields (see [3]).

After the $EWSB$, the $SU(2)_L \times U(1)_Y$ symmetry is spontaneously broken to the electromagnetic $U(1)_Q$ symmetry (where Q is the electric charge quantum number). Three of the four degrees of freedom of the doublet scalar field turn out to be absorbed in the longitudinal polarisation component of each of the three weak gauge bosons, W^\pm and Z , whilst the fourth one is the physical SM Higgs state h . At this stage, the fermion

¹The theory of the strong interactions between the colored quarks.

²It respects the requirement of renormalisability.

masses are generated through the Yukawa interaction with the same scalar field and its conjugate one.

Although the phenomenological power of this theory is remarkable (it has been deeply tested in various experimental scenarios), there is still no (either direct or indirect) evidence of the scalar sector impact in the probed phenomenology, in other words the Higgs boson has not been observed yet.

The urgency of discovering the Higgs boson (and consequently establishing the nature of *EWSB*) has driven the Physics community to devote major efforts to the realisation of more and more powerful accelerators.

For this, since decades a large number of machines (as LEP, SLC, Tevatron, etc.) has tried to investigate the *SM* to the high-precision measurement level (per mille accuracy), and apart from the astonishing agreement with the theoretical prediction concerning the fermion and vector boson sectors of the theory, the Higgs boson (the most important ingredient of the theoretical picture) is currently missing.

At the same time, the recent observation of the pattern of neutrino oscillations (for a complete review, see [4–6]) produced the evidence of the inadequateness of the *SM* (in its minimal version) in describing the mass properties of neutrinos.

Besides, dark matter (*DM*) evidence and related cosmological observations (see [7]) gave an hard blow to the minimal *SM* that, as well as for the massive neutrino case, can not be considered as a satisfactory theoretical framework for these phenomena.

Other than by experimental facts, the *SM* is also affected by several theoretical problems: firstly, quantum gravity is manifestely not included; secondly, the theory is affected by the so-called “Hierarchy problem” (see [8, 9]).

However, while finding a solution to the former could be “postponed” to energy scales that are close to the Plank-scale $\mathcal{O}(10^{19})GeV$, the latter is an indication of consistency problems already arising at the TeV energy scale.

All these aforementioned theoretical and experimental reasons call for some extension of the *SM*.

In fact, one could procede by extending the minimal *SM* by either top-down or bottom-up approaches. The former consist in the formulation of a theory that solves all the *SM* issues and can be broken down to a symmetry pattern that finally includes the *SM* as effective low-energy theory: a typical example of this approach is represented by supersymmetric scenarios as the (Next to) Minimal Supersymmetry Standard Model (*N*)*MSSM*, see [10]([11]).

The latter approach consists in piecing together a system of minimal extensions to give rise to the grandest possible system. In the context of this work, we choose to follow this approach in realising the so-called minimal $B - L$ extension of the SM .

1.2 A bottom-up approach: the minimal $B - L$ model

In order to realise a consistent extension of the SM , we exploit the fact that both the baryon (B) and the lepton (L) number are conserved quantities of the theory, as well as the $B - L$ one. Furthermore, it is important to notice that the $B - L$ number could be gauged in a $U(1)$ symmetry group in combination with an augmented neutrino sector, and this creates a model that is free from anomalies.

Hence, the minimal $B - L$ extension of the SM consists of augmenting the SM gauge groups $SU(3)_C \times SU(2)_L \times U(1)_Y$ by the aforementioned $U(1)_{B-L}$ symmetry (see [12, 13] and more recently [14–25]).

This choice is minimal on three respects:

- it is minimal in the gauge sector, enlarging the gauge group by adding one spontaneously broken $U(1)$ factor, which provides one new (neutral) gauge boson;
- it is minimal in the fermion sector, adding one new heavy neutrino per generation;
- it is minimal in the scalar sector, adding one new complex Higgs field, singlet under the SM gauge group.

This extension gives rise to a model:

- that is anomaly-free and gauge-invariant (see Section 2.1 for details);
- that provides an “elegant” way to generate the light neutrino masses by means of the so-called “see-saw” mechanism (see [26–31] and Section 2.4 for details).

This rather simple approach fulfils the phenomenological requirement of having a renormalisable theory that provides a mechanism for giving mass to light neutrinos as well as a good candidate for DM (see [32, 33]).

In addition, it is important to notice that $B - L$ symmetry breaking takes place at the TeV energy scale, hence leaving open the possibility of being part of a Grand Unified Theory (GUT) and giving rise to new and interesting TeV scale phenomenology.

In this work, we focus on the phenomenology arising from the main ingredients of EW plus $B - L$ spontaneous symmetry breaking, i.e., the Higgs sector phenomenology of the minimal $B - L$ model at present and future colliders.

1.3 Experimental frameworks: present and future colliders

In this Section we introduce the present and future machines that could possibly allow us to test the minimal $B - L$ model.

For this, two experimental frameworks have been taken into account:

- the Large Hadron Collider (LHC). It is a hadron-hadron collider. It is the only high-energy accelerator that is currently working. Up to now, it is the world's largest and highest-energy particle accelerator ever made.
- The International Linear Collider (ILC) and the Compact Linear Collider (CLIC). They are planned to be e^+e^- colliders. They are two proposed accelerators and the projects have not yet been approved. If realised, they will be the largest and highest-energy linear particle accelerators ever made.

1.3.1 The LHC

The LHC was built by the European Organization for Nuclear Research (CERN) with the intention of testing various predictions of high-energy physics, with emphasis on addressing the nature of the EW SB.

It is a circular collider and it is designed to investigate processes in which the initial state is characterised by either protons or heavy ions.

It consists of several detectors/experiments:

- ATLAS (A Toroidal LHC ApparatuS): together with CMS is one of the two general purpose detectors;
- CMS (Compact Muon Solenoid): together with ATLAS is one of the two general purpose detectors;
- ALICE (A Large Ion Collider Experiment): it is designed to investigate the so-called “quark-gluon plasma” and the (de)confinement scenarios;

- LHCb (Large Hadron Collider b): it is mainly designed to investigate the nature of CP -violation in interactions of b -hadrons.

In this work we focus on discovery physics, i.e., we are interested on proton-proton collisions and possible minimal $B - L$ signatures at both ATLAS and CMS.

1.3.2 Future linear collider prototypes

Although the LHC has finally entered its operational stage, a considerable part of the international physics community is focusing efforts in order to plan what the future of high-energy particle phenomenology and accelerators could be.

Nowadays, the community is working on the proposal of two linear accelerator prototypes: the ILC and the CLIC. Both of them represent the new generation of electron-positron colliders.

While the LHC and its multi-purpose detectors have been built with the aim of discovering new particles, the main goal that the new generation of linear colliders (LCs) is supposed to achieve is the subsequent profiling of the new physics whose evidence could arise in the next years at the LHC.

Specifically, there are many phenomenological aspects on which the LHC is insufficient in with respect to either ILC or CLIC:

- if existing, direct measuring of mass, spin and coupling of the Higgs and new gauge bosons;
- if existing, a complete profiling of any TeV scale extra-dimension;
- if existing, a better understanding of any supersymmetric scenario and related dark matter aspects.

In particular, in this work we are only interested in the minimal $B - L$ model Higgs sector. Therefore we will consider the two linear accelerator configurations only for the scope of probing the existence of a Higgs boson.

However, it is important to mention the fact that, if realised, the two accelerators will represent a unique way to precisely profile the Higgs sector of the minimal $B - L$ model.

1.4 Organisation of the work

This Thesis is organised as follows:

- in Chapter 2 we describe the minimal $B - L$ model in all its salient parts, with emphasis on the extended sectors, the $B - L$ symmetry breaking mechanism, some formal aspects related to the gauge-invariance and ghost fields, and the “see-saw” mechanism for generating the light neutrino masses;
- in Chapter 3 we perform a complete analysis of the experimental and theoretical constraints on the Higgs sector of the minimal $B - L$ model, focusing on the bounds on the Higgs masses coming from direct searches at LEP, unitarity and triviality arguments; then, we also present the experimental and theoretical constraints on the other parameters of the model and discuss the “fine-tuning” in the minimal $B - L$ model;
- in Chapter 4 we present our phenomenological results of the investigation of the minimal $B - L$ Higgs sector at colliders; we start with the study of Higgs branching ratios (BR), then we discuss some peculiar signatures at both the LHC and future LCs;
- in Chapter 5 we summarise our result and we also conclude our work discussing some open issues of our research;
- in Appendix A we list the potential of the minimal $B - L$ scalar effective-Lagrangian; this part is useful in analysing formal aspects of theory, as it will be clear in Section 3.2;
- in Appendix B we list the Feynman rules of the minimal $B - L$ model adopting the Feynman-gauge.

Chapter 2

The minimal $B - L$ model

In this Chapter we introduce the minimal $B - L$ model by a detailed description of the terms of its Lagrangian.

As we have already intimated, this model is an extension of the SM , following the symmetry pattern:

$$SU(3)_C \times SU(2)_L \times U(1)_Y \rightarrow SU(3)_C \times SU(2)_L \times U(1)_Y \times U(1)_{B-L}. \quad (2.1)$$

As we shall see, the charges of the two $U(1)$ factors of the extended gauge group are associated with the SM weak hypercharge Y , and with the total (Baryon - Lepton) number $B - L$ ¹.

The quantum consistency (anomaly cancellation) of the theory, together with the phenomenological requirement of generating neutrino masses, are fully satisfied by extending also the fermion content with a right-handed neutrino ν_R (singlet under the SM gauge group) for each family.

Finally, the requirement of giving mass to the extra neutral gauge boson Z' is fulfilled by a minimal extension of the scalar sector as well, with the introduction of a scalar field χ , singlet under the SM gauge group but not under the $U(1)_{B-L}$ (since it carries $B - L$ charge).

In Section 2.1 we begin by identifying the model Lagrangian in all its parts. In Section 2.2 we then proceed with a discussion of the extended Higgs mechanism, breaking $SU(2)_L \times$

¹In the general $B - L$ model, this identification is not generally possible since the presence of “mixing” makes it basis-dependent, therefore the covariant derivative is generally non-diagonal. Indeed, it is always possible to diagonalize the covariant derivative by defining an “effective charge” Y^P (with the corresponding coupling g^P), which is a linear combination of Y and $B - L$, but in this case a more careful treatment should be done and it lie outside of our purposes.

$U(1)_Y \times U(1)_{B-L}$ down to $U(1)_Q$, and of the ensuing spectrum of gauge bosons, fermions and scalars. In Section 2.3 we present a brief analysis of the minimal $B - L$ gauge-fixing. In Section 2.4 we introduce the principles of the so-called “see-saw” mechanism. Finally, in Section 2.5 we conclude this Chapter with a summary of the introduced parameters in comparison with the SM case.

It is important to mention the fact that the content of this Chapter will allow one to get all the necessary elements to implement the minimal $B - L$ model in any Feynman-rules generator (as *LanHEP* [34], *FeynRules* [35], etc.). In Appendix B we collect the Feynman rules of the model that we have obtained by mean of the *LanHEP* package.

2.1 The Lagrangian and the parameterisation

The minimal $U(1)_{B-L}$ extension of the SM is realised by augmenting the symmetry structure by a $U(1)$ gauge group, that is related to the $B - L$ symmetry.

Without loss of generality, the classical gauge-invariant Lagrangian for the class of models under consideration (obeying the $SU(3)_C \times SU(2)_L \times U(1)_Y \times U(1)_{B-L}$) can be decomposed as:

$$\mathcal{L} = \mathcal{L}_s + \mathcal{L}_{YM} + \mathcal{L}_f + \mathcal{L}_Y, \quad (2.2)$$

where the various terms represents the scalar, Yang-Mills, fermion and Yukawa part, respectively.

The general structure is similar to the SM Lagrangian, although (due to the different symmetry structure) each term takes into account the differences in the gauge, fermion and scalar sectors.

In the following, sector by sector, we will highlight analogies and differences with respect to the SM case.

2.1.1 The Yang-Mills sector

As in the SM , the vector fields are uniquely determined by the choice of the gauge group, and by the transformation in their adjoint representation. Hence, in the \mathcal{L}_{YM} , the non-Abelian field strengths therein are the same (as in the SM) and the only difference is contained in the Abelian terms.

Explicitly, it is formalised as follows:

$$\mathcal{L}_{YM} = -\frac{1}{4}G_{\mu\nu}^{\alpha}G^{\mu\nu\alpha} - \frac{1}{4}W_{\mu\nu}^aW^{\mu\nu a} - \frac{1}{4}F^{\mu\nu}F_{\mu\nu} - \frac{1}{4}F'^{\mu\nu}F'_{\mu\nu}, \quad (2.3)$$

where

$$F_{\mu\nu} = \partial_{\mu}B_{\nu} - \partial_{\nu}B_{\mu}, \quad (2.4)$$

$$F'_{\mu\nu} = \partial_{\mu}B'_{\nu} - \partial_{\nu}B'_{\mu}; \quad (2.5)$$

here, B and B' are the gauge fields associated with $U(1)_Y$ and $U(1)_{B-L}$, respectively.

2.1.2 The fermion sector

The fermion content of the model is the same of the minimal SM , except for the addition of a right-handed neutrino ν_R (singlet under the SM gauge group) for each of the three lepton families.

As we already mentioned, this addition is essential both for anomaly cancellation and preserving gauge invariance.

Following the field-basis notation introduced in Subsection 2.1.1, the covariant derivatives of the $B - L$ model are defined as the usual SM non-Abelian part plus an Abelian part:

$$D_{\mu} \equiv \partial_{\mu} + ig_S \mathcal{T}^{\alpha} G_{\mu}^{\alpha} + ig T^a W_{\mu}^a + ig_1 Y B_{\mu} + i(\tilde{g}Y + g'_1 Y_{B-L})B'_{\mu}. \quad (2.6)$$

In the minimal version of the $B - L$, $\tilde{g} = 0$ is assumed (i.e., no mixing between the two $U(1)$ factors)² and the covariant derivative becomes:

$$D_{\mu} \equiv \partial_{\mu} + ig_S \mathcal{T}^{\alpha} G_{\mu}^{\alpha} + ig T^a W_{\mu}^a + ig_1 Y B_{\mu} + ig'_1 Y_{B-L} B'_{\mu}. \quad (2.7)$$

Then, the fermionic Lagrangian is given by:

$$\begin{aligned} \mathcal{L}_f = & \sum_{k=1}^3 \left(i\overline{q_{kL}}\gamma_{\mu}D^{\mu}q_{kL} + i\overline{u_{kR}}\gamma_{\mu}D^{\mu}u_{kR} + i\overline{d_{kR}}\gamma_{\mu}D^{\mu}d_{kR} + \right. \\ & \left. + i\overline{l_{kL}}\gamma_{\mu}D^{\mu}l_{kL} + i\overline{e_{kR}}\gamma_{\mu}D^{\mu}e_{kR} + i\overline{\nu_{kR}}\gamma_{\mu}D^{\mu}\nu_{kR} \right), \end{aligned} \quad (2.8)$$

where the charges of the fields are the usual SM ones, plus the $B - L$ ones:

²It is important to highlight that this condition holds at the EW scale only: if we assume the running of \tilde{g} , then it will monotonically grow spoiling the “minimality” of the model (see Subsection 3.2.2 for details).

- $Y_{B-L} = 1/3$ for quarks,
- $Y_{B-L} = -1$ for leptons.

Assuming that the conjecture of “universality” is true, no distinction between generations has been made.

2.1.3 The scalar sector

The model under study has an extended gauge sector, with an additional neutral gauge boson Z' with respect to the SM . In order to realise a consistent Higgs mechanism (giving mass not only to the SM weak bosons but also to the Z') it is necessary to enlarge the SM Higgs sector by means of a further complex Higgs singlet χ .

The $B - L$ charges of the two scalar fields are set to be:

- $Y_{B-L}^H = 0$,
- $Y_{B-L}^\chi = +2$;

this choice is essential to preserve the gauge invariance of the model.

The most general gauge-invariant and renormalisable scalar Lagrangian is:

$$\mathcal{L}_s = (D^\mu H)^\dagger D_\mu H + (D^\mu \chi)^\dagger D_\mu \chi - V(H, \chi), \quad (2.9)$$

with the scalar potential given by

$$\begin{aligned} V(H, \chi) &= m^2 H^\dagger H + \mu^2 |\chi|^2 + \begin{pmatrix} H^\dagger H & |\chi|^2 \end{pmatrix} \begin{pmatrix} \lambda_1 & \frac{\lambda_3}{2} \\ \frac{\lambda_3}{2} & \lambda_2 \end{pmatrix} \begin{pmatrix} H^\dagger H \\ |\chi|^2 \end{pmatrix} \\ &= m^2 H^\dagger H + \mu^2 |\chi|^2 + \lambda_1 (H^\dagger H)^2 + \lambda_2 |\chi|^4 + \lambda_3 H^\dagger H |\chi|^2. \end{aligned} \quad (2.10)$$

2.1.4 The Yukawa term

To complete the description of the Lagrangian in equation (2.2), it is necessary to perform a treatment of the Yukawa couplings.

In addition to the Yukawa couplings of the minimal SM , we have two new types of Yukawa interactions involving right-handed neutrinos:

$$\begin{aligned} \mathcal{L}_Y &= -y_{jk}^d \overline{q_{Lj}} d_{Rk} H - y_{jk}^u \overline{q_{Lj}} u_{Rk} \tilde{H} - y_{jk}^e \overline{l_{Lj}} e_{Rk} H \\ &\quad - y_{jk}^\nu \overline{l_{Lj}} \nu_{Rk} \tilde{H} - y_{jk}^M \overline{(\nu_R)_j^c} \nu_{Rk} \chi + \text{h.c.}, \end{aligned} \quad (2.11)$$

where $\tilde{H} = i\sigma^2 H^*$ and i, j, k run from 1 to 3.

It is important to notice that the Yukawa interactions can generate both Dirac mass terms and Majorana mass terms for right-handed neutrinos (both of them in the second line of equation (2.11)). As we will see in Section 2.4 these are the essential ingredients of the “see-saw” mechanism for giving mass to light and heavy neutrinos.

As aforementioned, it is now clear, from the terms involving the χ scalar field, that $Y_{B-L}^\chi = +2$ is needed in order to ensure the gauge invariance.

2.2 Spontaneous $SU(2)_L \times U(1)_Y \times U(1)_{B-L}$ breaking

We generalise the *SM* discussion of spontaneous *EWSB* to the more complicated case represented by the potential of equation (2.10).

To determine the condition for $V(H, \chi)$ to be bounded from below, it is sufficient to study its behaviour for large field values, controlled by the matrix in the first line of the aforementioned equation. Requiring such a matrix to be positive-definite gives the conditions:

$$4\lambda_1\lambda_2 - \lambda_3^2 > 0, \quad (2.12)$$

$$\lambda_1, \lambda_2 > 0. \quad (2.13)$$

If the above conditions are satisfied, the choice of parameters is consistent with a well-defined potential, hence we can proceed to the minimisation of V as a function of constant Vacuum Expectation Values (*VEVs*) for the two Higgs fields.

Since the minimisation procedure is not affected by the choice of the gauge, it is not restrictive to define the two *VEVs* in the following way:

$$\langle H \rangle \equiv \begin{pmatrix} 0 \\ v \\ \frac{v}{\sqrt{2}} \end{pmatrix}, \quad \langle \chi \rangle \equiv \frac{x}{\sqrt{2}}, \quad (2.14)$$

with v and x real and non-negative.

Then, the search for extrema of V is made by mean of the following differential set of equations:

$$\begin{cases} \frac{\partial V}{\partial v}(v, x) = v \cdot \left(m^2 \lambda_1 v^2 + \frac{\lambda_3^2}{2} x^2 \right) = 0 \\ \frac{\partial V}{\partial x}(v, x) = x \cdot \left(\mu^2 \lambda_2 x^2 + \frac{\lambda_3^2}{2} v^2 \right) = 0 \end{cases} \quad (2.15)$$

The physically interesting solutions are the ones obtained for $v, x > 0$:

$$v^2 = \frac{-\lambda_2 m^2 + \frac{\lambda_3}{2} \mu^2}{\lambda_1 \lambda_2 - \frac{\lambda_3^2}{4}}, \quad (2.16)$$

$$x^2 = \frac{-\lambda_1 \mu^2 + \frac{\lambda_3}{2} m^2}{\lambda_1 \lambda_2 - \frac{\lambda_3^2}{4}}. \quad (2.17)$$

Since the denominator in equations (2.16)-(2.17) is always positive (assuming that the potential is well-defined), it follows that the numerators are forced to be positive in order to guarantee a positive-definite non-vanishing solution for v and x .

In order to identify the extrema, we need to evaluate the Hessian matrix:

$$\mathcal{H}(v, x) \equiv \begin{pmatrix} \frac{\partial^2 V}{\partial v^2} & \frac{\partial^2 V}{\partial v \partial x} \\ \frac{\partial^2 V}{\partial v \partial x} & \frac{\partial^2 V}{\partial x^2} \end{pmatrix} = \begin{pmatrix} 2\lambda_1 v^2 & \lambda_3 v x \\ \lambda_3 v x & 2\lambda_2 x^2 \end{pmatrix}. \quad (2.18)$$

From this equation, it is straightforward to verify that the solutions are minima if and only if equations (2.12)-(2.13) are satisfied.

2.2.1 The scalar mass spectrum

To compute the scalar masses, one must expand the potential in equation (2.10) around the minima found in equations (2.16)-(2.17).

Since the physical mass eigenvalues are gauge invariant, we define the Higgs fields following the unitary-gauge prescription:

$$H \equiv \begin{pmatrix} 0 \\ \frac{h+v}{\sqrt{2}} \end{pmatrix}, \quad \chi \equiv \frac{h'+x}{\sqrt{2}}. \quad (2.19)$$

After standard manipulations, the explicit expressions for the scalar mass eigenvalues are:

$$M_{h_1}^2 = \lambda_1 v^2 + \lambda_2 x^2 - \sqrt{(\lambda_1 v^2 - \lambda_2 x^2)^2 + (\lambda_3 x v)^2}, \quad (2.20)$$

$$M_{h_2}^2 = \lambda_1 v^2 + \lambda_2 x^2 + \sqrt{(\lambda_1 v^2 - \lambda_2 x^2)^2 + (\lambda_3 x v)^2}, \quad (2.21)$$

where h_1 and h_2 are the scalar fields of definite masses M_{h_1} and M_{h_2} respectively, and we conventionally choose $M_{h_1}^2 < M_{h_2}^2$.

These eigenvalues are related to the following eigenvectors:

$$\begin{pmatrix} h_1 \\ h_2 \end{pmatrix} = \begin{pmatrix} \cos \alpha & -\sin \alpha \\ \sin \alpha & \cos \alpha \end{pmatrix} \begin{pmatrix} h \\ h' \end{pmatrix}, \quad (2.22)$$

where $-\frac{\pi}{2} \leq \alpha \leq \frac{\pi}{2}$ fulfils³:

$$\sin 2\alpha = \frac{\lambda_3 x v}{\sqrt{(\lambda_1 v^2 - \lambda_2 x^2)^2 + (\lambda_3 x v)^2}}, \quad (2.23)$$

$$\cos 2\alpha = \frac{\lambda_2 x^2 - \lambda_1 v^2}{\sqrt{(\lambda_1 v^2 - \lambda_2 x^2)^2 + (\lambda_3 x v)^2}}. \quad (2.24)$$

For completeness, it is useful to write the isomorphic transformation between the two λ_1 - λ_2 - λ_3 and M_{h_1} - M_{h_2} - α spaces.

From equations (2.20)-(2.21)-(2.23), it is straightforward to have:

$$\begin{aligned} \lambda_1 &= \frac{M_{h_1}^2}{2v^2} + \frac{(M_{h_2}^2 - M_{h_1}^2)}{2v^2} \sin^2 \alpha = \frac{M_{h_1}^2}{2v^2} \cos^2 \alpha + \frac{M_{h_2}^2}{2v^2} \sin^2 \alpha \\ \lambda_2 &= \frac{M_{h_1}^2}{2x^2} + \frac{(M_{h_2}^2 - M_{h_1}^2)}{2x^2} \cos^2 \alpha = \frac{M_{h_1}^2}{2x^2} \sin^2 \alpha + \frac{M_{h_2}^2}{2x^2} \cos^2 \alpha \\ \lambda_3 &= \frac{(M_{h_2}^2 - M_{h_1}^2)}{2vx} \sin(2\alpha). \end{aligned} \quad (2.25)$$

2.2.2 The gauge mass spectrum

To determine the gauge boson spectrum, we have to expand the scalar kinetic terms as in the SM case. From consistency arguments, we expect that there exists a massless gauge boson (the photon) and the other gauge bosons acquiring mass.

Moreover, we expect that the SM charged vector boson spectrum is not affected by the extension (since it involves the non-Abelian part only). As for the Abelian vector bosons, using the unitary-gauge parameterisation, we write the kinetic terms in equation (2.9) as:

$$\begin{aligned} &(D^\mu H)^\dagger D_\mu H = \\ &= \frac{1}{2} \partial^\mu h \partial_\mu h + \frac{1}{8} (h+v)^2 (0 \ 1) \left[g W_a^\mu \sigma_a + g_1 B^\mu \right]^2 \begin{pmatrix} 0 \\ 1 \end{pmatrix} \\ &= \frac{1}{2} \partial^\mu h \partial_\mu h + \frac{1}{8} (h+v)^2 \left[g^2 |W_1^\mu - iW_2^\mu|^2 + (gW_3^\mu - g_1 B^\mu)^2 \right], \end{aligned} \quad (2.26)$$

³In all generality, the whole interval $0 \leq \alpha < 2\pi$ is halved because an orthogonal transformation is invariant under $\alpha \rightarrow \alpha + \pi$.

and

$$(D^\mu \chi)^\dagger D_\mu \chi = \frac{1}{2} \partial^\mu h' \partial_\mu h' + \frac{1}{2} (h' + x)^2 (g'_1 2B'^\mu)^2. \quad (2.27)$$

In equation (2.26) we can easily identify the SM charged gauge bosons W^\pm , with $M_W = gv/2$.

As for the other fields, the vanishing mixing between the two $U(1)$ factors (i.e., the assumption $\tilde{g} = 0$) allow us to immediately identify both the SM -like pieces and the new vector boson $Z' \equiv B'$.

Once we set the B^μ , W_3^μ and B'^μ as field basis, the explicit expression for the squared mass matrix is:

$$\begin{aligned} \mathcal{M}^2 &= \frac{v^2}{4} \begin{pmatrix} g_1^2 & -gg_1 & 0 \\ -gg_1 & g^2 & 0 \\ 0 & 0 & 16\frac{x^2}{v^2}(g'_1)^2 \end{pmatrix} \\ &= \frac{v^2}{4} (g^2 + g_1^2) \begin{pmatrix} \sin^2 \vartheta_w & -\cos \vartheta_w \sin \vartheta_w & 0 \\ -\cos \vartheta_w \sin \vartheta_w & \cos^2 \vartheta_w & 0 \\ 0 & 0 & \frac{16x^2(g'_1)^2}{v^2(g^2 + g_1^2)} \end{pmatrix}, \end{aligned} \quad (2.28)$$

where we have made use of the well-known relations:

$$\cos \vartheta_w = \frac{g}{\sqrt{g^2 + g_1^2}}, \quad \sin \vartheta_w = \frac{g_1}{\sqrt{g^2 + g_1^2}}. \quad (2.29)$$

As in the SM case, if we want to diagonalise the 2×2 sub-matrix in equation (2.28), we need to apply a rotation along the $B'(Z')$ field, defined by:

$$R_{EW}(\vartheta_w) = \begin{pmatrix} \cos \vartheta_w & -\sin \vartheta_w & 0 \\ \sin \vartheta_w & \cos \vartheta_w & 0 \\ 0 & 0 & 1 \end{pmatrix}, \quad (2.30)$$

and this allow us to isolate each mass eigenvalue:

$$R_{EW}(\vartheta_w) \mathcal{M}^2 [R_{EW}(\vartheta_w)]^{-1} = \begin{pmatrix} 0 & 0 & 0 \\ 0 & \frac{v^2}{4} (g^2 + g_1^2) & 0 \\ 0 & 0 & 4x^2 (g'_1)^2 \end{pmatrix}. \quad (2.31)$$

Finally, we can associate the mass eigenvalues with the corresponding physical vector boson eigenstates:

$$\begin{aligned} M_A &= 0, \\ M_Z &= \frac{v}{2}\sqrt{g^2 + g_1^2}, \\ M_{Z'} &= 2xg'_1. \end{aligned} \tag{2.32}$$

2.3 The Feynman-gauge and the ghost Lagrangian

Once the Lagrangian is established and the gauge symmetries are spontaneously broken, the gauge bosons acquire their masses and we have constructed a consistent theory.

However, the way we treated the Higgs mechanism so far is too simplistic: assuming the unitary-gauge framework, we have not depicted any exhaustive description of the computational Feynman rules of the minimal $B - L$ model, hence we are not ready for any phenomenological analysis yet.

Moreover, as we shall see in Subsection 3.2.1, we are missing a correct treatment of formal unitarity aspects of the theory.

Finally, it is well known that if the definition of each model is delivered in the Feynman-gauge the public softwares dedicated to the computation of amplitudes/cross-sections (as *CalcHEP* [36, 37], *MadGraph* [38], *FeynArts-FormCalc* [39], etc.) increase their computational power, hence with an explicit parametrisation of the Goldstone contribution within the Higgs potential.

For this, in the Subsection 2.3.1 we will introduce a standard parametrisation for the Higgs fields in the Feynman-gauge.

As for the aforementioned unitarity of the theory, it will be apparently spoiled by the fact that the Feynman gauge will introduce the effects of unphysical particles in the computational formalism. In order to cancel this effects, in the Subsection 2.3.2 we will define a gauge-fixing Lagrangian, using the Fadeev-Popov method, in order to restore the computational consistency of the the minimal $B - L$ model.

2.3.1 The Feynman gauge

We focus again on the scalar sector of the Lagrangian described in Subsection 2.1.3.

Following the prescription of the Feynman-gauge parametrisation of the Higgs doublet and singlet of the minimal $B - L$ model, we consider not only the Higgs fields and their VEV s, but also the so-called Goldstone bosons.

Hence, H and χ are now defined in the following way:

$$H = \frac{1}{\sqrt{2}} \begin{pmatrix} -i(w^1 - iw^2) \\ v + (h + iz) \end{pmatrix}, \quad \chi = \frac{1}{\sqrt{2}}(x + (h' + iz')), \quad (2.33)$$

where $w^\pm = w^1 \mp iw^2$, z and z' are the Goldstone bosons of W^\pm , Z and Z' , respectively.

From this definition and the set of relations described by equations (2.20)-(2.25), we can calculate the explicit rules of the interactions (i.e., the Feynman rules) in terms of mass eigenstates and couplings.

As we will show in Subsection 3.2.1, a particular interesting aspect of the structure of the scalar Lagrangian in the Feynman gauge is that it fully describes the interaction of longitudinally polarised vector bosons and Higgs bosons in the high energy limit (“equivalence theorem”, see the Chapter 21 of [1] and [40]).

Moreover, if we assume that the couplings of the theory are perturbative and small then we can also apply the prescription $D_\mu \simeq \partial_\mu$ in order to obtain the would-be-Goldstone scalar sector: to all intents it works as an effective high energy theory of the longitudinally polarised vector bosons and Higgs bosons interactions.

For this, the would-be-Goldstone effective theory is a particularly useful tool for analysing the perturbative unitarity stability of longitudinally polarised vector boson scatterings in the high energy limit, and we list the complete set of the functions appearing in the would-be-Goldstone Lagrangian, in Appendix A.

2.3.2 The Fadeev-Popov Lagrangian

Since there is no mixing in the neutral boson sector, the gauge-fixing in the minimal $B - L$ model is fulfilled by a rather easy procedure.

Firstly, the Higgs doublet gauge-fixing Lagrangian is not affected by the $B - L$ extension. Hence, following the notation of [1], the ghost Lagrangian in the Feynman gauge is the usual SM -like one:

$$\mathcal{L}_{FP_H} = \bar{c}^a \left[-(\partial_\mu D^\mu)^{ab} - g^2 (T^a \langle H \rangle) \cdot T^b H \right] c^b, \quad (2.34)$$

where the c 's are the gauge-fixing fields corresponding to the W 's and Z gauge bosons.

Due to the fact that the χ field belongs to an Abelian gauge symmetry structure, we have to extract the gauge-fixing for the Abelian case in the Feynman gauge.

To begin, we focus on the spontaneously broken term of the scalar Lagrangian in equation (2.9):

$$\mathcal{L}_{sAb} = (D^\mu \chi)^\dagger D_\mu \chi - V(H, \chi), \quad (2.35)$$

with $D_\mu = \partial_\mu + 2ig_1' Z'_\mu$. From the second equation of (2.33), we obtain:

$$\mathcal{L}_{sAb} = \frac{1}{2}(\partial_\mu h' - 2g_1' Z'_\mu z')^2 + \frac{1}{2}(\partial_\mu z' + 2g_1' Z'_\mu (x + h'))^2 - V(H, \chi). \quad (2.36)$$

This Lagrangian is invariant under an exact local symmetry:

$$\delta h' = -\alpha(x)z', \quad \delta z' = \alpha(x)(x + h'), \quad \delta Z'_\mu = -\frac{1}{2g_1'}\partial_\mu \alpha(x). \quad (2.37)$$

Due to the existence of this local symmetry, in order to define the functional integral over the variables h' , z' , Z' , we must introduce the Fadeev-Popov gauge-fixing.

Following the standard techniques (see the Chapter 9 of [1]), we define the functional integral:

$$Z = \int \mathcal{D}(Z')\mathcal{D}(h')\mathcal{D}(z') \exp \left[i \int \mathcal{L}_{sAb} \right]. \quad (2.38)$$

Introducing a gauge-fixing constraint we find:

$$Z = C \int \mathcal{D}(Z')\mathcal{D}(h')\mathcal{D}(z') \exp \left[i \int \mathcal{L}_{sAb} \right] \delta(G(Z', h', z')) \det \left(\frac{\delta G}{\delta \alpha} \right), \quad (2.39)$$

where C is a constant proportional to the “volume” of the gauge group and G is a gauge-fixing condition. At this point, we can introduce the gauge-fixing constraint as $\delta(G(x) - \omega(x))$ and integrate over $\omega(x)$ with a Gaussian weight, to obtain:

$$Z = C' \int \mathcal{D}(Z')\mathcal{D}(h')\mathcal{D}(z') \exp \left[i \int d^4x (\mathcal{L}_{sAb} - \frac{1}{2}G^2) \right] \det \left(\frac{\delta G}{\delta \alpha} \right). \quad (2.40)$$

The gauge-fixing function G is arbitrary, and a common choice in the Feynman-gauge is:

$$G = \partial^\mu Z'_\mu - 2g_1' x z'. \quad (2.41)$$

From the gauge-fixing condition, it is straightforward to obtain the Lagrangian of ghost for the Abelian terms of the scalar Lagrangian. Firstly, we evaluate the gauge variation

of G :

$$\frac{\delta G}{\delta \alpha} = -\frac{1}{2g_1'} \partial^2 - 2g_1' x(x + h') = \frac{1}{2g_1'} \left(-\partial^2 - (2g_1' x)^2 \left(1 + \frac{h'}{x} \right) \right). \quad (2.42)$$

The determinant of this operator is related to the ghost Lagrangian by the equation:

$$\det \left(\frac{\delta G}{\delta \alpha} \right) = \int \mathcal{D}c \mathcal{D}\bar{c} \exp \left[-i \int d^4x \mathcal{L}_{FP_x} \right], \quad (2.43)$$

where

$$\mathcal{L}_{FP_x} = \bar{c}^{Z'} \left(2g_1' \frac{\delta G}{\delta \alpha} \right) c^{Z'} = \bar{c}^{Z'} \left(-\partial^2 - M_{Z'}^2 \left(1 + \frac{h'}{x} \right) \right) c^{Z'}. \quad (2.44)$$

In the last equation, $M_{Z'} = 2g_1' x$ and $c^{Z'}$'s are the ghost fields related to the Z' boson.

It is interesting to notice that since this belongs to an Abelian gauge structure, the ghost fields does not couple directly to the gauge field, but only to the physical Higgs field.

2.4 See-saw mechanism and neutrino masses

In the SM framework, there is not a straightforward way to generate the experimentally observed neutrino masses and oscillations: any isolated extension that solve this open issue (effective Majorana mass terms, sterile right-handed neutrinos, etc.) is affected by consistency problems (they spoil either renormalisability or gauge invariance, see [4] for details).

The minimal $B - L$ model provides an elegant “natural” solution: the presence of right-handed neutrinos in the Yukawa Lagrangian (equation (2.11)) gives raise to the so-called “see-saw” mechanism.

In details, after the spontaneous breaking of the gauge symmetry, the Dirac neutrinos combine to six Majorana mass eigenstates, and the mass matrix is:

$$\mathcal{M} = \begin{pmatrix} 0 & m_D \\ m_D^T & M \end{pmatrix}, \quad (2.45)$$

where m_D and M are respectively the Dirac and Majorana mass matrices, defined as:

$$m_D = \frac{(y^\nu)^*}{\sqrt{2}} v, \quad M = \sqrt{2} y^M x. \quad (2.46)$$

Once assumed that the hierarchy $\Lambda_D \ll \Lambda_M$ (where Λ indicates the energy scale) is true, the diagonalization of the mass matrix realises the “see-saw” mechanism.

After this procedure, we are left with three light Majorana neutrinos ν_l and three heavy Majorana neutrinos ν_h , whose 3×3 mass matrices, denoted by M_l and M_h respectively, are given by:

$$\begin{aligned} M_l &\simeq m_D M^{-1} m_D^T = \frac{1}{2\sqrt{2}} y^\nu (y^M)^{-1} (y^\nu)^T \frac{v^2}{x}, \\ M_h &\simeq M = \sqrt{2} y^M x. \end{aligned} \quad (2.47)$$

In equations (2.47) we can appreciate the “see-saw” effect: the greater is M , the smaller is M_l .

As explicit example we consider the case in which there is no mixing between the three generations, hence the matrices m_D and M are two diagonal matrices: in this case the 6×6 matrix splits in three 2×2 matrices.

Thereafter, the diagonalisation is realised by the transformation

$$\begin{pmatrix} \cos \alpha_i & -\sin \alpha_i \\ \sin \alpha_i & \cos \alpha_i \end{pmatrix} \begin{pmatrix} 0 & m_D^i \\ m_D^i & M^i \end{pmatrix} \begin{pmatrix} \cos \alpha_i & \sin \alpha_i \\ -\sin \alpha_i & \cos \alpha_i \end{pmatrix} \simeq \text{diag} \left(-\frac{(m_D^i)^2}{M^i}, M^i \right), \quad (2.48)$$

where $i = 1, 2, 3$ denotes one of the three generations and $\alpha^i = \arcsin(m_D^i/M^i)$.

We can roughly estimate the mass-scale Λ_M needed to obtain neutrino masses in agreement with phenomenological constraints [41, 42].

By taking $\Lambda_l < 1$ eV and $\Lambda_D \sim EW$ scale we get:

$$\Lambda_l \simeq \frac{\Lambda_D^2}{\Lambda_M} < 1 \text{ eV} \Rightarrow \Lambda_M > 10^{13} \text{ GeV}. \quad (2.49)$$

We should keep in mind, however, that Λ_D could well be several orders of magnitudes smaller than the weak scale (for example, the electron mass): in such a case, much smaller scales for Λ_M are allowed.

Anyway, starting from equations (2.46), a generalised condition could be:

$$v|y^\nu| \ll x|y^M|. \quad (2.50)$$

It is important to recall that in the general case, in order to extract the individual mass eigenvalues and eigenstates of the mixed neutrinos eigensystem, we must separately diagonalise the two mass matrices M_l and M_h . In the case of M_l , the diagonalisation gives rise to the well-known mixing U_{PMNS} (see [43–46]) matrix with 6 real independent parameters, 3 angles and 3 phases.

2.5 Counting of parameters

The SM contains 18 real parameters (3 in the gauge sector, 2 in the Higgs sector, 13 in the fermion sector).

Once we add neutrino masses to the SM via the see-saw mechanism, and assume no mixing in the right-handed neutrino sector⁴, 12 more real parameters are introduced (6 neutrino masses and the 6 parameters of U_{PMNS}), for a total of 30.

The Yang-Mills sector contains 1 more parameter than in the SM model: the gauge coupling constant g'_1 .

Finally, The scalar potential depends on 7 real parameters, the two scalar masses (m^2 , μ^2), the three couplings (λ_1 , λ_2 , λ_3) and the two $VEVs$ (v , x): three of them are equivalent to the corresponding SM parameters, thus we have here 4 additional parameters with respect to the SM .

In conclusion, the total number of parameters is 35.

⁴This is realised by neglecting the additional complex parameters of their Yukawa couplings. Let's remind that in this work we are mainly interested in colliders and discovery physics, hence allowing any mixing either in the heavy or light neutrino sector does not affect our conclusions.

Chapter 3

The Higgs sector parameter space

As we have already seen in Section 2.5, the $B - L$ extension of the SM introduces a new set of parameters.

Apart from the Higgs boson mass, all the parameters involved in the definition of the SM Lagrangian have been set by experiments; when we call for the minimal $B - L$ extension, it opens a new parameter space defined by 12 parameters (from the neutrino sector¹), 1 parameter (from the $B - L$ gauge boson sector²) and 4 parameters (from the Higgs bosons sector³).

In principle, this could allow to explore potentially infinite new phenomenological implications, nevertheless one has to take into account the experimental and theoretical constraints that affects each sector.

As for the Higgs sector, in the past four decades an enormous effort has been made to improve both the theoretical and experimental techniques that allow us to understand what is the forbidden parameter space.

We can split these procedures in two sets: “experimental” and “theoretical”.

The ones belonging to the former give constraints:

- by EW precision tests (Subsection 3.1.1),
- by direct searches (Subsection 3.1.2);

the ones belonging to the latter give constraints:

¹The 6 neutrino masses and the 6 parameters of U_{PMNS} .

²The g'_1 coupling.

³The 3 λ 's and the x .

- by perturbative unitarity arguments (Subsection 3.2.1-3.2.3),
- by triviality and vacuum stability (Subsection 3.2.2-3.2.3),
- by “naturalness” arguments (Subsection 3.2.4).

In this Chapter we present the main results that we have obtained by the application of these techniques to the minimal $B - L$ model and their major implications.

3.1 Experimental constraints on the Higgs boson sector

Despite the fact that the Higgs boson(s) has(have) not been discovered yet, we know by consistency that the Higgs sector should participate to the known phenomenology.

Firstly, the Higgs bosons (as well as the other new particles of this model: heavy neutrinos and Z') must contribute to the quantum corrections to the high-precision EW observables⁴, and this could impose boundaries on the free parameters.

Moreover, there are constraints coming from direct searches of Higgs bosons at colliders, in particular from LEP.

In this Section we will summarise the main results of these indirect and direct (respectively) constraints.

3.1.1 High-precision data and constraints on the Higgs sector

Even if the $B - L$ model is a minimal extension of the SM , it shows a phenomenological richness that imposes an accurate approach to the EW precision data analysis.

In principle, if one assumes that the symmetry group of new physics (NP) is still $SU(3)_C \times SU(2)_L \times U(1)_Y$, it is possible to parametrise the radiative corrections in such a way that the contributions from NP could be easily implemented and confronted with EW precision data (a popular example is the well-known Peskin-Takeuchi parametrisation in [47, 48]).

However, it is important to mention the fact that the parametrisation is based on the fact that the Higgs bosons must be the only source of quantum corrections.

Obviously, this is not the case of the minimal $B - L$ model, because of its extra $U(1)$ extension.

⁴In the last twenty years an enormous amount of EW precision data have been collected by the e^+e^- colliders LEP and SLC.

Indeed, in this case we have not only a new gauge boson Z' that affects the choice of the precision parameters parametrisation, but also the presence of heavy neutrinos that are not weakly coupled with the boson sector: this spoils the first assumption.

In the absence of new gauge bosons or heavy neutrinos, many successful attempts have been made to profile the constraints on the Higgs sector parameter space (in the multiple Higgs scenario, some interesting study has been performed in [49]), but unfortunately the $B - L$ model falls outside these conclusions.

Hence, in this work we have not considered any boundary condition coming from the EW precision analysis. However, we borrow a qualitative conclusion from the aforementioned multiple Higgs scenario paper: we assume that the Higgs bosons inversion limit $\alpha \rightarrow \pi/2$ is not allowed.

3.1.2 Direct searches and constraints on the Higgs sector

The minimal SM Higgs boson has been searched in the LEP experiments, firstly at energies close to the Z boson peak (LEP1), then with center of mass energies up to $\sqrt{s} \sim 200$ GeV (LEP2).

The main production modes that have been explored at LEP1 are the so-called Bjorken process ($Z \rightarrow HZ \rightarrow Hf\bar{f}$) and the $Z \rightarrow H\gamma$ (through triangular loops of t 's and W 's).

In order to avoid the large hadronic background, Higgs boson have been unsuccessfully searched in the two aforementioned channels (see [50–53]), leading to a 95% Confidence Level (CL) limit of $M_H > 65$ GeV on the SM Higgs mass.

In the LEP2 energy regime, the Higgs boson have been searched in its dominant production process: the Higgs-strahlung, $Z \rightarrow HZ$.

LEP collaborations have explored several topologies, combining their results in the analysis of the Z boson recoil energy that led to the well known exclusion limit of the SM Higgs boson mass (see [54]):

$$M_H > 114.4 \text{ GeV} \tag{3.1}$$

at the 95% CL from the non-observation.

In the $B - L$ model (as well as in other extensions of the SM), this limit is shifted back in mass by the fact that Higgs bosons have non-standard coupling to the Z (it is reduced

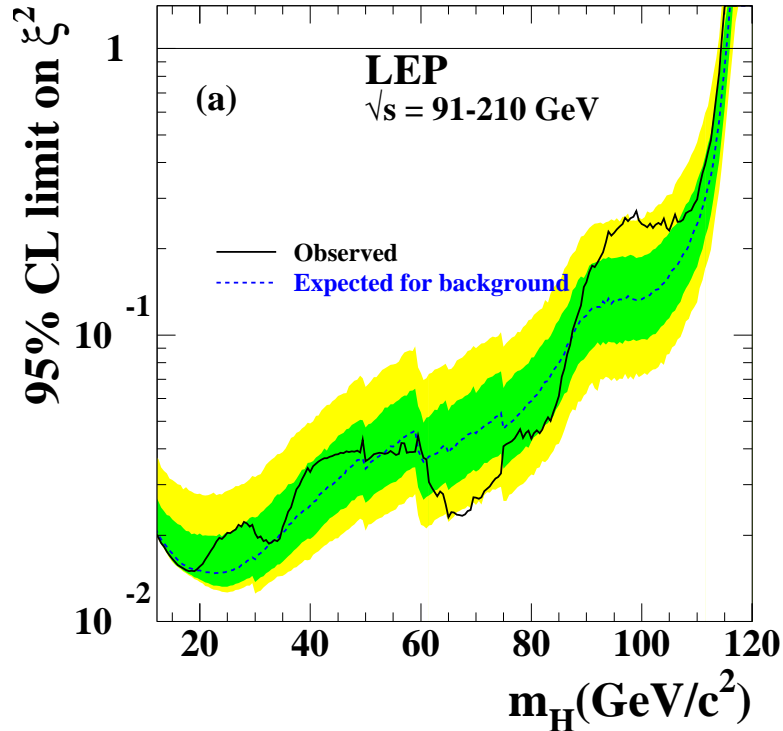


FIGURE 3.1: The 95% CL upper bound on the reduced coupling $\xi = g_{HZZ}/g_{HZZ}^{SM}$ set by the LEP collaborations; in the minimal $B-L$ model $\xi = \cos \alpha(\sin \alpha)$ for $H = h_1(h_2)$.

by $\cos \alpha$):

$$\frac{\sigma_{SM}(e^+e^- \rightarrow HZ)}{\sigma_{B-L}(e^+e^- \rightarrow H_1Z)} = \cos^2 \alpha. \quad (3.2)$$

Indeed, the LEP collaborations have also released a detailed analysis of the 95% CL exclusion limits on the (lightest) Higgs boson mass as function of the reduced coupling $\xi^2 = \cos^2 \alpha(\sin^2 \alpha)$ for the $h_1(h_2)$, and it is shown in figure 3.1.

In this work, we will consider the latter as the only experimental constraint on the $B-L$ Higgs sector parameter space.

3.1.3 Other experimental constraints

In view of an extensive numerical analysis of the phenomenological implications at colliders, one has to have a complete understanding of how other experimental bounds could affect the $B-L$ parameter space.

For this, we briefly present the experimental constraints on the gauge boson and neutrino sectors that we are going to consider in the rest of this work.

- $M_{Z'}$, the new gauge boson mass. An indirect constraint on $M_{Z'}$ comes from analyses at LEP of precision EW data (see [55], based on the analysis of experimental data published in [56–60])⁵:

$$\frac{M_{Z'}}{g'_1} \geq 7 \text{ TeV} . \quad (3.3)$$

Further limits have been obtained at Tevatron [20, 62, 63]. Both have been taken into account in this work.

- m_{ν_i} , the SM (or light) neutrino masses. We use the cosmological upper bound $\sum_i m_{\nu_i} < 1 \text{ eV}$ [64]. Ultimately, they have been taken to be $m_{\nu_i} = 10^{-2} \text{ eV}$. Since we are mainly interested in the discovery and collider physics phenomenological aspects, we remind that in the rest of our work, for our illustrative purposes, we take all neutrino masses (both light and heavy) to be degenerate.

3.2 Theoretical constraints on the Higgs boson sector

Several theoretical methods have been developed to establish what are the constraints on the Higgs parameter space.

In this Section we apply them to the minimal $B - L$ model.

They typically follow from general principles, like the assumption that the perturbative unitarity and the couplings of a theory are preserved to some energy scale (Subsection 3.2.1), as well as the stability of the symmetry breaking vacuum expectation value (Subsection 3.2.2).

These arguments could also be extended to different sectors of the theory in order to constrain other free parameters, as g'_1 , as we will show in the Subsection 3.2.3.

Finally, one could also propose some conjecture about the “naturalness” of the model, finding reasonable to indicate some “natural” range of value for the allowed parameter space of the theory in order to minimise the so-called “fine-tuning” problem (Subsection 3.2.4).

3.2.1 Perturbative unitarity

Even if there is no evidence of the $(B)SM$ Higgs boson(s), the need of such kind of particle in order to guarantee the perturbative unitarity of a theory is of fundamental concern.

⁵A less conservative approach, based on Fermi-type effective four-fermions interactions, gives the weaker constraint $\frac{M_{Z'}}{g'_1} \geq 6 \text{ TeV}$ [61].

In fact, the potential problem that affects the SM and its extensions is the following: in the absence of the Higgs boson contributions, the longitudinally polarised vector boson interactions violate unitarity at some energy scale.

To see this, we must recall some general properties of the scattering amplitudes; firstly, the amplitude A of a $2 \rightarrow 2$ process could be decomposed into partial waves a_l of orbital angular momentum l :

$$A = 16\pi \sum_{l=0}^{\infty} (2l+1) P_l(\cos \theta) a_l, \quad (3.4)$$

where P_l are the Legendre polynomials and θ is the diffusion angle; this leads to the following expression for the cross-section:

$$\sigma = \frac{16\pi}{s} \sum_{l=0}^{\infty} (2l+1) |a_l|^2. \quad (3.5)$$

From the optical theorem (see Chapter 7 of [1]) we also know that the cross-section is proportional to the imaginary part of the amplitude in the forward direction:

$$\sigma = \frac{1}{s} \text{Im}[A(\theta=0)] = \frac{16\pi}{s} \sum_{l=0}^{\infty} (2l+1) |a_l|^2. \quad (3.6)$$

From this, we have the relation $|a_l|^2 = \text{Im}(a_l)$, that leads to the well-known condition (see [65])

$$|\text{Re}(a_l(s))| \leq \frac{1}{2}. \quad (3.7)$$

In the SM context, the pioneeristic work of [66] showed that, when M_H is greater than a critical value $\simeq 1$ TeV (known as unitarity bound), the elastic spherical wave describing the scattering of the longitudinally polarised vector bosons at very high energy ($\sqrt{s} \rightarrow \infty$) violates the condition in equation 3.7, and the perturbative stability of the theory breaks down.

In the past, several efforts have been devoted to apply these methodology to a variety of models, in order to extract any possible information on their allowed parameter space. In particular, it has been already applied to scenarios with extended scalar sectors yet with same gauge structure as the SM , like those with additional singlets (for example, see [67]), doublets (for example, see [68] and [69] for non-Supersymmetric scenarios and [70] for Supersymmetric ones), triplets (for example, see [71]). It has also been shown that this approach is successful with respect to $U(1)$ gauge group extensions of the SM (for example, for the case of E_6 superstring-inspired minimal $U(1)$ extensions, see [72]).

Then, our aim is to show how this methods could also be successfully applied to the minimal $B-L$ case, taking into account the presence of two Higgs fields and four massive vector bosons.

In fact, by mean of the so-called Equivalence Theorem we are allowed to compute the amplitude of any process with external longitudinal vector bosons V_L ($V = W^\pm, Z, Z'$), in the high energy limit $M_V^2 \ll s$, by substituting each one of them with the related Goldstone bosons $v = w^\pm, z, z'$ and its general validity is proven (see [40]); schematically, if we consider a process with four longitudinal vector bosons: $A(V_L V_L \rightarrow V_L V_L) = A(vv \rightarrow vv) + O(m_V^2/s)$.

The intermediate vector boson exchange does not play a fundamental role in the Higgs boson(s) limits⁶, hence, as we intimated in Subsection 2.3.1, we simplify our approach by employing a theory of interacting would-be Goldstone bosons $v = w^\pm, z, z'$ described by the scalar Lagrangian in Appendix A.

In order to study the unitarity constraints in the $B-L$ model, we calculate the tree-level amplitudes for all two-to-two processes involving the full set of possible (pseudo)scalar fields (the most relevant subset is given by table 3.1).

Given a tree-level scattering amplitude between two spin-0 particles $A(s, \theta)$, where θ is the scattering (polar) angle, we know that the partial wave amplitude with angular momentum l is given by

$$a_l = \frac{1}{32\pi} \int_{-1}^1 d(\cos \theta) P_l(\cos \theta) A(s, \theta). \quad (3.8)$$

It turns out that only $l = 0$ (corresponding to the spherical partial wave contribution) leads to some bound, so we will not discuss the higher partial waves any further.

It is well known (and we have verified) that, in the high energy limit, only the four-point vertices (related to the four-point functions of the interacting potential, equations (A.1)-(A.3) of Appendix A) contribute to the $J = 0$ partial wave amplitudes, and this is consistent with many other aforementioned works that exploit the same methodology.

Hence, we present the main results of our study focusing only on the relevant subset of all spherical partial wave amplitudes that is shown in table 3.1. Here, we should notice that, as one can conclude from direct computation, in the high energy limit the contributions in table 3.1 ticked with \sim are just a double counting of the channels ticked with \surd or combinations of them.

⁶This is not generally true in gauge group extensions, nevertheless for this particular purpose we assume that g'_1 is perturbative and small, in such a way that any t -channel represents a subleading contribution to the scattering amplitude.

	zz	w^+w^-	$z'z'$	h_1h_1	h_1h_2	h_2h_2
zz	\checkmark	\checkmark	\checkmark	\checkmark	\checkmark	\checkmark
w^+w^-	\sim	\checkmark	\sim	\sim	\sim	\sim
$z'z'$	\sim	\sim	\checkmark	\checkmark	\checkmark	\checkmark
h_1h_1	\sim	\sim	\sim	\checkmark	\checkmark	\checkmark
h_1h_2	\sim	\sim	\sim	\sim	\checkmark	\checkmark
h_2h_2	\sim	\sim	\sim	\sim	\sim	\checkmark

TABLE 3.1: The most relevant subset of two-to-two scattering processes in the minimal $B - L$ model in the Higgs and would-be Goldstone boson sectors. The rows(columns) refer to the initial(final) state (or vice versa). The symbol \sim refers to processes that can be computed by appropriate rearrangements of those symbolised by \checkmark .

Moreover, the main contributions come from the so-called scattering eigenchannels, i.e., the diagonal elements of the “matrix” in table 3.1. In particular, for our choice of method, only $zz \rightarrow zz$ and $z'z' \rightarrow z'z'$, and to a somewhat lesser extent also $h_1h_1 \rightarrow h_1h_1$ and $h_2h_2 \rightarrow h_2h_2$, play a relevant role. For completeness, we list here all the a_0 's, eigenchannel by eigenchannel⁷:

$$a_0(zz \rightarrow zz) = \frac{3\alpha_W}{32M_W^2} [M_{h_1}^2 + M_{h_2}^2 + (M_{h_1}^2 - M_{h_2}^2) \cos(2\alpha)], \quad (3.9)$$

$$a_0(w^+w^- \rightarrow w^+w^-) = \frac{\alpha_W}{16M_W^2} [M_{h_1}^2 + M_{h_2}^2 + (M_{h_1}^2 - M_{h_2}^2) \cos(2\alpha)], \quad (3.10)$$

$$a_0(z'z' \rightarrow z'z') = \frac{3}{32\pi x^2} [M_{h_1}^2 + M_{h_2}^2 - (M_{h_1}^2 - M_{h_2}^2) \cos(2\alpha)], \quad (3.11)$$

$$\begin{aligned} a_0(h_1h_1 \rightarrow h_1h_1) &= \frac{3\alpha_W}{32M_W^2} [M_{h_1}^2 + M_{h_2}^2 + (M_{h_1}^2 - M_{h_2}^2) \cos(2\alpha)] \cos^4 \alpha \\ &\quad - \frac{3\sqrt{\alpha_W}}{64M_W\sqrt{\pi x}} (M_{h_1}^2 - M_{h_2}^2) \sin^3(2\alpha) \\ &\quad + \frac{3}{16\pi x^2} [M_{h_1}^2 - (M_{h_1}^2 - M_{h_2}^2) \cos^2 \alpha] \sin^4 \alpha, \end{aligned} \quad (3.12)$$

⁷Actually, in the high energy limit, $a_0(w^+w^- \rightarrow w^+w^-)$ differs from equation (3.10) by a quantity $\simeq \alpha_W$ due to photon and Z -boson exchange in the t -channel, but since we are applying the condition in equation (3.7) and $\alpha_W \ll \frac{1}{2}$, this correction does not change the picture of our Higgs boson mass limit search.

$$\begin{aligned}
a_0(h_1 h_2 \rightarrow h_1 h_2) &= \frac{\sqrt{\alpha_W}}{256 M_W \sqrt{\pi x}} (M_{h_1}^2 - M_{h_2}^2) (\sin(2\alpha) - 3 \sin(6\alpha)) \\
&+ \frac{3}{64 \pi x^2} [M_{h_1}^2 - (M_{h_1}^2 - M_{h_2}^2) \cos^2 \alpha] \sin^2(2\alpha) \\
&+ \frac{3\alpha_W}{64 M_W^2} [M_{h_1}^2 - (M_{h_1}^2 - M_{h_2}^2) \sin^2 \alpha] \sin^2(2\alpha), \quad (3.13)
\end{aligned}$$

$$\begin{aligned}
a_0(h_2 h_2 \rightarrow h_2 h_2) &= \frac{3}{16 \pi x^2} [M_{h_1}^2 - (M_{h_1}^2 - M_{h_2}^2) \cos^2 \alpha] \cos^4 \alpha \\
&- \frac{3\sqrt{\alpha_W}}{64 M_W \sqrt{\pi x}} (M_{h_1}^2 - M_{h_2}^2) \sin^3(2\alpha) \\
&+ \frac{3\alpha_W}{16 M_W^2} [M_{h_1}^2 - (M_{h_1}^2 - M_{h_2}^2) \sin^2 \alpha] \sin^4 \alpha, \quad (3.14)
\end{aligned}$$

where

$$\alpha_W = \frac{M_W^2}{\pi v^2}. \quad (3.15)$$

We remark upon the fact that in the high energy limit, $\sqrt{s} \rightarrow \infty$, only the a_0 partial wave amplitude (i.e., the four-point function as one can conclude by direct comparison between equations (3.9)-(3.14) and equations (A.1)-(A.3) in Appendix A) does not vanish, instead it approaches a value depending only on M_{h_1} , M_{h_2} and α . Therefore, by applying the condition in equation (3.7), we can obtain several different (correlated) constraints on the Higgs masses and mixing angle, i.e., we can find the M_{h_1} - M_{h_2} - α subspace in which the perturbative unitarity of the theory is valid up to any energy scale.

The most relevant scattering channels for the unitarity analysis are pure- z and pure z' -bosons scatterings. As one can see from equations (3.9)-(3.11), the limit coming from these two channels is unaffected by the transformation $\alpha \rightarrow -\alpha$, hence it is not restrictive to consider the half domain $\alpha \in [0, \frac{\pi}{2}]$ only. Furthermore, we remind the reader that we are still not allowing the inversion of the Higgs mass eigenvalues, i.e., we still require $M_{h_1} < M_{h_2}$.

Afterwards, we analyse the space of the parameters α , M_{h_1} and M_{h_2} , once it has been specified by the unitarity condition applied to the spherical partial wave scattering amplitudes listed in the previous Section in the very high energy limit.

We want to start our analysis in the M_{h_1} - M_{h_2} subspace, hence we “slice” the 3-dimensional parameter space we are dealing with by keeping the Higgs mixing angle fixed.

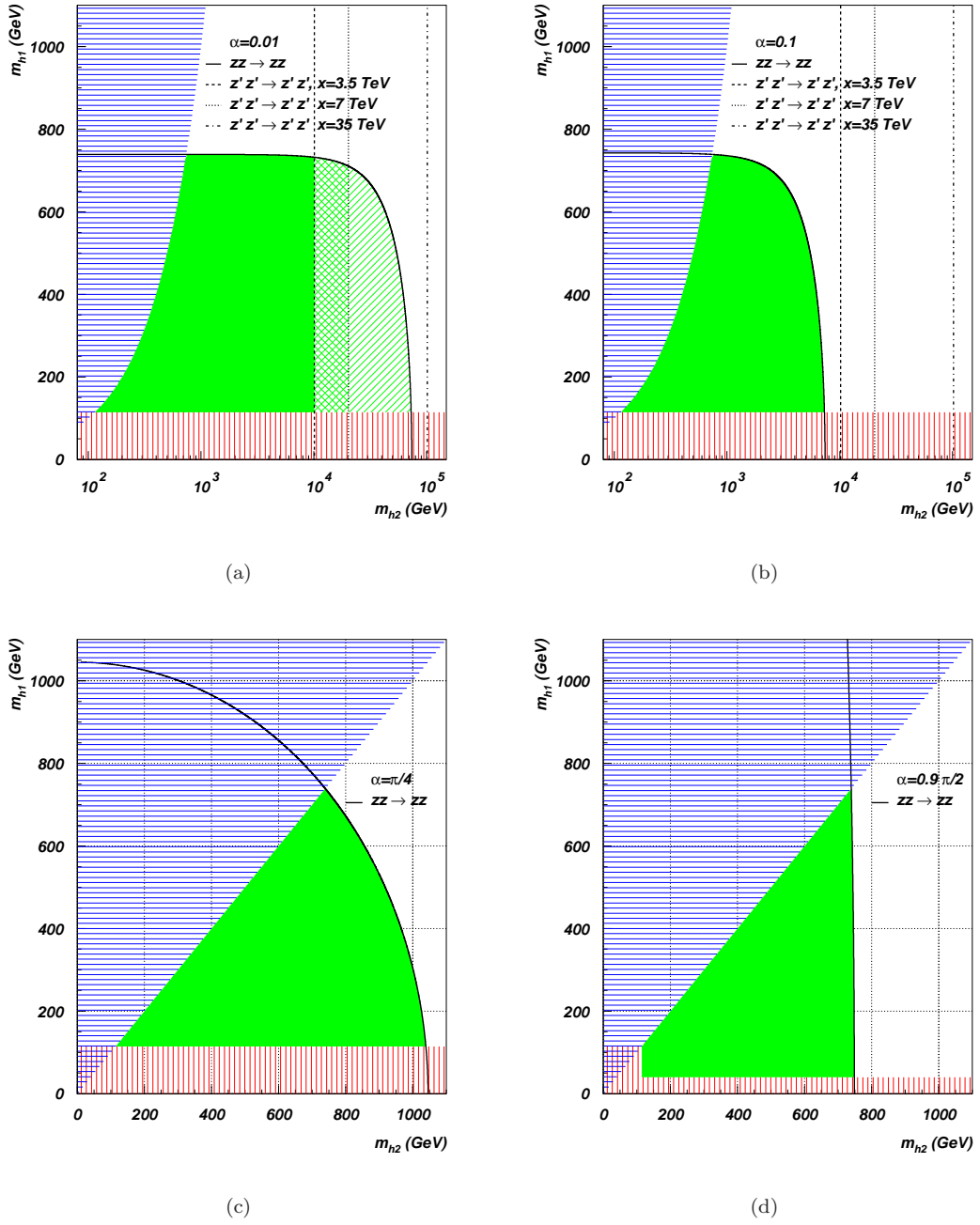


FIGURE 3.2: Higgs bosons mass limits in the $B-L$ model coming from the unitarity condition $|\text{Re}(a_0)| \leq \frac{1}{2}$ applied to the $zz \rightarrow zz$ and $z'z' \rightarrow z'z'$ scatterings for several values of x , for $\alpha = 0.01$ (3.2(a)), $\alpha = 0.1$ (3.2(b)), $\alpha = \pi/4$ (3.2(c)) and $\alpha = 0.9\pi/2$ (3.2(d)). The (blue) horizontal shadowed region corresponds to the unphysical configuration $M_{h_1} > M_{h_2}$. The (red) vertical shadowed region is excluded by the LEP experiments.

By applying the unitarity constraint to the spherical partial waves listed in the previous Section, one discovers that for a mixing angle α such that

$$\arctan\left(\frac{M_W}{x\sqrt{\pi}\alpha_W}\right) \leq \alpha \leq \frac{\pi}{2}, \quad (3.16)$$

the allowed parameter space is completely defined by the $zz \rightarrow zz$ eigenchannel.

We will call “high-mixing domain” the parameter space defined by a choice of the mixing angle in this range, while the “low-mixing domain” is the complementary one. For example, since $x \geq 3.5$ TeV following the LEP analyses (Subsection 3.1.3), if we choose x to be exactly 3.5 TeV, then we say that the high-mixing domain, in this particular case, is the one for $0.073 \leq \alpha \leq \frac{\pi}{2}$ (and, conversely, the low-mixing one is in the interval $0 \leq \alpha < 0.073$).

We can appreciate how the size of the Higgs mixing affects the limits on the Higgs masses by looking at figure 3.2, in which we plot the allowed space for the latter, limitedly to the two eigenchannels $zz \rightarrow zz$ and $z'z' \rightarrow z'z'$, for four different values of α and three of x (the latter affects only the limit coming from the $z'z' \rightarrow z'z'$ scattering).

We see that in both cases, as expected, the light Higgs mass upper bound does not exceed the *SM* one (which is $\simeq 700$ GeV, according to [65]), and it runs to the experimental lower limit from LEP (figure 3.1) as the heavy Higgs mass increases. This is because the two Higgses ‘cooperate’ in the unitarisation of the eigenchannels so that, if one Higgs mass tends to grow, the other one must become lighter and lighter in order to keep the scattering matrix elements unitarised.

While we are in the high-mixing domain, as in figure 3.2(b)-3.2(c)-3.2(d) (where $\alpha = 0.1$, $\alpha = \frac{\pi}{4}$, $\alpha = 0.9 \frac{\pi}{2}$, respectively⁸), the allowed region coming from the $zz \rightarrow zz$ scattering is completely included in the $z'z' \rightarrow z'z'$ allowed area, and the highest value allowed for the heavy Higgs mass only depends on the mixing angle via

$$\text{Max}(M_{h_2}) = 2\sqrt{\frac{2}{3}} \frac{M_W}{\sqrt{\alpha_W} \sin \alpha}. \quad (3.17)$$

When we move to figure 3.2(a) (where $\alpha = 0.01$, low-mixing domain) we are able to appreciate some interplay between the two scattering processes. In fact, in this case, while the $zz \rightarrow zz$ scattering eigenchannel allows the existence of a heavy Higgs of more than 10 TeV, the $z'z' \rightarrow z'z'$ scattering channel strongly limits the allowed mass region, with a “cut-off” on the heavy Higgs mass almost insensible to the light Higgs mass (and the value of the mixing angle, since we are in the low-mixing domain), that is

$$\text{Max}(M_{h_2}) \simeq 2\sqrt{\frac{2\pi}{3}} x, \quad (3.18)$$

⁸For the last of these values of the mixing angle, the lower limit from LEP experiments on the light Higgs boson is $M_{h_1} > 40$ GeV, while for the first it is almost equal to the *SM* lower limit ($M_{h_1} > 115$ GeV), as illustrated in figure 3.2.

which is in agreement (under different theoretical assumptions, though) with the result in [72]; from a graphical point of view, in figure 3.2(a) the (green) hollow area represents the allowed configuration space at $x = 3.5$ TeV, while at $x = 10$ TeV the allowed portion of the M_{h_1} - M_{h_2} subspace increases until the (green) double-lines shadowed region, finally the constraint relaxes to the (green) single line shadowed region when $x = 35$ TeV.

This interplay effect arising (somewhat unintuitively) for Higgs low-mixing is due to the fact that the consequent decoupling between the two Higgs states requires the light(heavy) Higgs state to independently keep the scattering matrix elements of the $z^{(\prime)}z^{(\prime)} \rightarrow z^{(\prime)}z^{(\prime)}$ process unitary, thus realising two separate constraints: the first on the light (SM -like) Higgs mass due to the $zz \rightarrow zz$ unitarisation and the second on the heavy Higgs mass due to the $z'z' \rightarrow z'z'$ unitarisation.

To summarise, given a value of the singlet Higgs VEV x (compatible with experiment), the upper bound on the light Higgs boson mass varies between the SM limit and the experimental lower limit from LEP as long as the upper bound for the heavy Higgs mass increases. Moreover, when α assumes a value included in the high-mixing domain, the strongest bound comes from the unitarisation of the z -boson scattering, whilst in the low-mixing domain the bound on the heavy Higgs mass coming from that channel relaxes and the unitarisation induced by the z' -boson scattering becomes so important to also impose a cut-off (which depends linearly on x) on the heavy Higgs mass.

This is a very important result, because it allows us to conclude that, whichever the Higgs mixing angle, both Higgs boson masses of the $B - L$ model are bounded from above. As examples of typical values for the heavy Higgs mass, in table 3.2, we show some upper bounds that universally apply (i.e., no matter what the mixing angle is) once the singlet Higgs VEV is given.

x (TeV)	Max(M_{h_2}) (TeV)
3.5	$\simeq 10$
7	$\simeq 20$
10	$\simeq 30$
20	$\simeq 60$
35	$\simeq 100$

TABLE 3.2: Universal upper bound on the heavy Higgs mass, M_{h_2} , in the $B - L$ model as a function of the singlet Higgs VEV , x .

Before we move on, it is also worth re-emphasising that, if the Higgs mixing angle is such that we are in the high-mixing case, the upper bound on the heavy Higgs boson mass coming from z -boson scattering is more stringent than the one coming from z' -boson scattering and it is totally independent from the chosen singlet Higgs VEV .

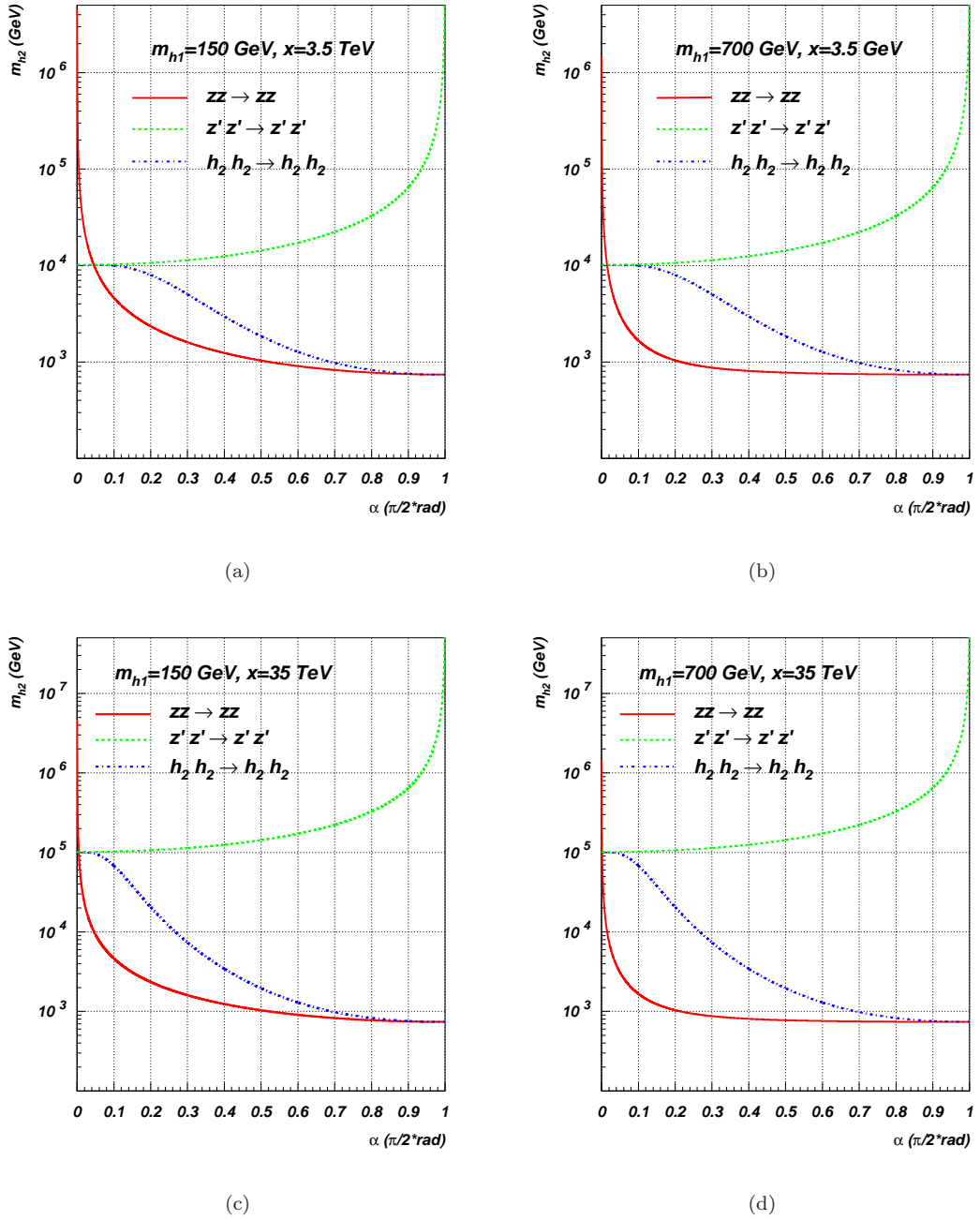


FIGURE 3.3: Heavy Higgs boson mass limits plotted against the mixing angle α in the minimal $B - L$ model. We have applied the unitarity condition $|\text{Re}(a_0)| \leq \frac{1}{2}$ on $zz \rightarrow zz$ (red straight line), $z'z' \rightarrow z'z'$ (green dashed line) and $h_2 h_2 \rightarrow h_2 h_2$ (blue dashed-dotted line) scatterings. This has been plotted for two fixed values of the light Higgs boson mass ($M_{h_1} = 150$ GeV (3.3(a), 3.3(c)) and $M_{h_1} = 700$ GeV (3.3(b), 3.3(d))) and of the singlet Higgs VEV ($x = M_{Z'}/(2g'_1) = 3.5$ TeV (3.3(a), 3.3(b)) and $x = M_{Z'}/(2g'_1) = 35$ TeV (3.3(c), 3.3(d))).

Nowadays, it is important to refer in our analysis to the possibility of a Higgs boson discovery at the Large Hadron Collider (LHC). Thus, if we suppose that a light or heavy Higgs mass M_{h_1} has been already measured by an experiment it is interesting to study the α - M_{h_2} parameter space, to see whether an hitherto unassigned Higgs state can be

consistent with a minimal $B - L$ scenario.

To this end, in figure 3.3 we fix M_{h_1} and x at two extreme configurations: we take $M_{h_1} = 150$ GeV as minimum value (conservatively, taking a figure that is allowed by the experimental lower bound established by LEP for a SM Higgs boson) and $M_{h_1} = 700$ GeV as maximum value (close to the maximum allowed by unitarity constraints, as we saw before). Then, we take $x = 3.5$ TeV as minimum value (that is, the lower limit established by LEP data for the existence of a Z' of $B - L$ origin) and $M_{h_1} = 35$ TeV as maximum value (that is, one order of magnitude bigger than the smallest VEV allowed by experiment).

Even in this case we can separate the 2-dimensional subspace in a low-mixing region and a high-mixing region, as before. We can identify the first(second) as the one in which the upper bound is established by unitarisation through the $z'(z)$ -boson scattering. The value of the mixing angle that separates the two regions in this case is given by

$$\alpha = \arccos \sqrt{\frac{(3M_{h_1}^2 - 8\pi x^2) \alpha_W}{6M_{h_1}^2 \alpha_W - 8\pi x^2 \alpha_W - 8M_W^2}}. \quad (3.19)$$

Once the light Higgs boson mass is fixed, we can see how the heavy Higgs boson mass is bounded from above through the value defined by equation (3.18) through the $z'z' \rightarrow z'z'$ channel, and this occurs in the low-mixing region. In particular, we can notice how the z' -constraining function reaches a plateau and overlaps with the $h_2h_2 \rightarrow h_2h_2$ eigenchannel bound. Moreover, if we pay attention to the high-mixing region, we see that, if M_{h_1} is fixed to some low value, then the bound on the heavy Higgs mass relaxes much more as the mixing gets smaller and smaller with respect to the the situation in which M_{h_1} is large, where the unitarisation is shared almost equally by M_{h_2} and M_{h_1} .

3.2.2 Triviality and vacuum stability bounds

It is very well known that because of quantum corrections, the parameters which appear in the $B - L$ Lagrangian (as well as in the SM Lagrangian) are energy-scale dependent (see [22] for details).

This is also true for the quartic Higgs couplings as well as the gauge couplings which will be monotonically increasing with the energy scale, and this growth leads to constraints on the parameter space.

It is important to highlight the fact that we have previously defined the minimal $B - L$ by setting $\tilde{g} = 0$ in equation (2.6). However, \tilde{g} is scale-dependent, and it increases with

the energy-scale, so it is more appropriate to say that we define the minimal $B - L$ by setting $\tilde{g} = 0$ at the EW energy-scale.

From this, it is clear that a correct estimate of the evolution of the couplings must include the \tilde{g} contribution.

Therefore, the variation of the parameters is described by the Renormalisation Group Equation (RGE), and from [22, 73] we know that the running of λ_i 's is described by:

$$\begin{aligned}\frac{d(\lambda_1)}{d(\log \Lambda)} &\simeq \frac{1}{16\pi^2} (24\lambda_1^2 + \lambda_3^2 + 12\lambda_1 y_t^2 - 9\lambda_1 g^2 - 3\lambda_1 g_1^2 - 3\lambda_1 \tilde{g}^2), \\ \frac{d(\lambda_2)}{d(\log \Lambda)} &\simeq \frac{1}{8\pi^2} (10\lambda_2^2 + \lambda_3^2 + 4\lambda_2 \text{Tr} [(y^M)^2] - 24\lambda_2 (g_1')^2), \\ \frac{d(\lambda_3)}{d(\log \Lambda)} &\simeq \frac{\lambda_3}{8\pi^2} (6\lambda_1 + 4\lambda_2 + 2\lambda_3),\end{aligned}\tag{3.20}$$

and the running of the gauge couplings is described by:

$$\begin{aligned}\frac{d(g_1)}{d(\log \Lambda)} &= \frac{1}{16\pi^2} \left[\frac{41}{6} g_1^3 \right], \\ \frac{d(g_1')}{d(\log \Lambda)} &= \frac{1}{16\pi^2} \left[12g_1'^3 + 2\frac{16}{3} g_1'^2 \tilde{g} + \frac{41}{6} g_1' \tilde{g}^2 \right], \\ \frac{d(\tilde{g})}{d(\log \Lambda)} &= \frac{1}{16\pi^2} \left[\frac{41}{6} \tilde{g} (\tilde{g}^2 + 2g_1^2) + 2\frac{16}{3} g_1' (\tilde{g}^2 + g_1^2) + 12g_1'^2 \tilde{g} \right].\end{aligned}\tag{3.21}$$

Once we know the RGE s in equations (3.20)-(3.21), we must fix the boundary conditions for the evolution of the parameters. We choose the EW gauge coupling to be set by experiment ($g_1(EW) \simeq 0,36$) as well as the “top”-Yukawa ($y_t \simeq 1$).

Regarding the neutrinos, for simplicity we consider them degenerate and we fix their masses to $M_{\nu h}^{1,2,3} = 200$ GeV (hence, $y^M \simeq m_{\nu h}/x\sqrt{2}$)⁹, since this value has been proven to be related to interesting phenomenological scenarios (see [16]).

Moreover, another boundary condition is set by the definition of the model: $\tilde{g}(EW) = 0$.

Focusing on the scalar sector, the free parameters in our study are then M_{h_1} , M_{h_2} , α and x . The general philosophy is to fix in turn some of the free parameters and scan over the other ones, individuating the allowed regions fulfilling the aforementioned set of conditions (as we previously did in Subsection 3.2.1).

⁹For simplicity we assume that y_t and y^M do not evolve, nevertheless their evolution could in principle affect quantitatively (not qualitatively) our conclusions (see [22] for further details).

We firstly define a parameter to be “perturbative” for values less than unity. This is a conservative definition, as we could relax it by an order of magnitude and still get values of the parameters for which the perturbative series will converge¹⁰.

Then, *RGE* evolution can constrain the parameter space of the scalar sector in two complementary ways: from one side, the couplings must be perturbative,

$$0 < \lambda_{1,2,3}(Q') < 1 \quad \forall Q' \leq Q, \quad (3.22)$$

and it is usually referred to as the “triviality” condition; on the other side, the vacuum of the theory must be well-defined at any scale, that is, to guarantee the validity of eqs. (2.12) and (2.13) at any scale $Q' \leq Q$:

$$0 < \lambda_{1,2}(Q') \quad \text{and} \quad 4\lambda_1(Q')\lambda_2(Q') - \lambda_3^2(Q') > 0 \quad \forall Q' \leq Q, \quad (3.23)$$

and it is usually referred to as the “vacuum stability” condition.

Given the simplicity of the scalar sector in the *SM*, the triviality and vacuum stability conditions can be studied independently and they both constrain the Higgs boson masses, providing an upper bound and a lower bound, respectively. In more complicated models than the one considered here, it might be more convenient to study the overall effect of equations (3.22)-(3.23), since there are regions of the parameter space in which the constraints are evaded simultaneously. This is the strategy we decided to follow.

Figure 3.4 shows the allowed region in the parameter space M_{h_1} - M_{h_2} for increasing values of the mixing angle α , for fixed *VEV* $x = 7.5$ TeV and heavy neutrino masses $M_{\nu_h} = 200$ GeV, corresponding to Yukawa couplings whose effect on the *RGE* running can be considered negligible.

For $\alpha = 0$, the allowed values for M_{h_1} are the *SM* ones and the extended scalar sector is completely decoupled. The allowed space is therefore the simple direct product of the two, as we can see in figure 3.4(a). When there is no mixing, the bounds that we get for the new heavy scalar are quite loose, allowing a several TeV range for M_{h_2} , still depending on the scale of validity of the theory. We observe no significant lower bounds (i.e., $M_{h_2} > 0.5$ GeV), as the right-handed Majorana neutrino Yukawa couplings are negligible.

As we increase the value for the angle, the allowed space deforms towards smaller values of M_{h_1} . If for very small scales Q of validity of the theory such masses have already been excluded by LEP, for big enough values of Q , at a small angle as $\alpha = 0.1$, the presence

¹⁰Notice that the parameters upon which the perturbative expansion is performed are usually of the form $\sqrt{\alpha} = g/\sqrt{4\pi}$, rather than being g itself.

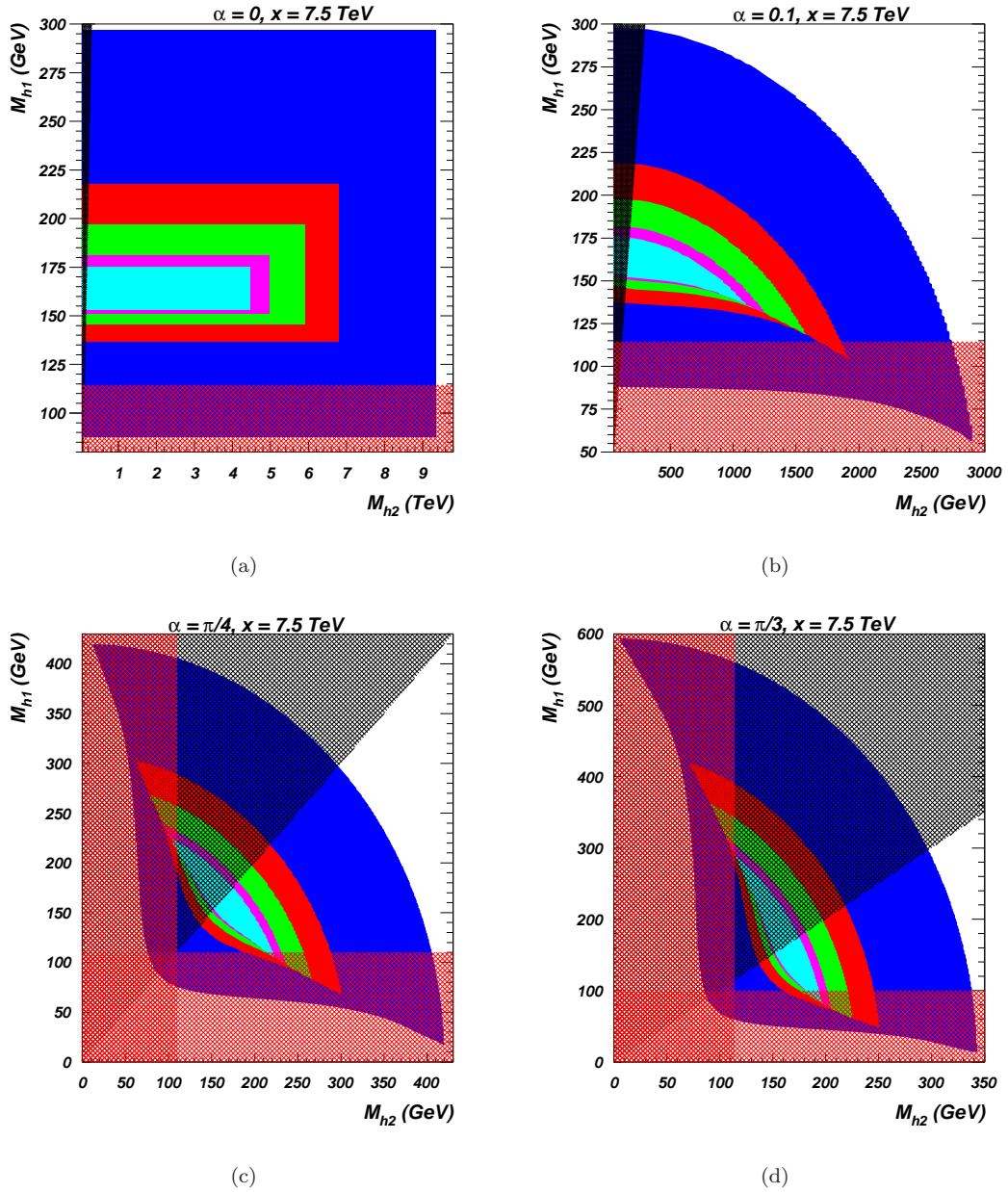


FIGURE 3.4: Allowed values in the M_{h_1} vs. M_{h_2} space in the $B-L$ model by eqs. (3.22) and (3.23), for (3.4(a)) $\alpha = 0$, (3.4(b)) $\alpha = 0.1$, (3.4(c)) $\alpha = \pi/4$ and (3.4(d)) $\alpha = \pi/3$. Colours refer to different values of Q/GeV : blue (10^3), red (10^7), green (10^{10}), purple (10^{15}) and cyan (10^{19}). The shaded black region is forbidden by our convention $M_{h_2} > M_{h_1}$, while the shaded red region refers to the values of the scalar masses forbidden by LEP. Here: $x = 7.5$ TeV, $M_{\nu_h} = 200$ GeV.

of a heavier boson allows the model to survive up to higher scales for smaller h_1 masses if compared to the SM (in which just h_1 would exist). Correspondingly, the constraints on M_{h_2} become tighter. Moving to bigger values of the angle, the mixing between h_1 and h_2 grows up to its maximum, at $\alpha = \pi/4$, where h_1 and h_2 both contain an equal amount of doublet and singlet scalars. The situation is therefore perfectly symmetric, as one can see from figure 3.4(c). Finally, in figure 3.4(d), we see that the bounds on M_{h_2}

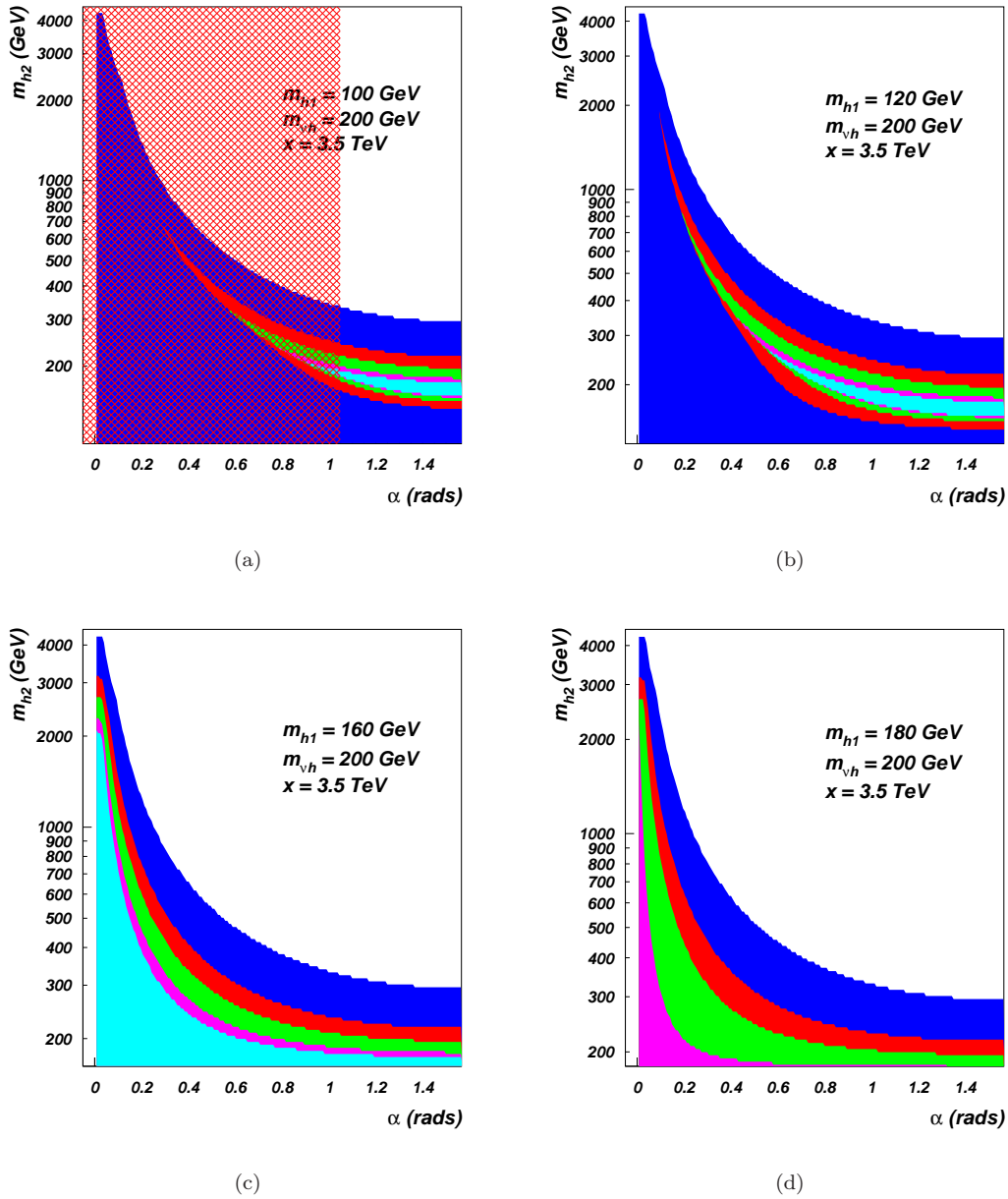


FIGURE 3.5: Allowed values in the M_{h_2} vs. α space in the $B-L$ model by eqs. (3.22) and (3.23), for (3.5(a)) $M_{h_1} = 100 \text{ GeV}$, (3.5(b)) $M_{h_1} = 120 \text{ GeV}$, (3.5(c)) $M_{h_1} = 160 \text{ GeV}$ and (3.5(d)) $M_{h_1} = 180 \text{ GeV}$. Colours refer to different values of Q/GeV : blue (10^3), red (10^7), green (10^{10}), purple (10^{15}) and cyan (10^{19}). The plots already encode our convention $M_{h_2} > M_{h_1}$ and the shaded red region refers to the values of α forbidden by LEP. Here: $x = 3.5 \text{ TeV}$, $M_{\nu_h} = 200 \text{ GeV}$.

are getting tighter, approaching the SM ones, and those for M_{h_1} are relaxing. That is, for values of the angle $\pi/4 < \alpha < \pi/2$, the situation is qualitatively not changed, but now h_2 is the SM -like Higgs boson. Visually, one can get the allowed regions at a given angle $\pi/2 - \alpha$ by simply taking the specular figure about the $M_{h_1} = M_{h_2}$ line of the plot for the given angle α .

Complementary to the previous study, we can now fix the light Higgs mass at specific,

experimentally interesting¹¹, values, i.e., $M_{h_1} = 100, 120, 160$ and 180 GeV, and show the allowed region in the M_{h_2} vs. α plane. This is done in figure 3.5.

From this figures it is clear that the transition of h_2 from the new extra scalar to the SM -like Higgs boson as we scan on the angle. As we increase M_{h_1} (up to $M_{h_1} = 160$ GeV), a bigger region in M_{h_2} is allowed for the model to be valid up to the Plank scale (the most inner regions, in cyan). Nonetheless, such a region exists also for a value of the light Higgs mass excluded by LEP for the SM , $M_{h_1} = 100$ GeV, but only for big values of the mixing angle. No new regions (with respect to the SM) in which the model can survive up to the Plank scale open for $M_{h_1} > 160$ GeV, as the allowed space deforms towards smaller values of M_{h_1} .

Combining the results of this Subsection with those on the previous one (Subsection 3.2.1), we are now in a position to investigate the production and decay phenomenology of both Higgs states of the minimal $B - L$ model at present and future accelerators. This will be realised in Chapter 4.

3.2.3 Unitarity and triviality constraints on g'_1

As well as constraining the Higgs sector parameters, the perturbative unitarity and RGE -based techniques are also helpful to constraining the g'_1 parameter.

For this reason, in this Subsection, we apply this methods to the analysis of the $B - L$ gauge coupling.

Focusing on the computational aspects of this analysis, in Subsection 3.2.1 we have already seen that perturbative unitarity violation at high energy occurs only in vector and Higgs bosons elastic scatterings, our interest is focused on the corresponding sectors.

We have also already made use of the Equivalence Theorem, which guarantees that we can replace the gauge bosons and Higgses interacting Lagrangian with the corresponding Goldstone and Higgs bosons effective theory (further details of this formalism can be found in Subsection 3.2.1 and in [21].)

Moreover, since we want to focus on g'_1 limits, we assume that the two Higgs bosons of the model have masses such that no significant contribution to the spherical partial wave amplitude will come from the scalar four-point and three-point functions. Taking Higgs boson masses smaller than the unitarity limits is therefore a way to exclude any other source of unitarity violation different from the possible largeness of the g'_1 gauge coupling.

¹¹The chosen values maximise the probability for the decays $h_1 \rightarrow b\bar{b}$, $h_1 \rightarrow \gamma\gamma$, $h_1 \rightarrow W^+W^-$ and $h_1 \rightarrow ZZ$, respectively.

In the search for the g'_1 upper limits, we assume that we can neglect all the gauge couplings in the covariant derivative but g'_1 , and the equation (2.7) becomes:

$$D_\mu \simeq \partial_\mu + 2ig'_1 Z'_\mu. \quad (3.24)$$

The inclusion of g'_1 in the covariant derivative gives rise to two new Feynman rules with respect to the set described in Appendix A, i.e.:

$$Z' h_1 z' = -2ig'_1 \sin \alpha (p_{h_1}^\mu - p_{z'}^\mu), \quad (3.25)$$

$$Z' h_2 z' = 2ig'_1 \cos \alpha (p_{h_2}^\mu - p_{z'}^\mu), \quad (3.26)$$

where all the momenta are considered incoming and z' is the would-be-Goldstone boson associated with the new Z' gauge field.

Now that the background is set, we focus on the techniques that we have used to obtain the unitarity bounds (Subsection 3.2.1) in combination with the *RGE* analysis (Subsection 3.2.2).

Firstly, we recall that equations (3.21) and the boundary conditions where $g_1(EW) \simeq 0.36$ and $\tilde{g}(EW) = 0$ fully fix the evolution of g'_1 with the scale.

In the search for the maximum $g'_1(EW)$ allowed by theoretical constraints, we previously showed that the contour condition

$$g'_1(\Lambda) \leq k, \quad (3.27)$$

also known as the triviality condition, is the assumption that enables to solve the system of equations and gives the traditional upper bound on g'_1 at the *EW* scale (where it is usually assumed either $k = 1$ or $k = \sqrt{4\pi}$, calling for a coupling that preserves the perturbative convergence of the theory).

Nevertheless, what is important to say is that this is an “ad hoc” assumption, while our aim is to extract the boundary condition by perturbative unitarity arguments, showing that under certain conditions it represents a stronger constraint on the domain of g'_1 .

While in the search for the Higgs boson mass bound it is widely accepted to assume small values for the gauge couplings and large Higgs boson masses, for our purpose we reverse such argument with the same logic: we assume that the Higgs boson masses are compatible with the unitarity limits and we study the two-to-two scattering amplitudes of the whole scalar sector, pushing the largeness of g'_1 to the perturbative limit.

By direct computation, also in this case it turns out that only $J = 0$ (corresponding to the spherical partial wave contribution) leads to some bound, and the only divergent contribution to the spherical amplitude is due to the size of the coupling g'_1 in the intermediate Z' vector boson exchange contributions. Hence, the only relevant channels are: $z'z' \rightarrow h_1h_1$, $z'z' \rightarrow h_1h_2$, $z'z' \rightarrow h_2h_2$.

As an example, we evaluate the a_0 partial wave amplitude for $z'z' \rightarrow h_1h_1$ scattering in the $s \gg M_{Z'}, M_{h_1}$ limit.

Firstly, we know that:

$$M(s, \cos \theta) \simeq (2g'_1 \sin \alpha)^2 \left(1 - \frac{4s}{s(1 - \cos \theta) + 2M_{Z'}^2 \cos \theta} \right), \quad (3.28)$$

and by mean of the integration proposed in equation (3.8), we extract the $J = 0$ partial wave:

$$a_0(z'z' \rightarrow h_1h_1) = \frac{(2g'_1)^2}{16\pi} \left(1 + 2 \log \left(\frac{M_{Z'}^2}{s} \right) \right) \sin^2 \alpha. \quad (3.29)$$

It is important to notice that the mass of the Z' acts as a natural regularisator that preserves both the amplitude and the spherical partial wave from any collinear divergence.

Considering the three aforementioned scattering channels, their spherical partial wave (in the high energy limit $s \gg M_{Z'}, M_{h_{1,2}}$) is represented by the following matrix:

$$a_0 = f(g'_1, s; x) \begin{pmatrix} 0 & \frac{1}{2} \sin^2 \alpha & -\frac{1}{\sqrt{2}} \sin \alpha \cos \alpha & \frac{1}{2} \cos^2 \alpha \\ \frac{1}{2} \sin^2 \alpha & 0 & 0 & 0 \\ -\frac{1}{\sqrt{2}} \sin \alpha \cos \alpha & 0 & 0 & 0 \\ \frac{1}{2} \cos^2 \alpha & 0 & 0 & 0 \end{pmatrix}, \quad (3.30)$$

where, according to equation (2.32),

$$f(g'_1, s; x) = \frac{(2g'_1)^2}{16\pi} \left(1 + 2 \log \left(\frac{(2g'_1 x)^2}{s} \right) \right), \quad (3.31)$$

and the elements of the matrix are related to the system consisting of $\frac{1}{\sqrt{2}}z'z'$, $\frac{1}{\sqrt{2}}h_1h_1$, h_1h_2 , $\frac{1}{\sqrt{2}}h_2h_2$.

The most stringent unitarity bound on the g'_1 coupling is derived from the requirement that the magnitude of the largest eigenvalue combined with the function $f(g'_1, s; x)$ does not exceed 1/2 (see equation (3.7)).

If we diagonalise the matrix in equation (3.30), we find that the maximum eigenvalue¹² and the corresponding eigenvector are:

$$\frac{1}{2} \Rightarrow \frac{1}{2} (z'z' + h_1h_1 \sin^2 \alpha - h_1h_2 \sin(2\alpha) + h_2h_2 \cos^2 \alpha). \quad (3.32)$$

Combining the informations of equations (3.31)-(3.32), together with the perturbative unitarity condition in equation (3.7), we obtain:

$$|\text{Re}(a_0)| = \frac{(2g'_1)^2}{32\pi} \left| 1 + 2 \log \left(\frac{(2g'_1 x)^2}{s} \right) \right| \leq \frac{1}{2}. \quad (3.33)$$

In the last equation, s represents the scale of energy squared at which the scattering is consistent with perturbative unitarity, i.e. $s = \Lambda^2$, where Λ is the evolution energy scale cut-off.

Finally, if we consider the contour of this inequality, we find exactly the boundary condition that solve the set of differential equations in (3.21), giving us the upper limit for g'_1 at the *EW* scale.

Evaluating the set of differential equations (3.21) by means of the well-known Runge-Kutta algorithm, and imposing both the unitarity and triviality condition as a two-point boundary value with a simple shooting method¹³, we have made a comparison between the two arguments for several values of x , the Higgs singlet *VEV*: the results are plotted in figure 3.6.

By direct comparison of the two formulae in equations (3.27)-(3.33), it is easy to see that the unitarity bounds become more important than the triviality bounds when

$$\frac{\Lambda}{x} \simeq \exp \left(\frac{16\pi + 4}{16} \right), \quad (3.34)$$

with the assumption that $M_{Z'} \sim x$ and $k = 1$.

From this equation, it is straightforward to see that the ‘‘ad hoc’’ choice of the triviality parameter k is crucial for establishing which limit is the most stringent one.

If we then choose a value of the *VEV* x that is compatible with the experimental limits and still in the TeV range, $x \in [3.5, 35]$ TeV (see equation (3.3)), we find that the unitarity bounds are more stringent than the triviality ones when the energy scale is

¹²It is important to mention the fact that the maximum eigenvalue does not depend on α , hence also the unitarity condition is α -independent.

¹³It consisted in varying the initial conditions in dichotomous-converging steps until the unitarity bound was fulfilled.

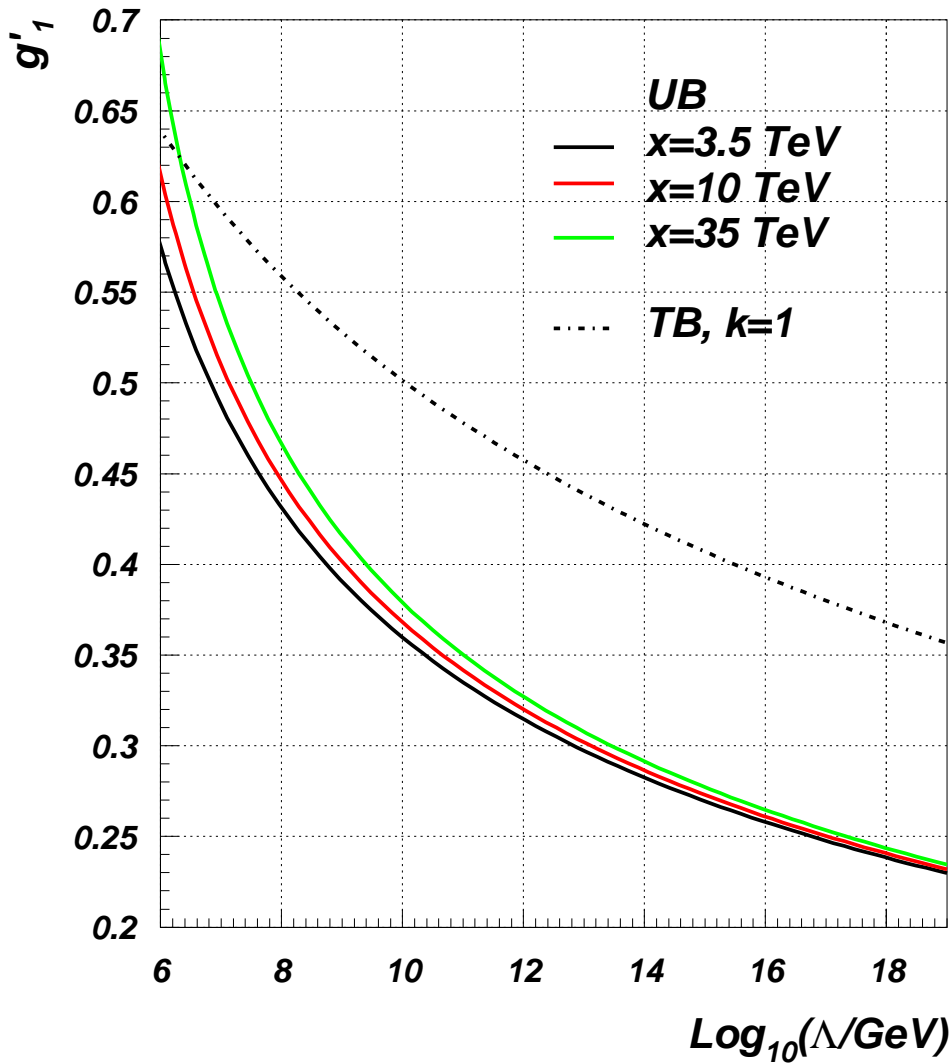


FIGURE 3.6: Triviality (assuming $k = 1$, dotted-dashed line) and unitarity (continuous and dashed lines) limits on the g'_1 coupling of the minimal $B-L$ model, plotted against the energy cut-off Λ in \log_{10} -scale, for several choices of the singlet VEV ($x = 3.5 \text{ TeV}$, black lines; $x = 10 \text{ TeV}$, red (dark grey) lines; $x = 35 \text{ TeV}$, green (light grey) lines).

greater than a critical value of $\Lambda_c \simeq 10^6 \text{ GeV}$, and this is consistent with the results in figure 3.6.

In order to summarise these results, in table (3.3) we present a comparison between the triviality and the unitarity bounds for several energy scales and $(B-L)$ -breaking VEV s.

Though these results are scale dependent, we see that, if $\Lambda \gg \Lambda_c$, our method basically refines the triviality bound by an absolute value of $\simeq 0.1$, that represents a correction of (at least) 20% on the results that have recently appeared in the literature (see [22]).

$\text{Log}_{10}(\Lambda/\text{GeV})$	7	10	15	19
TB, $g'_1(k=1)$	0.595	0.501	0.407	0.357
UB, $g'_1(x=3.5 \text{ TeV})$	0.487	0.360	0.269	0.230
UB, $g'_1(x=10 \text{ TeV})$	0.510	0.368	0.273	0.232
UB, $g'_1(x=35 \text{ TeV})$	0.542	0.379	0.277	0.234

TABLE 3.3: Triviality bounds, equation (3.27) with $k=1$, and unitarity bounds, equation (3.33) with $x=3.5, 10, 35 \text{ TeV}$, for g'_1 in the minimal $B-L$ model for several values of the energy scale Λ .

In conclusion, we have shown that, by combining perturbative unitarity and *RGE* methods, one can significantly constrain the g'_1 coupling of the minimal $B-L$ extension of the SM , by imposing limits on its upper value that are more stringent than standard triviality bounds¹⁴.

3.2.4 The fine-tuning constraint

In this Subsection we discuss the “naturalness” aspects of the model through the theoretical indication on the Higgs mass value that comes from the “fine-tuning” problem: this is introduced by the analysis of the one-loop radiative corrections to the Higgs boson mass(es).

In the SM framework, the dominant contributions to the quantum corrections are

$$M_H^2 = (M_H^0)^2 + \frac{3\Lambda^2}{8\pi^2 v^2} (M_H^2 + 2M_W^2 + M_Z^2 - 4M_t^2), \quad (3.35)$$

where Λ is the energy-scale cut-off and M_H^0 is the bare mass contained in the unrenormalised Lagrangian. This induced correction is quadratically divergent rather than the usual logarithmic ones. If Λ is large (for example of the order of the grand unification scale), a fine adjustment between the bare mass and the corrections is needed in order to have a physical Higgs boson with a mass in the range of EW symmetry breaking scale: this is the “naturalness” problem of the SM .

However, following the Veltman conjecture (see [74]), if the following relation holds:

$$M_H^2 \simeq 4M_t^2 - 2M_W^2 - M_Z^2, \quad (3.36)$$

not only the fine-tuning problem is smoothed, but we could have an indirect indication of the SM Higgs mass ($\sim 320 \text{ GeV}$).

¹⁴Moreover, as unitarity is more constraining than triviality, the stability of the perturbative solution obtained through the former is already guaranteed by the latter.

We apply this argument to the $B - L$ model: firstly, we have two Higgs bosons and two related expressions for the mass radiative corrections:

$$\begin{aligned}
& \Delta M_{h_1}^2 = \\
& = \frac{\Lambda^2}{64M_{Z'}^2\pi^2v^2} (3M_{h_1}^2 (3M_{Z'}^2 + 8(g'_1)^2v^2) + M_{h_2}^2 (3M_{Z'}^2 + 8(g'_1)^2v^2)) \\
& - 12 (4M_t^2M_{Z'}^2 + 16c_a^4(g'_1)^2M_{\nu h}^2v^2 - M_{Z'}^2 (2M_W^2 + M_Z^2 + 4v^2 ((g'_1)^2 - 2c_a^2s_a^2(y^\nu)^2))) \\
& + 4 (M_{h_1}^2 (3M_{Z'}^2 - 8(g'_1)^2v^2) + 3 (16c_a^4(g'_1)^2M_{\nu h}^2v^2 \\
& + M_{Z'}^2 (-4M_t^2 + 2M_W^2 + M_Z^2 - 4v^2 ((g'_1)^2 + 2c_a^2s_a^2(y^\nu)^2)))) \cos(2\alpha) \\
& - 12(g'_1)M_{Z'}v (M_{h_1}^2 - M_{h_2}^2 + 16\sqrt{2}c_a^3M_{\nu h}s_av(y^\nu)) \sin(2\alpha) \\
& + (M_{h_1}^2 - M_{h_2}^2) ((3M_{Z'}^2 + 8(g'_1)^2v^2) \cos(4\alpha) + 2(g'_1)M_{Z'}v \sin(4\alpha)), \tag{3.37}
\end{aligned}$$

and

$$\begin{aligned}
& \Delta M_{h_2}^2 = \\
& = \frac{\Lambda^2}{64M_{Z'}^2\pi^2v^2} (M_{h_1}^2 (3M_{Z'}^2 + 8(g'_1)^2v^2) + 3 (M_{h_2}^2 (3M_{Z'}^2 + 8(g'_1)^2v^2)) \\
& + 4 (-16c_a^4(g'_1)^2M_{\nu h}^2v^2 + M_{Z'}^2 (-4M_t^2 + 2M_W^2 + M_Z^2 + 4v^2 ((g'_1)^2 - 2c_a^2s_a^2(y^\nu)^2)))) \\
& - 4 (M_{h_2}^2 (3M_{Z'}^2 - 8(g'_1)^2v^2) + 3 (16c_a^4(g'_1)^2M_{\nu h}^2v^2 \\
& + M_{Z'}^2 (-4M_t^2 + 2M_W^2 + M_Z^2 - 4v^2 ((g'_1)^2 + 2c_a^2s_a^2(y^\nu)^2)))) \cos(2\alpha) \\
& + 12(g'_1)M_{Z'}v (-M_{h_1}^2 + M_{h_2}^2 + 16\sqrt{2}c_a^3M_{\nu h}s_av(y^\nu)) \sin(2\alpha) \\
& - (M_{h_1}^2 - M_{h_2}^2) ((3M_{Z'}^2 + 8(g'_1)^2v^2) \cos(4\alpha) + 2(g'_1)M_{Z'}v \sin(4\alpha)), \tag{3.38}
\end{aligned}$$

where we have chosen the neutrinos being degenerate ($M_{\nu h}^{1,2,3} \sim M_{\nu h}$, $y_{1,2,3}^\nu \sim y^\nu$) and their mixing angles being averaged ($s_{a1,a2,a3} \sim s_a$).

By mean of the Veltman conjecture, we set the radiative one-loop corrections to be small (~ 0), obtaining a set of two equations in two variables, M_{h_1} and M_{h_2} , and the solution is:

$$\begin{aligned}
& M_{h_1}^2 \simeq \\
& \simeq (3 ((g'_1)M_{Z'}v (12c_a^4M_{\nu h}^2 - 8M_t^2 + 4M_W^2 + 2M_Z^2 - 3M_{Z'}^2 - 16c_a^2s_a^2v^2(y^\nu)^2) \\
& + (g'_1)M_{Z'}v (-12c_a^4M_{\nu h}^2 - 8M_t^2 + 4M_W^2 + 2M_Z^2 + 3M_{Z'}^2 - 16c_a^2s_a^2v^2(y^\nu)^2) \cos(2\alpha) \\
& + 8c_a^4(g'_1)^2M_{\nu h}^2v^2 \sin(2\alpha) + M_{Z'}^2 (-4M_t^2 + 2M_W^2 + M_Z^2 - 2(g'_1)^2v^2) \sin(2\alpha) \\
& - 8c_a^2M_{Z'}^2s_a^2v^2(y^\nu)^2 \sin(2\alpha) - 4\sqrt{2}c_a^3M_{\nu h}s_av(y^\nu) (2 \cos(\alpha) \sec(2\alpha) \sin(\alpha) \times \\
& \times (8(g'_1)^2v^2 \cos^2(\alpha) + 3M_{Z'}^2 \sin^2(\alpha)) + 3(g'_1)M_{Z'}v \sin(2\alpha) \tan(2\alpha))) \div \\
& \div (-12(g'_1)M_{Z'}v \cos(2\alpha) + (-3M_{Z'}^2 + 4(g'_1)^2v^2) \sin(2\alpha)), \tag{3.39}
\end{aligned}$$

and

$$\begin{aligned}
M_{h_2}^2 &\simeq \\
&\simeq (3((g'_1)M_{Z'}v(-12c_a^4M_{\nu h}^2 + 8M_t^2 - 4M_W^2 - 2M_Z^2 + 3M_{Z'}^2 + 16c_a^2s_a^2v^2(y^\nu)^2) \\
&+ (g'_1)M_{Z'}v(-12c_a^4M_{\nu h}^2 - 8M_t^2 + 4M_W^2 + 2M_Z^2 + 3M_{Z'}^2 - 16c_a^2s_a^2v^2(y^\nu)^2)\cos(2\alpha) \\
&+ 8c_a^4(g'_1)^2M_{\nu h}^2v^2\sin(2\alpha) + M_{Z'}^2(-4M_t^2 + 2M_W^2 + M_Z^2 - 2(g'_1)^2v^2)\sin(2\alpha) \\
&- 8c_a^2M_{Z'}^2s_a^2v^2(y^\nu)^2\sin(2\alpha) + 4\sqrt{2}c_a^3M_{\nu h}s_av(y^\nu)(2\cos(\alpha)\sec(2\alpha)\sin(\alpha)\times \\
&\times (3M_{Z'}^2\cos^2(\alpha) + 8(g'_1)^2v^2\sin^2(\alpha)) - 3(g'_1)M_{Z'}v\sin(2\alpha)\tan(2\alpha))) \div \\
&\div (-12(g'_1)M_{Z'}v\cos(2\alpha) + (-3M_{Z'}^2 + 4(g'_1)^2v^2)\sin(2\alpha)). \tag{3.40}
\end{aligned}$$

Indeed, it is important to say that the Veltman conjecture is only indicative of the one-loop behaviour¹⁵, and evaluating the stability of the Veltman solution at two-loops is not among the purposes of this work. However, it is interesting to notice that in the decoupled scenario $\alpha = 0$, the solution is:

$$M_{h_1}^2 \simeq 4M_t^2 - 2M_W^2 - M_Z^2 + 8c_a^2s_a^2v^2(y^\nu)^2, \tag{3.41}$$

$$M_{h_2}^2 \simeq 6c_a^4M_{\nu h}^2 - \frac{3M_{Z'}^2}{2}. \tag{3.42}$$

We find the *SM*-like solution plus a non-significative contribution from heavy neutrinos (equation (3.41)), while the second solution is totally ruled by the interplay between the heavy neutrinos and Z' boson mass (equation (3.42)).

Again, too many free-parameters are floating around, hence we can only give an illustrative example of a choice of parameters related to a reasonable amount of fine-tuning.

The role of heavy neutrinos in the first equation is absolutely negligible, so as in the *SM* case $M_{h_1} \simeq 320$ GeV represents a good choice for the light Higgs; assuming a relatively heavy right-handed neutrinos (~ 400 GeV) and a relatively light Z' boson (~ 700 GeV), the Veltman conjecture implies that a theory with a heavy Higgs boson with mass of ~ 470 GeV is the most “natural”.

¹⁵Moreover, since too many free parameters enter in the game, no significative study could be performed in the $B - L$ context.

Chapter 4

Higgs phenomenology at colliders

This Chapter is devoted to the presentation of the results of our phenomenological investigation of the $B - L$ Higgs sector.

Firstly, after a summary of our choice of parameters and computational details, we present the total decay width and the branching ratios (BRs) of the Higgs bosons, in order to set the background.

Then, we focus on the LHC experimental scenario, with emphasis on the possible peculiar signatures of the model.

Finally, we will present a set of possible signature cross sections that could represent a relevant test for the SM break-down at future LCs.

4.1 Parameter space and implementation of the model in CalcHEP

As spelled out in the previous Chapter, the independent physical parameters of the Higgs sector of the scenario considered here are:

- M_{h_1} , M_{h_2} and α , the Higgs boson masses and mixing angle. We investigate this parameter space spanning over continuous intervals in the case of the first two quantities while adopting discrete values for the third one (taking into account all the experimental and theoretical constraints presented in Chapter 3).

In order to explore efficiently the expanse of parameter space pertaining to the minimal $B - L$ model, we introduce two extreme conditions, which makes the model intuitive,

though at the end it should be borne in mind that intermediate solutions are phenomenologically favoured. The two conditions are obtained by setting:

1. $\alpha = 0$, this is the “decoupling limit”, with h_1 behaving like the *SM* Higgs.
2. $\alpha = \frac{\pi}{2}$, this is the so-called “inversion limit”, with h_2 behaving like the *SM* Higgs (though recall that this possibility is phenomenologically not viable, see Subsection 3.1.1).

Furthermore, concerning the strength of Higgs interactions, some of the salient phenomenological behaviours can be summarised as follows¹:

- *SM*-like interactions scale with $\cos \alpha(\sin \alpha)$ for $h_1(h_2)$;
- those involving the other new $B - L$ fields, like Z' and heavy neutrinos, scale with the complementary angle, i.e., with $\sin \alpha(\cos \alpha)$ for $h_1(h_2)$;
- triple (and quadruple) Higgs couplings are possible and can induce resonant behaviours, so that, e.g., the $h_2 \rightarrow h_1 h_1$ decay can become dominant if $M_{h_2} \sim 2M_{h_1}$.

Other than M_{h_1} , M_{h_2} and α , additional parameters are the following:

- g'_1 , the new $U(1)_{B-L}$ gauge coupling. We will adopt discrete perturbative values for this quantity, taking into account the analysis of the allowed parameter space of Subsection 3.2.3.
- $M_{Z'}$, the new gauge boson mass, considering the experimental limits presented in Subsection 3.1.3 (equation (3.3)).
- M_{ν_h} , the heavy neutrino masses, are assumed to be degenerate, diagonal and relatively light.
- M_{ν_l} , the *SM* (or light) neutrino masses; they have been conservatively taken to be $M_{\nu_l} = 10^{-2}$ eV in order to fulfil the cosmological bound requirement presented in Subsection 3.1.3; they are assumed to be degenerate and diagonal.

The numerical analysis was performed with CalcHEP [37] with the model introduced through LanHEP [34]. Moreover, the implementation has been enriched with the following plug-ins:

¹All of these results are a consequence of the way the particles couple, i.e., the Feynman rules in Appendix B.

- the one-loop vertices $g - g - h_1(h_2)^2$, $\gamma - \gamma - h_1(h_2)$ and $\gamma - Z(Z') - h_1(h_2)$ via W gauge bosons and heavy quarks (top, bottom and charm) have been implemented, adapting the formulae in [77].
- Running masses for top, bottom and charm quarks, evaluated at the Higgs boson mass: $Q = M_{h_1}(M_{h_2})$, depending on which scalar boson is involved in the interaction.
- Running of the QCD coupling constant, at two-loops with 5 active flavours.

4.2 Branching ratios and total widths

Moving to the Higgs boson decays, figure 4.1 shows the BRs for both the Higgs bosons, h_1 and h_2 , respectively. Only the two-body decay channels are shown here.

Regarding the light Higgs boson, the only new particle it can decay into is the heavy neutrino (we consider a very light Z' boson unlikely), if the channel is kinematically open. In figure 4.1(a) we show this case, for a small heavy neutrino mass, i.e., $M_{\nu_h} = 50$ GeV, and we see that the relative BR of this channel can be rather important, as the decay into b -quark pairs or into W boson pairs, in the range of masses $110 \text{ GeV} \leq M_{h_1} \leq 150 \text{ GeV}$. Such range happens to be critical in the SM since here the SM Higgs boson passes from decaying dominantly into b -quark pairs to a region in masses in which the decay into W boson pairs is the prevailing one. These two decay channels have completely different signatures and discovery methods. The fact that the signal of the Higgs boson decaying into b -quark pairs is many orders of magnitude below the natural QCD background spoils its sensitivity. In the case of the $B - L$ model, the decay into heavy neutrino pairs is therefore phenomenologically very important, besides being an interesting feature of the $B - L$ model if $M_{\nu_h} < M_W$, as it allows multilepton signatures of the light Higgs boson. Among them, there is the decay of the Higgs boson into 3ℓ , $2j$ and \cancel{E}_T (that we have already studied for the Z' case in reference [16]), into 4ℓ and \cancel{E}_T (as, again, already studied for the Z' case in reference [18]) or into 4ℓ and $2j$ (as already studied, when $\ell = \mu$, in the 4th family extension of the SM [78]). All these peculiar signatures allow the Higgs boson signal to be studied in channels much cleaner than the decay into b -quark pairs.

In the case of the heavy Higgs boson, further decay channels are possible in the $B - L$ model, if kinematically open. The heavy Higgs boson can decay in pairs of the light Higgs boson ($h_2 \rightarrow h_1 h_1$) or even in triplets ($h_2 \rightarrow h_1 h_1 h_1$), in pairs of heavy neutrinos

²Finally, the NLO QCD k -factor for the gluon fusion process [2, 75, 76] has been used. Regarding the other processes, we decided to not implement their k -factors since they are much smaller in comparison.

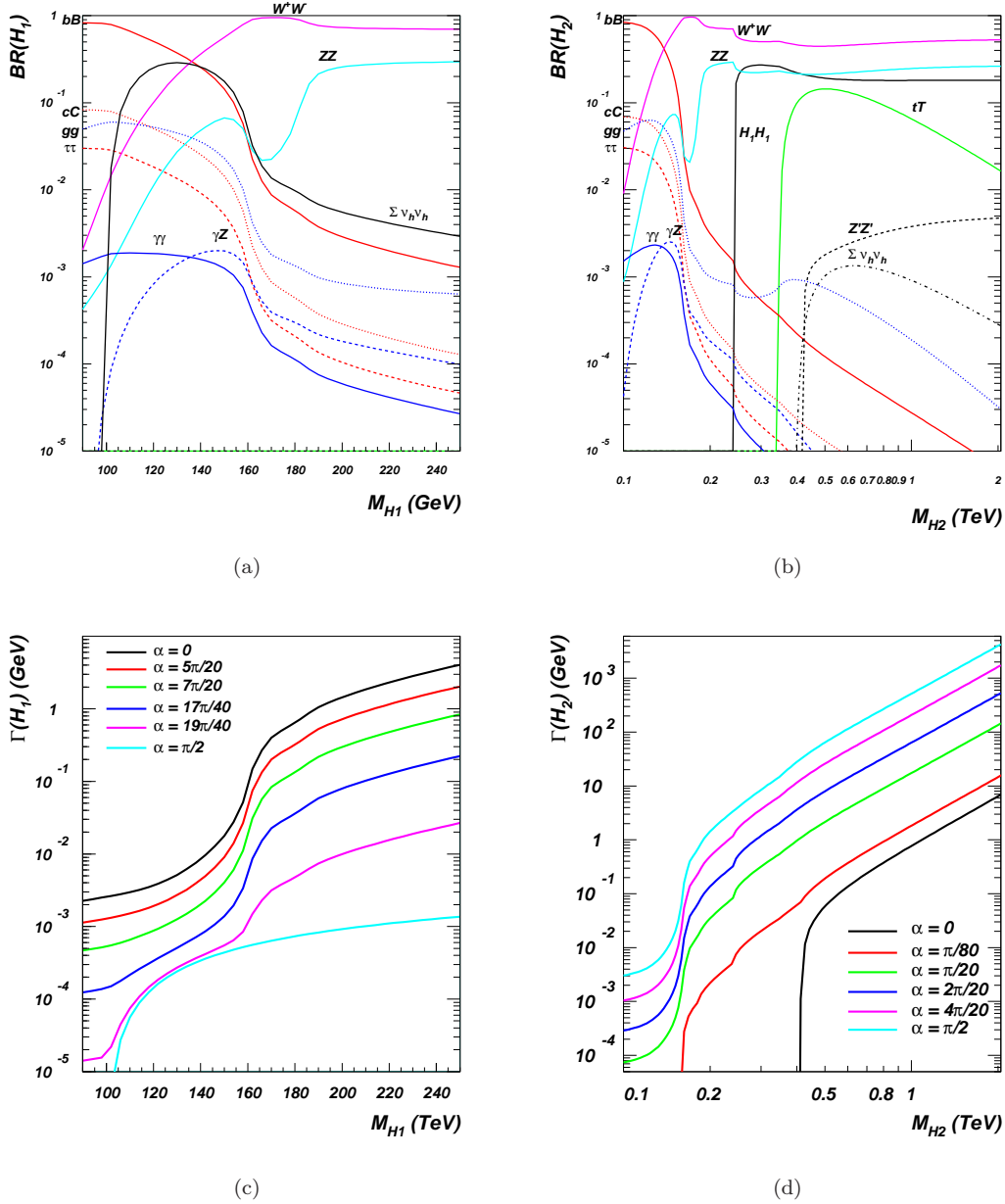


FIGURE 4.1: (4.1(a)) Branching ratios for h_1 for $\alpha = 2\pi/5$ and $M_{\nu_h} = 50$ GeV and (4.1(c)) h_1 total width for a choice of mixing angles and (4.1(b)) BRs for h_2 for $\alpha = 3\pi/20$ and $M_{h_1} = 120$ GeV, $M_{Z'} = 210$ GeV and $M_{\nu_h} = 200$ GeV and (4.1(d)) h_2 total width for a choice of mixing angles.

and Z' bosons. Even for a small value of the angle, figure 4.1(b) shows that the decay of a heavy Higgs boson into pairs of the light one can be quite sizeable, at the level of the decay into SM Z bosons for $M_{h_1} = 120$ GeV. It is important to note that this channel does not have a simple dependence on the mixing angle α , as we can see in figure 4.2.

The BRs of the heavy Higgs boson decaying into Z' boson pairs and heavy neutrino pairs decrease as the mixing angle increases, getting to their maxima (comparable to the W and Z ones) for a vanishing α , for which the production cross section is however

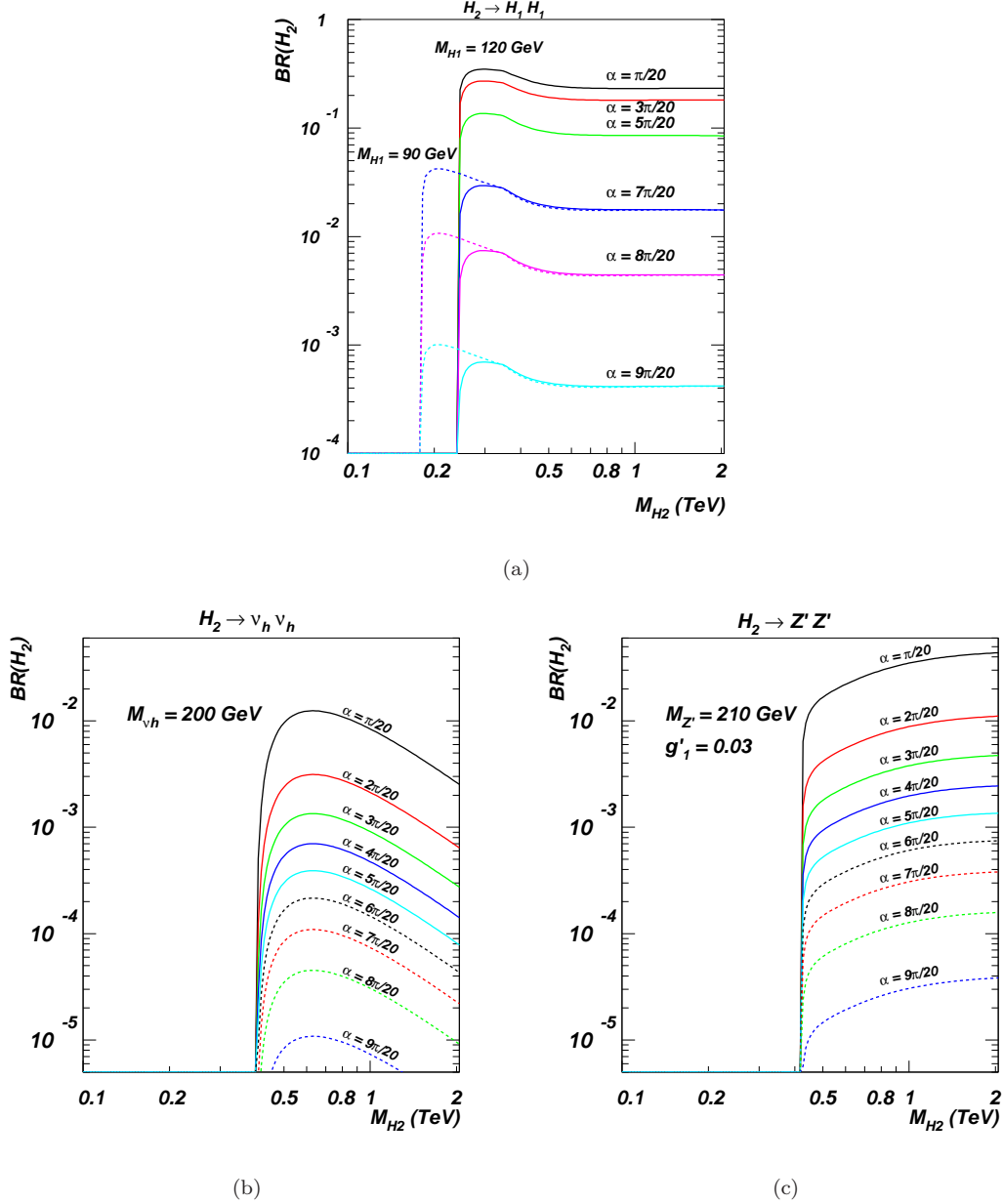


FIGURE 4.2: Dependence on the mixing angle α of (4.2(a)) $BR(h_2 \rightarrow h_1 h_1)$, of (4.2(b)) $BR(h_2 \rightarrow \nu_h \nu_h)$ and of (4.2(c)) $BR(h_2 \rightarrow Z' Z')$.

negligible. As usual, and also clear from figure 4.1(b), the decay of the heavy Higgs boson into Z' gauge bosons is always bigger than the decay into pairs of fermions (the heavy neutrinos, even when summed over the generations as plotted), when they have comparable masses (here, $M_{Z'} = 210$ GeV and $M_{\nu_h} = 200$ GeV).

The other standard decays of both the light and the heavy Higgs bosons are not modified substantially in the $B - L$ model (i.e., the decay of the Higgs boson to W boson pair is always dominant when kinematically open, while before that the decay into b -quarks is the prevailing one; further, radiative decays, such as Higgs boson decays into pairs of

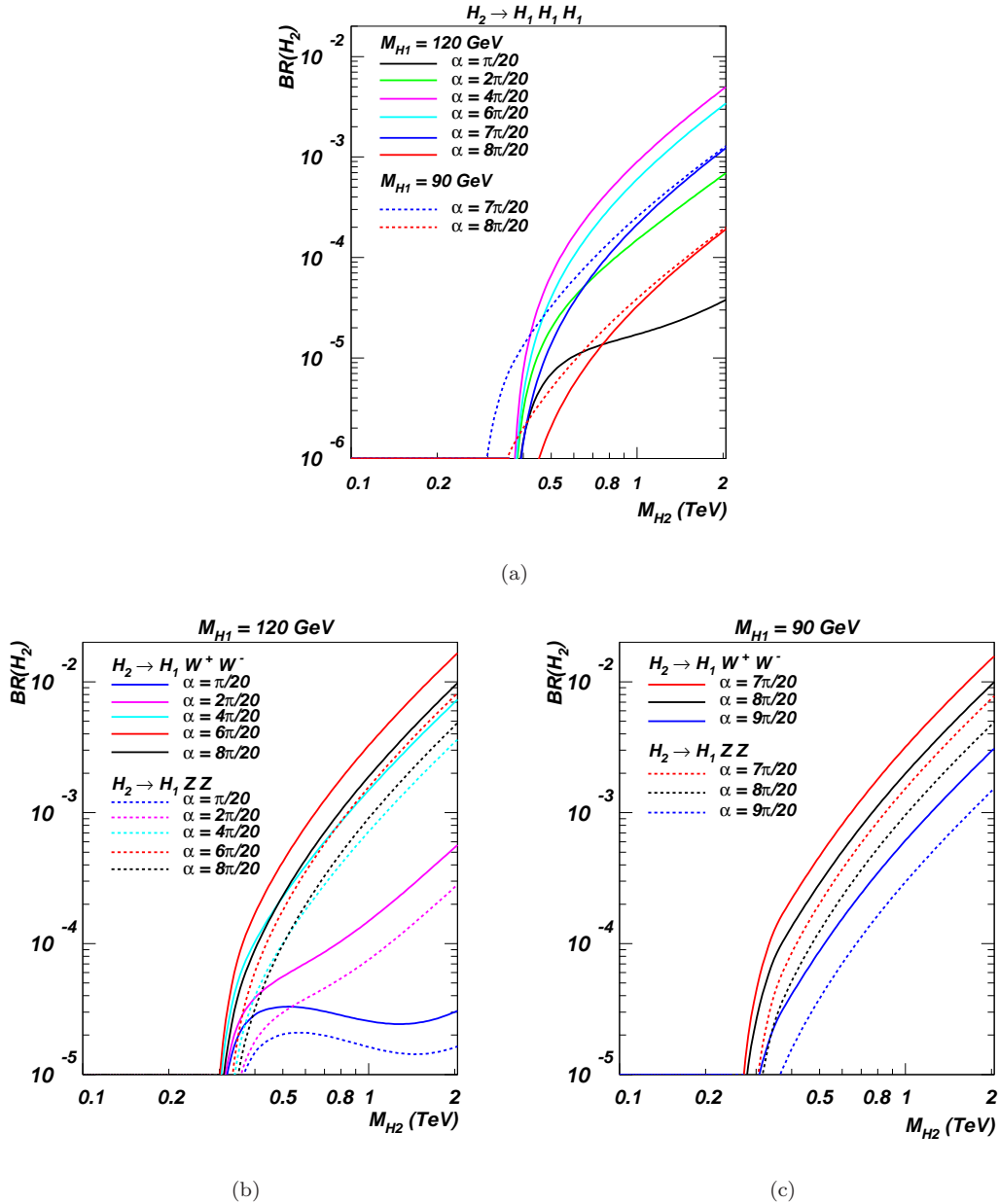


FIGURE 4.3: Dependence on the mixing angle α of the three body decays (4.3(a)) $BR(h_2 \rightarrow h_1 h_1 h_1)$ and (4.3(b)) $BR(h_2 \rightarrow h_1 V V)$ ($V = W^\pm, Z$) for $M_{h_1} = 120$ GeV and (4.3(c)) for $M_{h_1} = 90$ GeV, respectively.

photons, peak at around 120 GeV). Only when other new channels open, the standard decay channels alter accordingly. This rather common picture could be altered when the mixing angle α approaches $\pi/2$, but such situation is phenomenologically not viable (see Subsection 3.1.1).

Figures 4.1(c) and 4.1(d) show the total widths for h_1 and h_2 , respectively. In the first case, few thresholds are clearly recognisable, as the heavy neutrino one at 100 GeV (for angles very close to $\pi/2$ only), the WW and the ZZ ones. Over the mass range considered ($90 \text{ GeV} < M_{h_1} < 250 \text{ GeV}$), the particle's width is very small until the WW

threshold, less than 1 – 10 MeV, rising steeply to few GeV for higher h_1 masses and small angles (i.e., for a SM -like light Higgs boson). As we increase the mixing angle, the couplings of the light Higgs boson to SM particles is reduced, and so its total width.

On the contrary, as we increase α , the h_2 total width increases, as clear from figure 4.1(d). Also in this case, few thresholds are recognisable, as the usual WW and ZZ gauge boson ones, the light Higgs boson one (at 240 GeV) and the $t\bar{t}$ one (only for big angles, i.e., when h_2 is the SM -like Higgs boson). When the mixing angle is small, the h_2 total width stays below 1 GeV all the way up to $M_{h_2} \sim 300 \div 500$ GeV, rising as the mass increases towards values for which $\Gamma_{h_2} \sim M_{h_2} \sim 1$ TeV and h_2 loses the meaning of resonant state, only for angles very close to $\pi/2$. Instead, if the angle is small, i.e., less than $\pi/10$, the ratio of width over mass is less than 10% and the heavy Higgs boson is a well defined particle. In the decoupling regime, i.e., when $\alpha = 0$, the only particles h_2 couples to are the Z' and the heavy neutrinos. The width is therefore dominated by the decay into them and is tiny, as clear from figure 4.1(d).

As already mentioned, figure 4.2 shows the dependence on the mixing angle α of the BRs of h_2 into pairs of non- SM particles. In particular, we consider the decays $h_2 \rightarrow h_1 h_1$ (for two different h_1 masses, $M_{h_1} = 90$ GeV and $M_{h_1} = 120$ GeV, only for the allowed values of α), $h_2 \rightarrow \nu_h \nu_h$ and $h_2 \rightarrow Z' Z'$ (not influenced by M_{h_1}). As discussed in Section 4.1, the interaction of the heavy Higgs boson with SM (or non- SM) particles has an overall $\sin \alpha$ (or $\cos \alpha$, respectively) dependence. Nonetheless, the BRs in figure 4.2 depend also on the total width, that for $\alpha > \pi/4$ is dominated by the $h_2 \rightarrow W^+ W^-$ decay. Hence, when the angle assumes big values, the angle dependence of the h_2 BRs into heavy neutrino pairs and into Z' boson pairs follow a simple $\cot \alpha$ behaviour. Regarding $h_2 \rightarrow h_1 h_1$, its BR is complicated by the fact that the contribution of this process to the total width is not negligible when the mixing angle is small, i.e., $\alpha < \pi/4$. In general, this channel vanishes when $\alpha \rightarrow 0$, and it gets to its maximum, of around 10% \div 30% of the total width, as α takes a non-trivial value, being almost constant with the angle if it is small enough.

The heavy Higgs boson can be relatively massive and the tree-level three-body decays are interesting decay modes too. Besides being clear BSM signatures, they are crucial to test the theory beyond the observation of any scalar particle: its self-interactions and the quartic interactions with the vector bosons could be tested directly in these decay modes. In the $B - L$ model with no $Z - Z'$ mixing, the quartic interactions that can be tested as h_2 decay modes, if the respective channels are kinematically open, are: $h_2 \rightarrow h_1 h_1 h_1$, $h_2 \rightarrow h_1 W^+ W^-$ and $h_2 \rightarrow h_1 Z Z$, as shown in figure 4.3, again for $M_{h_1} = 90$ GeV and 120 GeV. Although possible, $h_2 \rightarrow h_1 Z' Z'$ is negligible always, even if the Z' boson is

light enough to allow the decay. For $M_{Z'} = 210$ GeV, $BR(h_2 \rightarrow h_1 Z' Z') \lesssim 10^{-5}$ for $M_{h_2} < 2$ TeV.

The BRs for both the $h_2 \rightarrow h_1 h_1 h_1$ and the $h_2 \rightarrow h_1 V V$ ($V = W^\pm, Z$) channels are maximised roughly when the mixing between the two scalars is maximum, i.e., when $\alpha \sim \pi/4$, regardless of M_{h_1} . The former channel, that is interesting because would produce three light Higgs bosons simultaneously, can contribute at most at 10^{-3} of the total width for h_2 , as we are neglecting values of M_{h_2} and α for which $\Gamma_{h_2} \sim M_{h_2}$ (see figure 4.1(d)). For instance, for $M_{h_2} = 800$ GeV, α needs to be less the $\pi/5$ to have a reasonable small width-over-mass ratio ($\sim 10\%$), and $BR(h_2 \rightarrow h_1 h_1 h_1) \leq 0.6 \cdot 10^{-3}$. The situation is similar for the latter channel, involving pairs of SM gauge bosons. Again, for $M_{h_2} = 800$ GeV and $\alpha = \pi/5$, $BR(h_2 \rightarrow h_1 W^+ W^-) = 2BR(h_2 \rightarrow h_1 Z Z) = 10^{-3}$ for $m_{h_1} = 120$ GeV. For $M_{h_1} = 90$ GeV, the mixing angle is constrained to be bigger than $7\pi/20$. For these values and the same M_{h_2} as before, such BRs are doubled.

4.3 Higgs bosons at the LHC

In this Section we present our results for the analysis of the scalar sector of the minimal $B - L$ model at the LHC. We shortly introduce the scheduled working plan at the accelerator. Then, we present cross sections at $\sqrt{s} = 7$ and 14 TeV for the two Higgs bosons. Finally, we will focus on some phenomenologically viable signatures and their event rates.

4.3.1 The LHC scheduled working plan

The scheduled programme is planned to be the following:

- 7 TeV is total energy of the two proton beams (energy in the hadronic center of mass) and 1 fb^{-1} is the scheduled integrated luminosity ($\sim 1 - 2$ operational years in the time scale). This is what we label as “early discovery scenario”.
- 14 TeV is total energy of the two proton beams (energy in the hadronic center of mass) and 300 fb^{-1} is the scheduled integrated luminosity (~ 10 operational years in the time scale). This is what we label as “full luminosity scenario”.

4.3.2 Standard production mechanisms

In figure 4.4 we present the cross sections for the most relevant production mechanisms, i.e., the usual SM processes such as gluon-gluon fusion, vector-boson fusion, $t\bar{t}$ associated

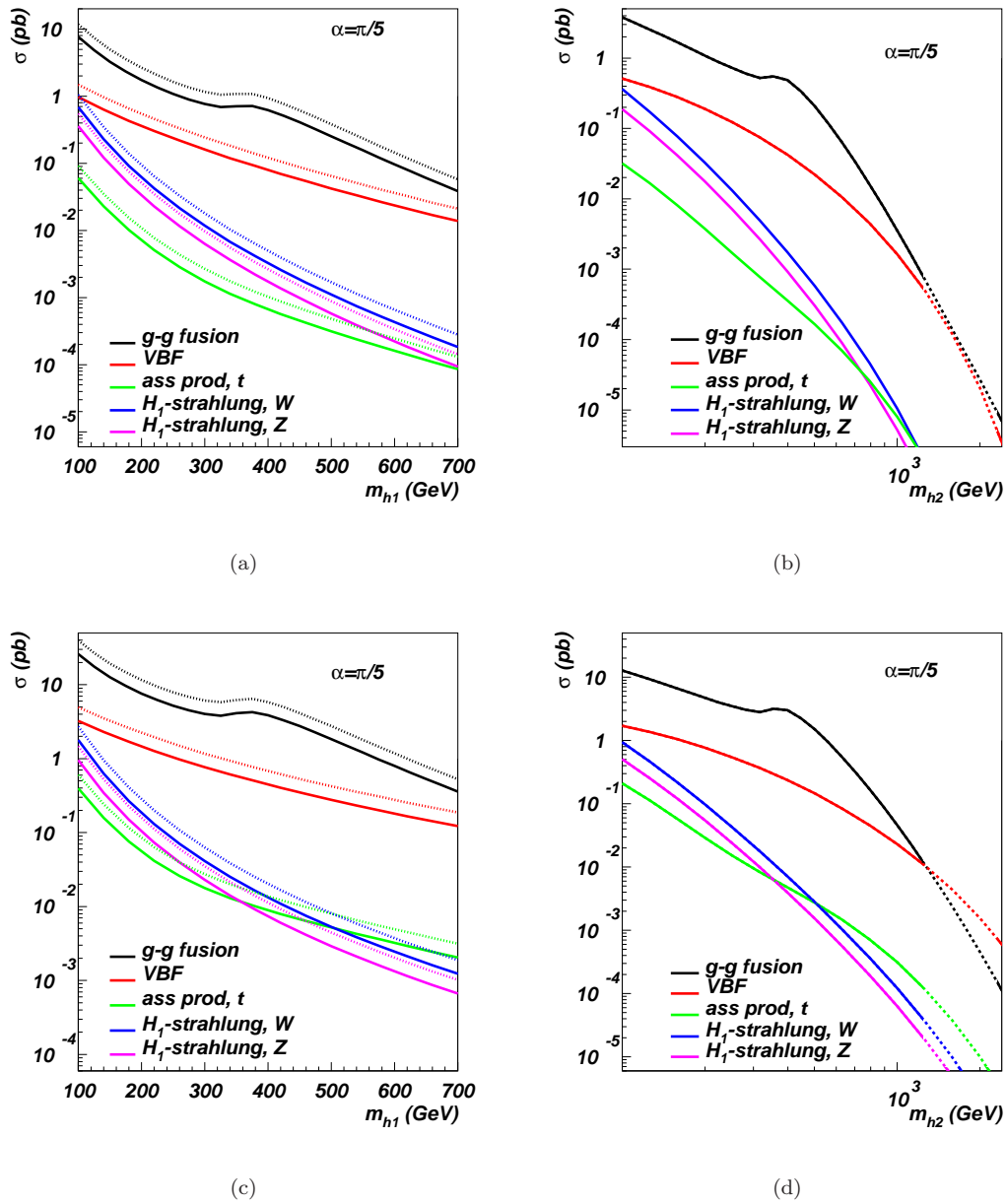


FIGURE 4.4: Cross sections in the minimal $B - L$ model for h_1 at the LHC (4.4(a)) at $\sqrt{s} = 7$ TeV and (4.4(c)) at $\sqrt{s} = 14$ TeV, and for h_2 (4.4(b)) at $\sqrt{s} = 7$ TeV and (4.4(d)) at $\sqrt{s} = 14$ TeV. Dashed lines in figures 4.4(a) and 4.4(c) refer to $\alpha = 0$. The dotted part of the lines in figure 4.4(d) refer to h_2 masses excluded by Unitarity (see Subsection 3.2.1).

production and Higgs-strahlung. For reference, we show in dashed lines the SM case (only for h_1), that corresponds to $\alpha = 0$.

Comparing figure 4.4(c) to figure 4.4(a), there is a factor two enhancement passing from a $\sqrt{s} = 7$ TeV to a $\sqrt{s} = 14$ TeV centre-of-mass energy at the LHC.

The cross sections are a smooth function of the mixing angle α , so, as expected, every sub-channel has a cross section that scales with $\cos \alpha$ ($\sin \alpha$), respectively for h_1 (h_2).

As a general rule, the cross section for h_1 at an angle α is equal to that one of h_2 for $\pi/2 - \alpha$. In particular, the maximum cross section for h_2 (i.e., when $\alpha = \pi/2$) coincides with the cross section of h_1 for $\alpha = 0$.

We notice that these results are in agreement with the ones that have been discussed in [79–81] in the context of a scalar singlet extension of the SM , having the latter the same Higgs production phenomenology. Moreover, as already showed in [79], also in the minimal $B - L$ context an high value of the mixing angle could lead to important consequences for Higgs boson discovery at the LHC: h_1 production could be suppressed below an observable rate at $\sqrt{s} = 7$ TeV and heavy Higgs boson production could be favoured, with peculiar final states clearly beyond the SM , or even hide the production of both (if no more than 1 fb^{-1} of data is accumulated). Instead, at $\sqrt{s} = 14$ TeV we expect that at least one Higgs boson will be observed, either the light one or the heavy one, or indeed both, thus shedding light on the scalar sector of the $B - L$ extension of the SM discussed in this work.

4.3.3 Non-standard production mechanisms

All the new particles in the $B - L$ model interact with the scalar sector, so novel production mechanisms can arise considering the exchange of new intermediate particles. Among the new production mechanisms, the associated production of the scalar boson with the Z' boson and the decay of a heavy neutrino into a Higgs boson are certainly the most promising, depending on the specific masses. Notice also that the viable parameter space, that allows a Higgs mass lighter than the SM limit of 114.4 GeV for certain $\alpha - M_{h_2}$ configurations, enables us to investigate also production mechanisms that in the SM are subleading, as the associated production of a Higgs boson with a photon. Figures 4.5 and 4.6 show the cross sections for the non-standard production mechanisms, for $\sqrt{s} = 14$ TeV and several values of α .

Figures 4.5(a) and 4.5(b) show the cross sections for associated production with the Z' boson of h_1 and of h_2 , respectively, for several combinations of Z' boson masses and g'_1 couplings. The process is

$$q \bar{q} \rightarrow Z'^* \rightarrow Z' h_{1(2)}, \quad (4.1)$$

and it is dominated by the Z' boson's production cross sections (see [16, 20]). Although never dominant (always below 1 fb), this channel is the only viable mechanism to produce h_2 in the decoupling scenario, i.e., $\alpha = 0$.

In figure 4.6 we plot the cross sections of the other non-standard production mechanisms against the light Higgs mass, for several choices of parameters (as explicitly indicated in

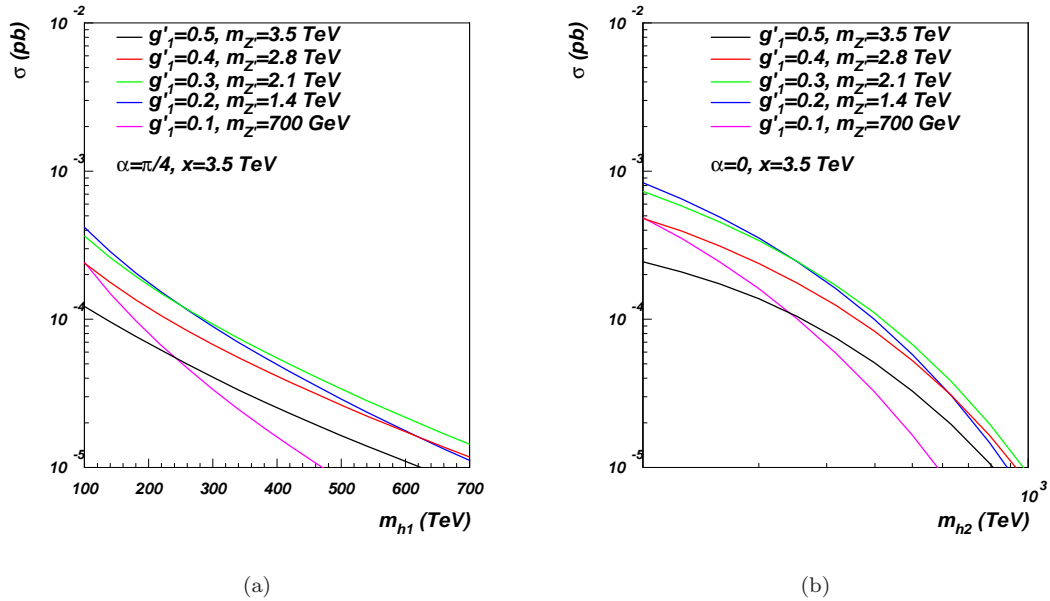


FIGURE 4.5: Cross sections in the minimal $B - L$ model for the associated production with the Z'_{B-L} boson (4.5(a)) of h_1 at $\alpha = \pi/4$ and (4.5(b)) of h_2 at $\alpha = 0$.

the labels). We superimposed the red-shadowed region in order to avoid any value of the cross section that has been already excluded by LEP constraints (see Subsection 3.1.2), mapping each value of the boundary cross section as produced by the related maximum value allowed for the light Higgs mass M_{h_1} (at fixed mixing angle α).

First of the showed plots is the decay of a heavy neutrino into a Higgs boson. The whole process chain is

$$q \bar{q} \rightarrow Z' \rightarrow \nu_h \nu_h \rightarrow \nu_h \nu_l h_{1(2)}, \quad (4.2)$$

and it requires to pair produce heavy neutrinos, again via the Z' boson (see [16, 82] for a detailed analysis of the $pp \rightarrow Z' \rightarrow \nu_h \nu_h$ process and other aspects of Z' and heavy neutrinos phenomenology in the minimal $B - L$ model). Although rather involved, this mechanism has the advantage that the whole decay chain can be of on-shell particles, besides the peculiar final state of a Higgs boson and a heavy neutrino. For a choice of the parameters that roughly maximises this mechanism ($M_{Z'} = 900 \text{ GeV}$, $g'_1 = 0.13$ and $M_{\nu_h} = 200 \text{ GeV}$), figure 4.6(a) shows that the cross sections for the production of the light Higgs boson (when only one generation of heavy neutrinos is considered) are above 10 fb for $M_{h_1} < 130 \text{ GeV}$ (and small values of α), dropping steeply when the light Higgs boson mass approaches the kinematical limit for the heavy neutrino to decay into it. Assuming the transformation $\alpha \rightarrow \pi/2 - \alpha$, the production of the heavy Higgs boson via this mechanism shows analogous features.

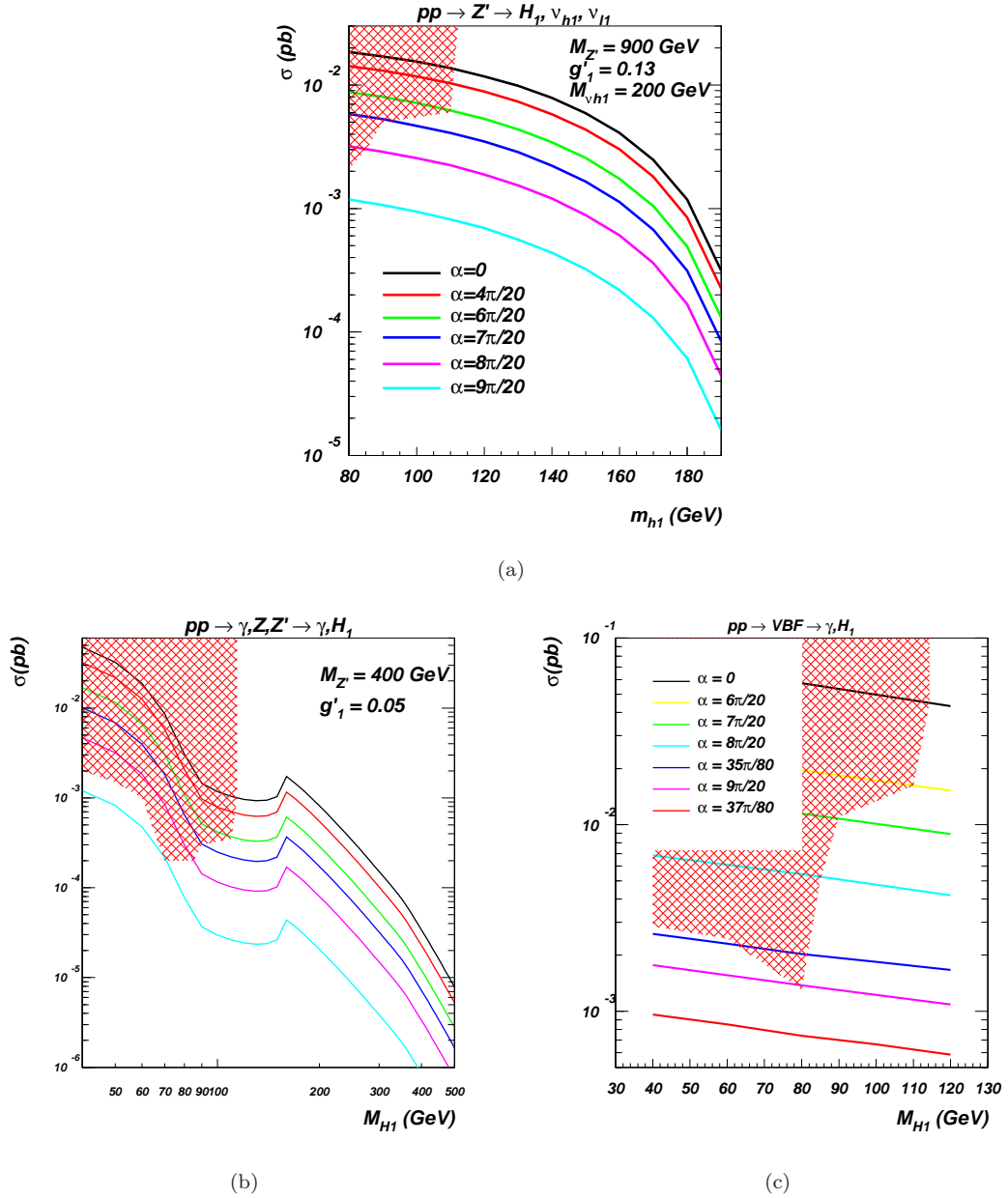


FIGURE 4.6: Cross sections in the minimal $B - L$ model for the associated production of h_1 (4.6(a)) with one heavy and one light neutrinos, (4.6(b)) with a photon via γ, Z and Z' bosons exchange (same legend as in figure 4.6(a) applies here) and (4.6(c)) in the vector-boson fusion, all at $\sqrt{s} = 14$ TeV. The red shading is the region excluded by LEP constraints (Subsection 3.1.2).

Next, figures 4.6(b) and 4.6(c) shows the associated production of the light Higgs boson with a photon. The processes are, respectively,

$$q\bar{q} \rightarrow \gamma/Z/Z' \rightarrow \gamma h_1 \quad (4.3)$$

via the SM neutral gauge bosons (γ and Z) and the new Z' boson, and

$$q q' \rightarrow \gamma h_1 q'' q''' , \quad (4.4)$$

through vector-boson fusion (only W and Z bosons).

In the first instance, we notice that the Z' sub-channel in equation (4.3) is always negligible, as there is no $Z' - W - W$ interaction and the $V - h - \gamma$ effective vertex is only via a t -quark loop (an order of magnitude lower than the $V - h - \gamma$ effective vertex via a W boson loop) [77]. What is relevant in these two channels is that the light Higgs boson mass can be considerably smaller than the LEP limit (they are valid for the SM , or equivalently when $\alpha = 0$ in the $B - L$ model). Hence, the phase space factor can enhance the mechanism of equation (4.3) for small masses, up to the level of 1 fb for $M_{h_1} < 60$ GeV (and suitable values of the mixing angle α , depending on the experimental and theoretical limits, see [21, 22] for a complete treatment of the allowed parameter space of the Higgs sector of the minimal $B - L$ model). Moreover, it has recently been observed that the associated production with a photon in the vector-boson fusion channel could be useful for low Higgs boson masses in order to trigger events in which the Higgs boson decays into b -quark pairs [83]. Complementary to that, the process in equation (4.3) can also be of similar interest, with the advantage that the photon will always be back-to-back relative to the b -quark pair. For comparison, figures 4.6(b) and 4.6(c) show the cross section for these processes³. Certainly, for a h_1 boson heavier than the SM limit, vector-boson fusion is the dominant process for associated production of h_1 with a photon, and this is also true for $M_{h_1} > 60$ GeV. However, for light Higgs boson masses lower than 60 GeV, the two mechanisms of eqs. (4.3) and (4.4) become equally competitive, up to the level of $\mathcal{O}(1)$ fb each, for suitable values of the mixing angle α .

4.3.4 Event Rates

In this Section we combine the results from the Higgs boson cross sections and those from the BR analysis in order to perform a detailed study of typical event rates for some Higgs signatures which are specific to the $B - L$ model.

Before all else, we remind the terminology previously introduced in Subsection 4.3.1: we will generally refer to an “early discovery scenario” by considering an energy in the hadronic CM of $\sqrt{s} = 7$ TeV and an integrated luminosity of $\int L = 1 \text{ fb}^{-1}$ (according to the official schedule, this is what is expected to be collected after the first couple of

³In order to produce figure 4.6(c), we included the following cuts: $P_t^{\gamma, \text{jet}} > 15$ GeV, $|\eta^\gamma| < 3$ and $|\eta^{\text{jet}}| < 5.5$, where “jet” refers to the actual final state, though we use partons here to emulate it [83].

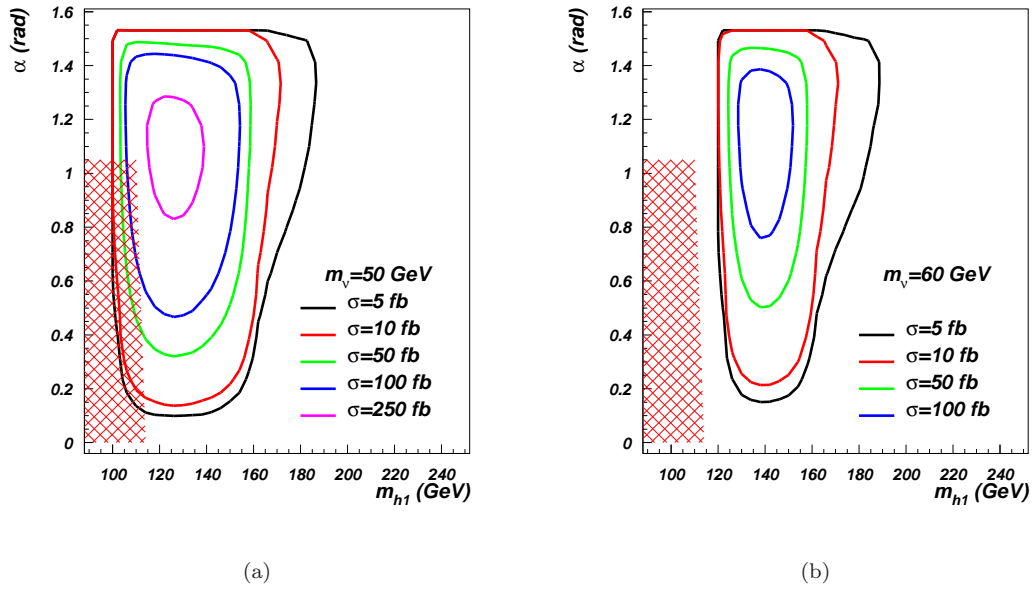


FIGURE 4.7: Cross section times BR contour plot for the $B-L$ process $pp \rightarrow h_1 \rightarrow \nu_h \nu_h$ at the LHC with $\sqrt{s} = 7$ TeV, plotted against M_{h_1} - α , with $M_{\nu_h} = 50$ GeV (4.7(a)) and $M_{\nu_h} = 60$ GeV (4.7(b)). Several values of cross section times BR have been considered: $\sigma = 5$ fb (black line), $\sigma = 10$ fb (red line), $\sigma = 50$ fb (green line), $\sigma = 100$ fb (blue line) and $\sigma = 250$ fb (violet line). The red-shadowed region is excluded by the LEP experiments.

years of LHC running) and to a “full luminosity scenario” by considering an energy in the hadronic CM of $\sqrt{s} = 14$ TeV and an integrated luminosity of $\int L = 300 \text{ fb}^{-1}$ (according to the official schedule, this is what is expected to be realistically collected at the higher energy stage).

As we shall see by combining the production cross sections and the decay BR s already presented, the two different scenarios open different possibilities for the detection of peculiar signatures of the model: in the “early discovery scenario” there is a clear possibility to detect a light Higgs state yielding heavy neutrino pairs while the “full luminosity scenario” affords the possibility of numerous discovery mechanisms (in addition to the previous mechanism, for the heavy Higgs state one also has decays of the latter into Z' boson and light Higgs boson pairs).

Firstly, we focus on the “early discovery scenario”: in this experimental configuration, the most important $B-L$ distinctive process is represented by heavy neutrino pair production via a light Higgs boson, through the channel $pp \rightarrow h_1 \rightarrow \nu_h \nu_h$. In figure 4.7 we show the explicit results for the $pp \rightarrow h_1 \rightarrow \nu_h \nu_h$ process at the LHC with $\sqrt{s} = 7$ TeV, for $M_{\nu_h} = 50$ GeV (figure 4.7(a)) and $M_{\nu_h} = 60$ GeV (figure 4.7(b)), obtained by combining the light Higgs boson production cross section via gluon-gluon fusion only (since it represents the main contribution) and the BR of the light Higgs boson to heavy neutrino pairs. The obtained rate is projected in the M_{h_1} - α plane and several values

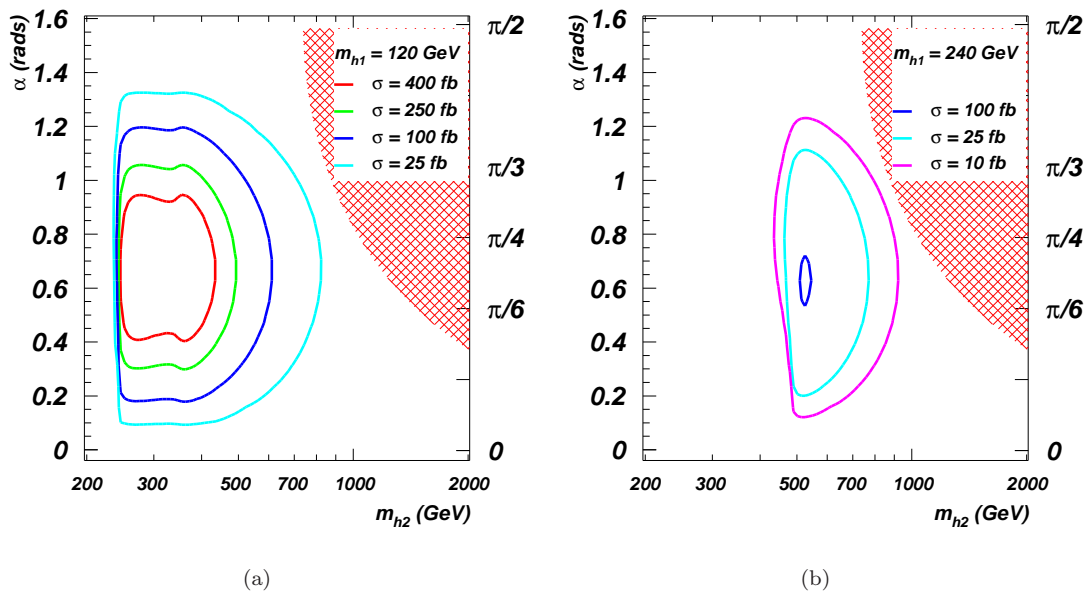


FIGURE 4.8: Cross section times BR contour plot for the $B-L$ process $pp \rightarrow h_2 \rightarrow h_1 h_1$ at the LHC with $\sqrt{s} = 14$ TeV, plotted against $M_{h_2}-\alpha$, with $M_{h_1} = 120$ GeV (4.8(a)) and $M_{h_1} = 240$ GeV (4.8(b)). Several values of cross section times BR have been considered: $\sigma = 10$ fb (violet line), $\sigma = 25$ fb (light-blue line), $\sigma = 100$ fb (blue line), $\sigma = 250$ fb (green line) and $\sigma = 400$ fb (red line). The red-shadowed region is excluded by unitarity constraints.

of the cross section times BR have been considered: $\sigma = 5, 10, 50, 100$ and 250 fb. The red-shadowed region takes into account the exclusion limits established by the LEP experiments.

Even considering a low-luminosity scenario (i.e., $\int L \simeq 1 \text{ fb}^{-1}$), there is a noticeable allowed parameter space for which the rate of such events is considerably large: in the case of $M_{\nu_h} = 50$ GeV, when the integrated luminosity reaches $\int L = 1 \text{ fb}^{-1}$, we estimated a collection of ~ 10 heavy neutrino pairs from the light Higgs boson production and decay for $100 \text{ GeV} < M_{h_1} < 170 \text{ GeV}$ and $0.05\pi < \alpha < 0.48\pi$, that scales up to $\sim 10^2$ events for $110 \text{ GeV} < M_{h_1} < 155 \text{ GeV}$ and $0.16\pi < \alpha < 0.46\pi$. In the case of $M_{\nu_h} = 60$ GeV, we estimated a collection of ~ 10 heavy neutrino pairs from Higgs production for $120 \text{ GeV} < M_{h_1} < 170 \text{ GeV}$ and $0.06\pi < \alpha < 0.48\pi$, that scales up to $\sim 10^2$ events for $125 \text{ GeV} < M_{h_1} < 150 \text{ GeV}$ and $0.25\pi < \alpha < 0.44\pi$.

If we consider instead the “full luminosity scenario”, there are several important distinctive signatures: $pp \rightarrow h_2 \rightarrow h_1 h_1$, $pp \rightarrow h_2 \rightarrow Z' Z'$ and $pp \rightarrow h_2 \rightarrow \nu_h \nu_h$. In figure 4.8 we show the results for light Higgs boson pair production from heavy Higgs boson decays at the LHC with $\sqrt{s} = 14$ TeV for $M_{h_1} = 120$ GeV (figure 4.8(a)) and $M_{h_1} = 240$ GeV (figure 4.8(b)). Again, if we project the rates on the bi-dimensional $M_{h_2}-\alpha$ plane, we can select the contours that relate the cross section times BR to some peculiar values.

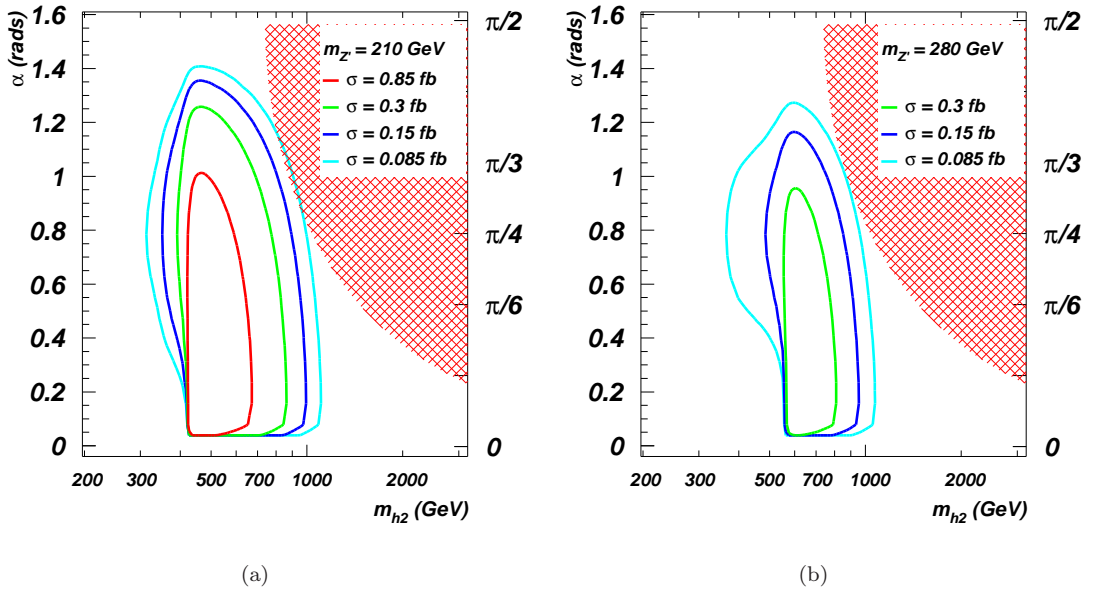


FIGURE 4.9: Cross section times BR contour plot for the $B-L$ process $pp \rightarrow h_2 \rightarrow Z'Z'$ at the LHC with $\sqrt{s} = 14$ TeV, plotted against $M_{h_2}-\alpha$, with $M_{Z'} = 210$ GeV (4.9(a)) and $M_{Z'} = 280$ GeV (4.9(b)). Several values of cross section times BR have been considered: $\sigma = 0.085$ fb (light-blue line), $\sigma = 0.15$ fb (blue line), $\sigma = 0.3$ fb (green line), $\sigma = 0.85$ fb (red line). The red-shadowed region is excluded by unitarity constraints.

Considering an integrated luminosity of 300 fb^{-1} , we can relate $\sigma = 25(250)$ fb to $7500(75000)$ events, hence for both choices of the light Higgs mass the $\alpha-M_{h_2}$ parameter space offers an abundant portion in which the event rate is noticeable for light Higgs boson pair production from heavy Higgs boson decays: when $M_{h_1} = 120$ GeV the process is accessible almost over the entire parameter space, with a cross section peak of 400 fb in the $240 \text{ GeV} < M_{h_2} < 400 \text{ GeV}$ and $0.13\pi < \alpha < 0.30\pi$ intervals, while in the $M_{h_1} = 240$ GeV case the significant parameter space is still large, even if slightly decreased, with a cross section peak of 25 fb in the $480 \text{ GeV} < M_{h_2} < 800 \text{ GeV}$ and $0.06\pi < \alpha < 0.32\pi$ region.

In figure 4.9 we show the results for Z' boson pair production from heavy Higgs boson decays at the LHC with $\sqrt{s} = 14$ TeV for $M_{Z'} = 210$ GeV (figure 4.9(a)) and $M_{Z'} = 280$ GeV (figure 4.9(b)). Again, if we project the rates on the bi-dimensional $M_{h_2}-\alpha$ plane, we can select the contours that relate the cross section times BR to some peculiar values. Here, we have that $\sigma = 0.085(0.85)$ fb corresponds to $25(250)$ events, hence for both choices of Z' mass the $\alpha-M_{h_2}$ parameter space offers an abundant portion in which the event rate could be interesting for Z' boson pair production from heavy Higgs boson decays: for $M_{Z'} = 210$ GeV the process has a peak of 0.85 fb in the $420 \text{ GeV} < M_{h_2} < 650$ GeV and $0.03\pi < \alpha < 0.25\pi$ region, while if $M_{Z'} = 280$ GeV a noticeable parameter space is still potentially accessible with a rate peak of 0.3 fb (100 events) in the $560 \text{ GeV} < M_{h_2} < 800 \text{ GeV}$ and $0.03\pi < \alpha < 0.19\pi$ region.

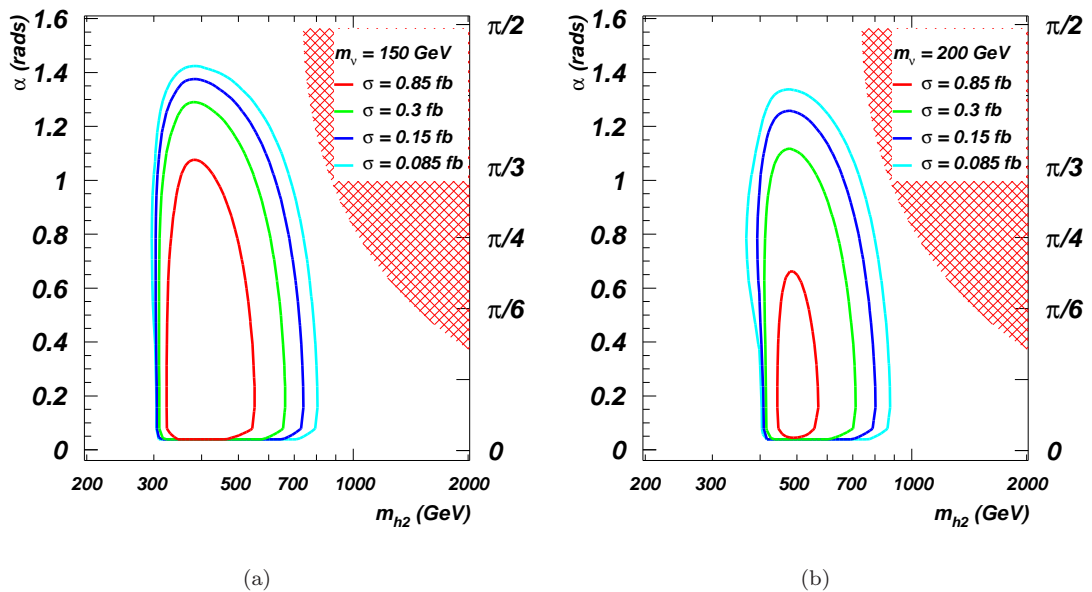


FIGURE 4.10: Cross section times BR contour plot for the $B - L$ process $pp \rightarrow h_2 \rightarrow \nu_h \nu_h$ at the LHC with $\sqrt{s} = 14$ TeV, plotted against M_{h_2} - α , with $M_{\nu_h} = 150$ GeV (4.10(a)) and $M_{\nu_h} = 200$ GeV (4.10(b)). Several values of cross section times BR have been considered: $\sigma = 0.085$ fb (light-blue line), $\sigma = 0.15$ fb (blue line), $\sigma = 0.3$ fb (green line), $\sigma = 0.85$ fb (red line). The red-shadowed region is excluded by unitarity constraints.

In analogy with the previous two cases, in figure 4.10 we show the results for heavy neutrino pair production at the LHC with $\sqrt{s} = 14$ TeV plus $M_{\nu_h} = 150$ GeV (figure 4.10(a)) and $M_{\nu_h} = 200$ GeV (figure 4.10(b)). The usual contour plot displays a sizable event rate in the α - M_{h_2} parameter space for both choices of the ν_h mass. For example, when $M_{\nu_h} = 150$ GeV we find a cross section times BR peak of 0.85 fb (~ 250 events) in the $320 \text{ GeV} < M_{h_2} < 520 \text{ GeV}$ and $0.03\pi < \alpha < 0.33\pi$ region, while if $M_{\nu_h} = 200$ GeV we find a peak of 0.85 fb in the $450 \text{ GeV} < M_{h_2} < 550 \text{ GeV}$ and $0.03\pi < \alpha < 0.21\pi$ region.

4.4 Higgs bosons at future linear colliders

In this Section we present our results for the scalar sector of the minimal $B - L$ model at future LCs. In general, sub-TeV CM energies ($\sqrt{s} = 500$ GeV) will be suitable for an ILC, multi-TeV CM energies ($\sqrt{s} = 3$ TeV) will be appropriate for CLIC while the case 1 TeV may be appropriate to both. In all cases, results will be shown for some discrete choices of the Z' mass and of the scalar mixing angle α . Their values have been chosen in each plot to highlight some relevant phenomenological aspects. Concerning single Higgs production, we will distinguish the standard production mechanisms (via SM gauge bosons) from the novel mechanisms present in the model under discussion

(emphasising in particular the role of the Z' gauge boson). Finally, plots for double Higgs production will also be presented.

4.4.1 The future linear collider running proposals

Although there are not official approvals of either ILC or CLIC yet, we already know what are the energy parameters of the two proposed machines:

- ILC: 500 GeV is the planned initial energy, with the open possibility of an upgrade to 1 TeV, and 500 fb^{-1} of integrated luminosity at fixed energy; moreover, the possibility is planned to span over the energy range up the maximum energy (500 GeV or 1 TeV) at 10 fb^{-1} of integrated luminosity.
- CLIC: 3 TeV is the planned initial energy, with the open possibility of an upgrade to 5 TeV; there is no scheduled integrated luminosity yet, then we conservatively assume that it will correspond to the ILC prototype, i.e. 500 fb^{-1} .

The standard Initial State Radiation (*ISR*) functions are implemented, according to the formulae in [19, 36, 84].

Finally, though the beam-strahlung parameters have only been set for the ILC prototype, in this work we assume that the same set of values holds for the CLIC framework, hence we will take into account these values as they appear in the “ILC Reference Design Report” (see [85]). We list them in table 4.1.

	Nominal value	Unit
Bunch population	2	$\times 10^{10}$
RMS bunch length	300	μm
RMS horizontal beam size	640	nm
RMS vertical beam size	5.7	nm

TABLE 4.1: Nominal values of beam parameters at the ILC (see [85]).

4.4.2 Standard single-Higgs production mechanisms

Figure 4.11 shows the cross sections for the standard production mechanisms of a single Higgs boson: vector boson fusion ($V = W^\pm, Z$), the strahlung from the Z boson and the associated production with a t -quark pair. These standard production mechanisms are modulated by a $\cos\alpha(\sin\alpha)$ prefactor in the vertices when considering $h_1(h_2)$, as generally true for all the scalar singlet extensions of the *SM*. Hence, we will not spend too much time in discussing them.

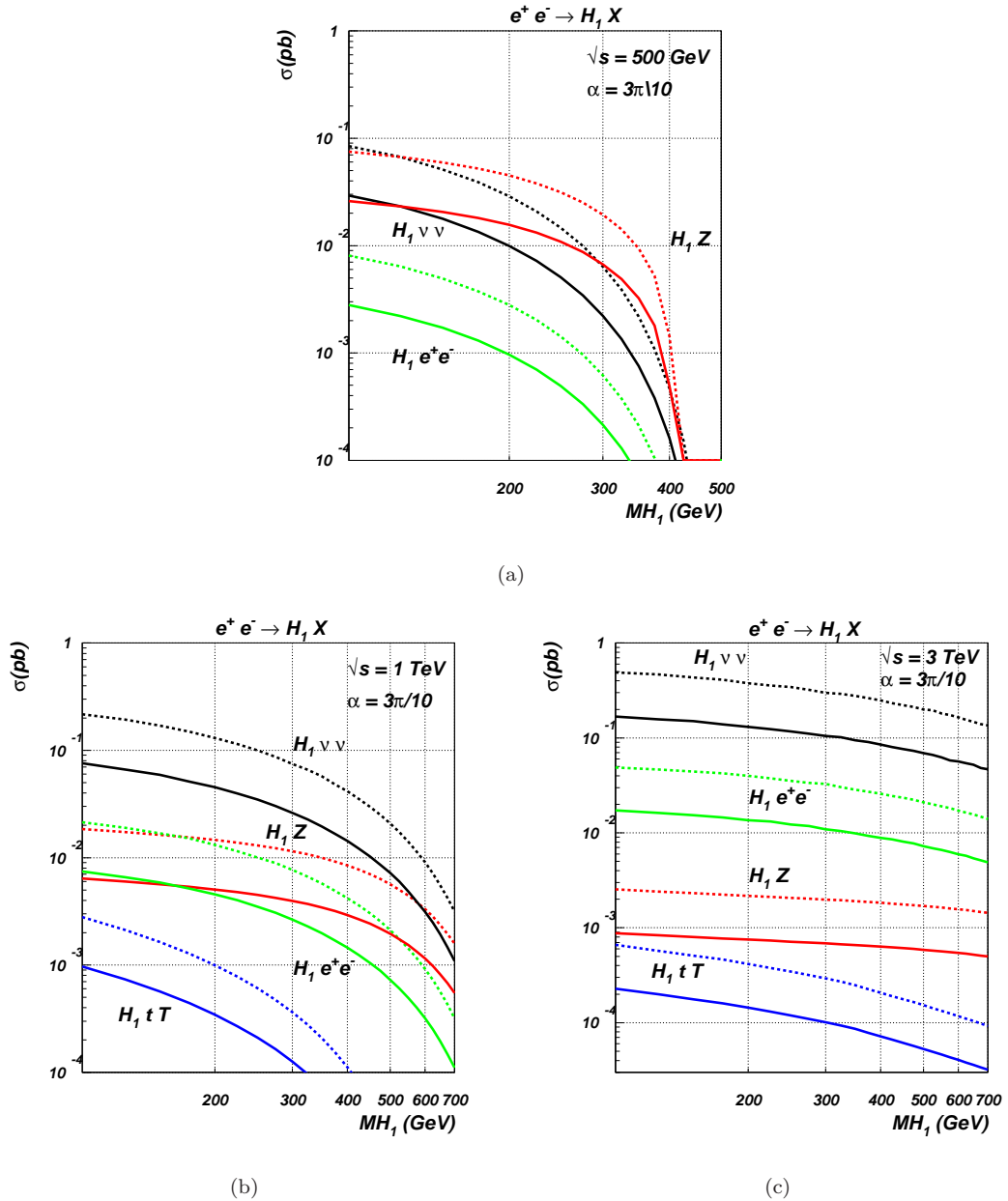


FIGURE 4.11: Cross sections for the process standard Higgs boson production mechanism as a function of the mass at the LC for $\alpha = 3\pi/10$ for (4.11(a)) h_1 and at $\sqrt{s} = 500$ GeV, for (4.11(b)) h_1 at $\sqrt{s} = 1$ TeV and for (4.11(c)) h_1 at $\sqrt{s} = 3$ TeV. The dashed lines refer to $\alpha = 0$.

As well known [2], for low energies, Higgs-strahlung from a Z boson is competitive with W -boson fusion, that becomes the main mechanism as we increase the CM energy. At $\sqrt{s} = 1$ TeV, the cross sections for a light Higgs boson vary from $\mathcal{O}(0.1)$ pb for $M_{h_1} = 100$ GeV to $\mathcal{O}(10)$ fb for $M_{h_1} = 600$ GeV, in the decoupling regime (i.e., for $\alpha = 0$, that corresponds to recovering the SM Higgs boson). All the cross sections are then scaled by a factor $\cos \alpha$ ($\sin \alpha$) when considering h_1 (h_2). At this value of CM energy then, the associated production with a t -quark pair reaches its highest value (for the CM energies we are plotting), i.e., $\mathcal{O}(1)$ fb for $M_{h_1} \leq 200$ GeV, depending on the mixing angle.

Not surprisingly, as we increase the CM energy towards $\sqrt{s} = 3$ TeV, W -boson fusion increases considerably, staying around fractions of pb for several masses and angles, for both Higgs bosons, while the Higgs-strahlung from the Z boson plunges towards cross sections of the order of few fb.

The associated production with a t -quark pair in the SM scenario is the least effective production mechanism, with cross sections of few fb at most. However, we will show in the following Subsection that this mode can be enhanced by the presence of the Z' boson.

4.4.3 Non-standard single-Higgs production mechanisms

In this Section we will discuss the novel mechanisms to produce a Higgs boson (both the light one or the heavy one) in the minimal $B - L$ model. All the new features arise from having a Z' that interacts with both the scalar and fermion sectors. We recall here another important feature: the Z' boson is dominantly coupled to leptons [16]. In fact:

$$\sum_{\ell} BR(Z' \rightarrow \ell\ell) \sim \frac{3}{4}; \quad (4.5)$$

$$\sum_q BR(Z' \rightarrow q\bar{q}) \sim \frac{1}{4}; \quad (4.6)$$

and in particular, $BR(Z' \rightarrow e^+e^-) \simeq 15\%$, which makes a lepton collider the most suitable environment for testing this model.

Again, the Z' mass and g'_1 gauge coupling values have been chosen to respect the constraints coming from LEP and Tevatron (Subsection 3.1.3).

We start by showing the cross section for the associated production of a Higgs boson and a Z' boson, as in figure 4.12. Due to the stringent bounds on the Z' boson mass and coupling to fermions, a sub-TeV CM energy collider is not capable of benefiting from this production mechanism, especially because of the naive kinematic limitation in the final state phase space. In other words, there is not enough energy to produce a Z' and a Higgs boson, if both are on-shell. This is clear in figures 4.12(a) and 4.12(b), where a light Z' boson (with mass of 500 GeV) gives cross sections below 0.1 fb. For a Z' boson of 700 GeV mass instead, the cross sections can be of the order of few fb, only for Higgs masses below 300 GeV, the kinematical limit. These results are similar to the LHC, in which the Z' strahlung process has cross sections below 1 fb (below 0.1 fb for $M_{h_2} > 400$ GeV) [24], even if the LC is expected to accumulate roughly an order of magnitude more integrated luminosity than the LHC.

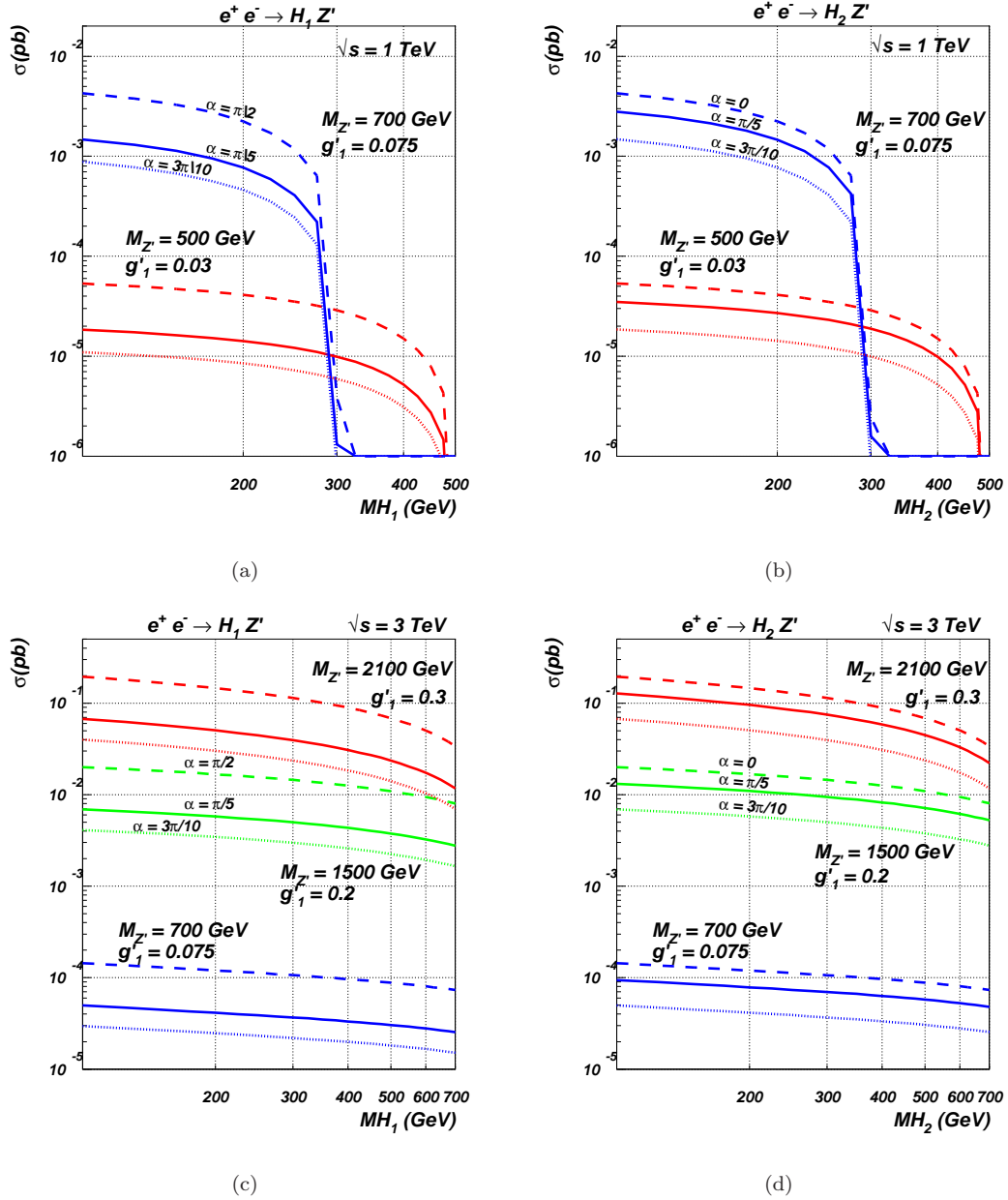


FIGURE 4.12: Cross sections for the process $e^+e^- \rightarrow Z'^* \rightarrow h_{1(2)}Z'$ (4.12(a)) for h_1 and (4.12(b)) for h_2 at the LC at $\sqrt{s} = 1$ TeV and (4.12(c)) for h_1 and (4.12(d)) for h_2 at the LC at $\sqrt{s} = 3$ TeV.

The situation is considerably improved for a multi-TeV collider, not anymore limited in kinematics. As shown in figures 4.12(c) and 4.12(d), a Higgs boson can be produced in association with a Z' boson of 1.5 TeV mass with cross sections of ~ 10 fb in the whole range of the scalar masses considered, rising to $\mathcal{O}(100)$ fb if $M_{Z'} = 2.1$ TeV is considered (and a suitable value for g'_1 is chosen). Although such configuration could suffer from kinematical limitations for the Higgs boson mass to be produced, the cross sections when the scalar mass is close to 700 GeV (the maximum value considered here) are still above those when a Z' boson of 1.5 TeV mass is considered, regardless of the

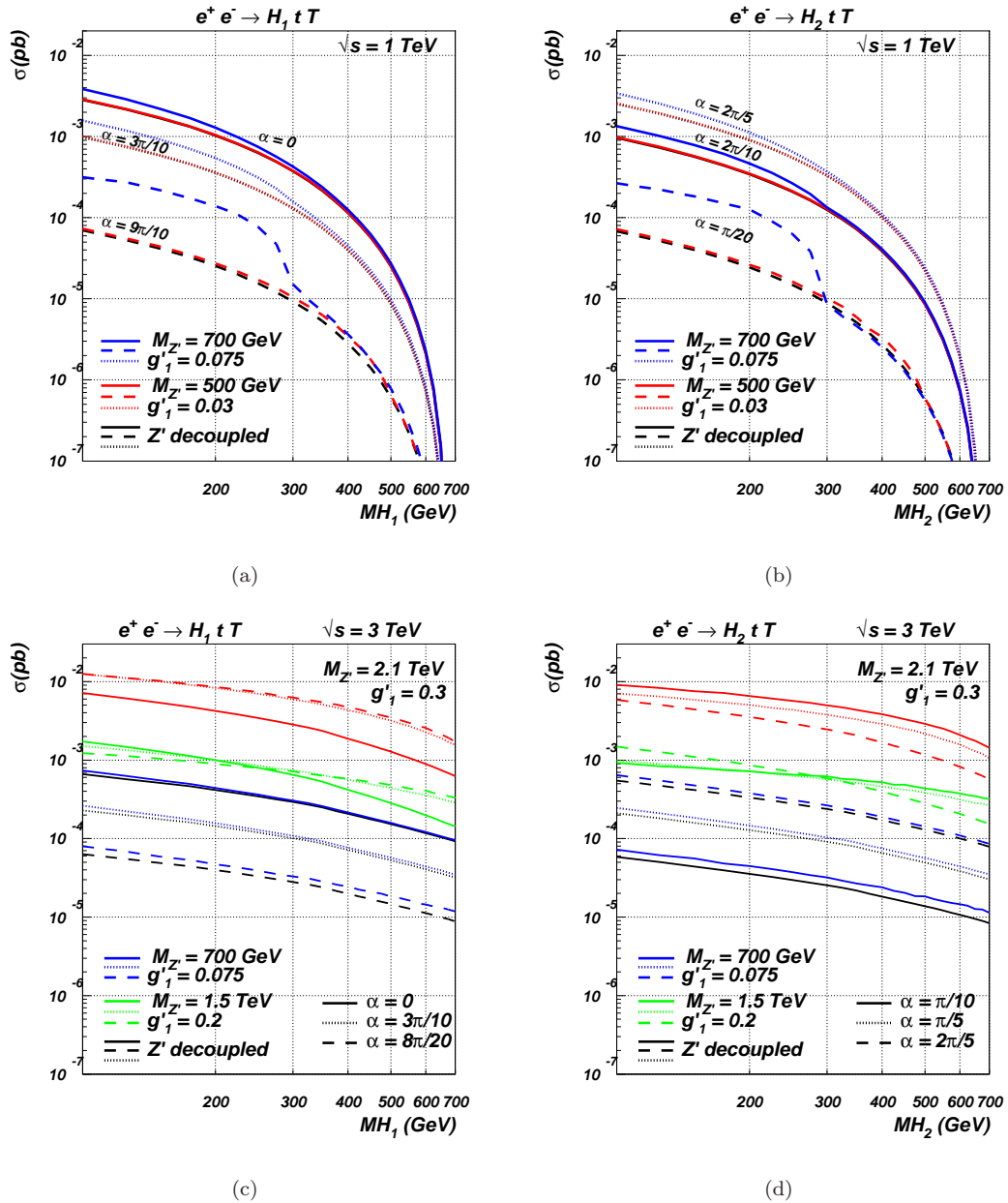


FIGURE 4.13: Cross sections for the process $e^+e^- \rightarrow h_{1(2)}t\bar{t}$ (4.13(a)) for h_1 and (4.13(b)) for h_2 , at the LC at $\sqrt{s} = 1$ TeV, (4.13(c)) for h_1 and (4.13(d)) for h_2 , at $\sqrt{s} = 3$ TeV, for several angles and $M_{Z'}$.

Higgs boson. It is crucial to note that this is the only production mechanism that can potentially lead to the discovery of the heavy Higgs boson in the decoupling limit, i.e., for $\alpha \rightarrow 0$. As previously stated, the strahlung from Z' is not suitable for the LHC, making a multi-TeV LC possibly the ultimate chance for its discovery.

As anticipated, the associated production with a t -quark pair can be enhanced exploiting the Z' boson. In figures 4.13(a) and 4.13(b) are shown the cross sections for the associated production of a Higgs boson and a pair of t -quarks, for $M_{Z'} = 500$ GeV, 700 GeV and in the case of a much heavier Z' boson, hence decoupled, for $\sqrt{s} = 1$ TeV. As

known, the Higgs boson in this channel can be radiated both by a t -(anti)quark or by the vector boson, even though the fraction of events with a Z boson is negligible with respect to the t -quark pair produced by a photon. Therefore, in the SM , the measure of the Higgs coupling to the t -quark is possible, though difficult because of the small cross sections [86]. We are therefore left to evaluate the relative contribution of the Z' boson, to check whether the same situation holds.

It is first interesting to note that, in the decoupling limit (i.e., for vanishing scalar mixing angle α), h_1 does not couple directly to the Z' boson. Nonetheless, the Z' boson can decay to t -quark pair, one of which then radiates the light Higgs boson. This channel has the same final state than the SM ones, and will therefore increase the total number of events, as clear from figure 4.13(a). Hence, the chances of measuring the (SM -like) Higgs boson to t -quark coupling are improved in this case, only slightly for $\sqrt{s} = 1$ TeV but quite considerably for $\sqrt{s} = 3$ TeV and a few TeV Z' boson mass.

As we increase the scalar mixing angle, the relative contribution of the Z' boson increases, although the total cross sections for $\sqrt{s} = 1$ TeV fall below the fraction of fb, making it even harder to be observed. The situation is opposite for the multi-TeV CM energy case (figures 4.13(c) and 4.13(d)), in which the Z' boson is produced abundantly and it can enhance the Higgs boson associated production with a t -quark pair. In this case, anyway, it is not true anymore that the majority of the events are those in which the Higgs boson is radiated by a t -quark: the Higgs-strahlung from the Z' boson is now an important channel, as clear from figures 4.12(c) and 4.12(d) and from the fact that, for low Z' masses, the total cross section is smaller as we start increasing the angle (due to the reduced coupling to the t -quark), while for TeV Z' boson masses it always increases. If the Z' boson mass is below the maximum CM energy of the collider, the fraction of strahlung events off the Z' boson can be reduced by tuning the CM energy and sitting at the peak of the Z' boson itself. In this case, the vast majority of Z' bosons are produced on-shell, enhancing the total cross sections and the portion of events in which the Z' boson decays into a t -quark pair, one of which will then radiate the Higgs boson. The possibility of sitting at the peak of the Z' boson is therefore very important phenomenologically, as it allows the Higgs coupling to the t -quark to be measured much more precisely than in the SM , as the cross section in the minimal $B - L$ model for this channel can rise up to $10 \div 100$ fb, depending on the Higgs boson mass and mixing angle. Notice that for h_1 the angle has to be small (i.e., less than $\pi/5$) to allow for this measurement, as only in this case h_1 couples more to the t -quark than to the Z' boson, though Z' strahlung events are still important (the ratio of the two subchannels is in fact $< 5\%$). This situation is exactly specular when the heavy Higgs boson is considered: when the CM energy is maximal, the associated production with a t -quark pair has good cross sections but it does not allow a direct measurement of the Higgs boson to

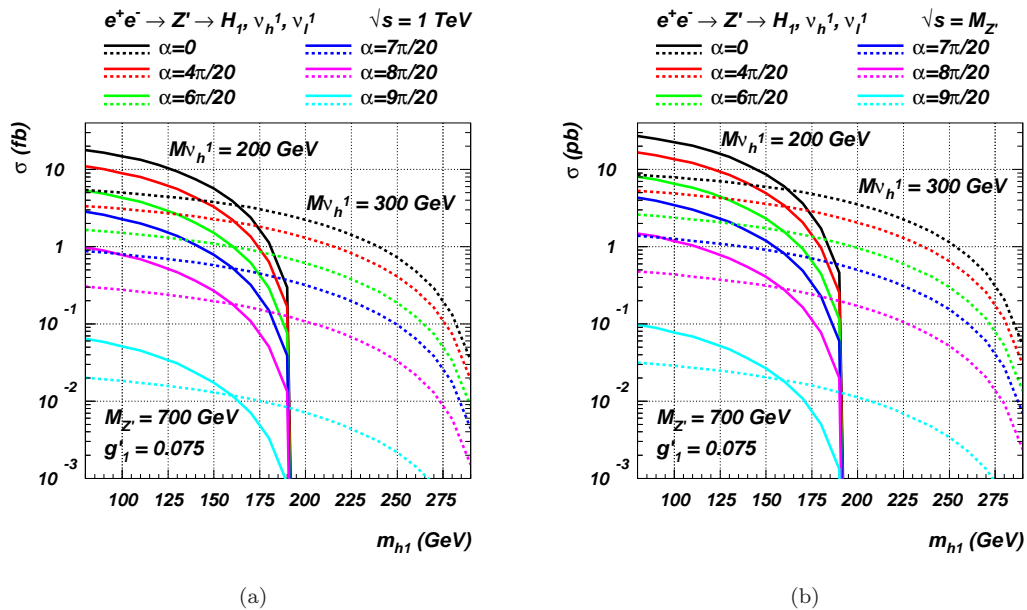


FIGURE 4.14: Cross sections for the associated production of the light Higgs boson and one heavy and one light first generation neutrinos (via $Z' \rightarrow \nu_h \nu_l$) at the LC (4.14(a)) for $\sqrt{s} = 1$ TeV and (4.14(b)) for $\sqrt{s} \equiv M_{Z'}$.

t -quark coupling, that instead is possible for big angles ($\alpha \gtrsim 3\pi/10$) when sitting at the Z' boson peak. Notice that, in this configuration, the total cross section is independent of the Z' boson mass, if the t -pair and the Higgs boson can be produced all on-shell. Otherwise, the cross sections are suppressed by the phase space.

Next, a possibility already highlighted in [16, 24] for the LHC is using the heavy neutrino as a source of light Higgs bosons. Besides to provide a further production mechanism and being a very peculiar feature of the minimal $B - L$ model, it also allows for a direct measure for the Higgs boson to heavy neutrinos coupling when the decay of the Higgs to neutrino pairs is kinematically forbidden. Though, in [24] is showed that it gives low cross sections at the LHC, making it hard to probe. In contrast, a LC is a more suitable environment to test this mechanism. One reason is that the Z' couples dominantly to leptons, as already intimated. Further, the possibility of tuning the CM energy and sitting exactly on the Z' peak will enhance the Z' production cross section by a factor of roughly 10^3 . Another key factor is that the BR of a heavy neutrino into a light Higgs boson and a light neutrino is $\sim 20\%$ (at the very most, see [16]), when kinematically allowed. This mechanism is not suitable for the heavy scalar though: since it is heavier than the light one, for sure one would observe the latter first. Altogether, for a Z' boson of 700 GeV mass, figure 4.14(a) shows the cross sections for the production of a (first generation only) heavy neutrino pair and the subsequent decay of one of them into a light Higgs boson, for two different masses of the heavy neutrino, at $\sqrt{s} = 1$ TeV. At this stage, the mechanism is giving $\mathcal{O}(1 \div 10)$ fb cross sections for a heavy neutrino of

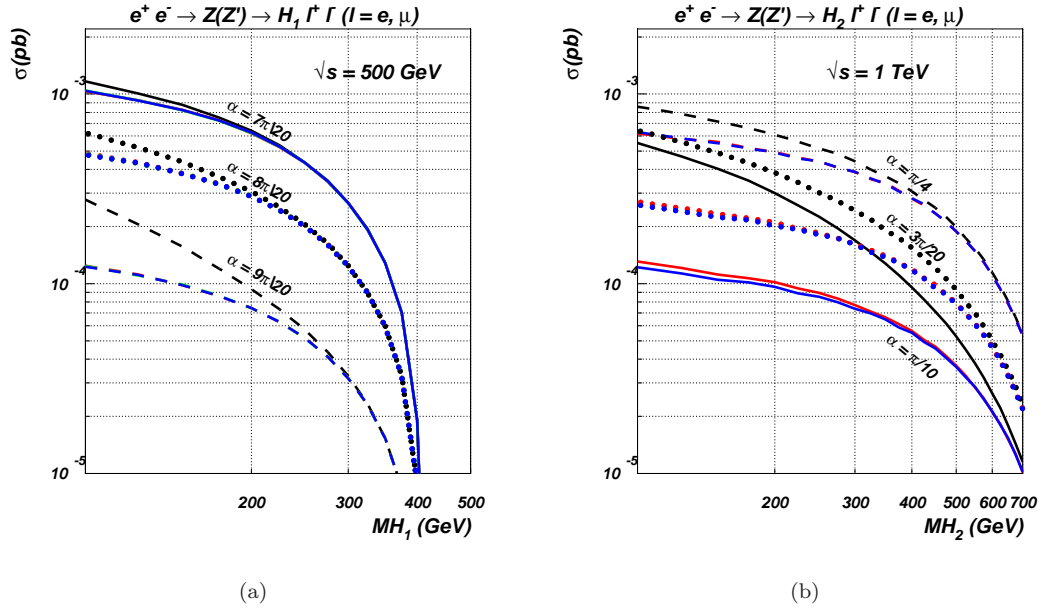


FIGURE 4.15: Cross section for $e^+e^- \rightarrow Z(Z')^* \rightarrow h_1 \ell^+ \ell^-$ ($\ell = e, \mu$). (4.15(a)) Black line is for $M_{Z'} = 420$ GeV, other lines for $M_{Z'} = 700, 1500, 7000$ GeV; $\sqrt{s} = 500$ GeV. (4.15(b)) Black line is for $M_{Z'} = 1050$ GeV, other lines for $M_{Z'} = 1400, 3500$ GeV; $\sqrt{s} = 1$ TeV.

200 GeV mass, decreasing to $\mathcal{O}(1)$ fb when a mass of 300 GeV is considered, for a good range in the mixing angle. Figure 4.14(b) shows the full potentiality of this model at a LC: by sitting on the Z' peak, the heavy neutrino pair production is enhanced by a factor $\sim 10^3$, giving cross sections well above the pb range for a large portion of the allowed parameter space, and staying above 10 fb whatever the mixing angle. When kinematically allowed though, this peculiar mechanism really carries the hallmark of the minimal $B-L$ model and it does not depend dramatically on the Z' mass, if below the maximum CM energy of the collider.

Finally, the interference between the Z and the Z' could play an important role in the scalar sector, besides the t -quark Yukawa coupling measure presented above. As well known, and remarked upon in [19], the negative interference between the neutral gauge bosons can be substantial. One could then look for information about a further neutral vector boson also by looking at the interference when a Higgs boson is radiated from the Z bosons. To highlight this effect, in this model it is possible to select just the leptonic decay modes of the vector bosons, reducing the predominance of the Z boson. Nonetheless, as shown in figure 4.15, such effects are minimal when the Z' boson mass is above the CM energy of the LC.

Other subleading processes for Higgs boson production consist of single production in association with two vector bosons and of double Higgs boson production. In these

contexts, many new mechanisms arise in this model, especially exploiting the Z' boson and because a resonant $h_2 \rightarrow h_1 h_1$ process is allowed.

4.4.4 Single scalar production in association with a pair of vector bosons

The SM gauge boson pair production has really large cross sections at the LC, therefore the radiation of a Higgs boson could still have observable rates. Also, once the Higgs boson has been seen in the main production mechanisms of Section 4.4.2, these subprocesses could be useful to test the quartic coupling to the SM gauge bosons. Figure 4.16 shows the case for $\sqrt{s} = 0.5, 1$ and 3 TeV CM energies. We neglect here final state photons: although the cross section of channels comprising the photon could be comparable to the WW subchannel (see, e.g., [2]), the absence of a direct coupling to the scalar bosons ensures that these channels would not provide further informations than the other processes that have been considered.

We then see that the WW channel is roughly an order of magnitude higher than the ZZ one and that, for low Higgs boson masses, the cross sections decrease as we increase the CM energy. However, a larger CM energy allows the production of more massive scalars and to avoid kinematic limitations. So that, if $\sqrt{s} = 1$ TeV is preferable to test these mechanisms for Higgs boson masses between 100 and 300 GeV (with comparable or higher cross sections to the case for $\sqrt{s} = 500$ GeV), the $\sqrt{s} = 3$ TeV configuration is essential for masses above 300 GeV, for both the light and heavy Higgs boson. Unless very high (and disfavoured) values of the mixing angle, the $h_1 WW$ channel has cross section above 0.1 fb for the whole range of scalar masses considered. The opposite is true for the heavy Higgs boson, for which only big values of α allow this channel to be above 0.1 fb. The case for the ZZ channel is different: since its cross sections are rather small, it has chances of being detected, staying above 0.1 fb, only for $\sqrt{s} = 500$ GeV and $\sqrt{s} = 1$ TeV. For $\sqrt{s} = 3$ TeV its observation requires very high statistics.

The cross sections for the case of one Z' boson in the final state could be important and comparable to the WW channel. Also, this particular channel is useful to test the absence of a tree-level $h - Z - Z'$ coupling. Figure 4.17 shows the cross sections for $\sqrt{s} = 3$ TeV for two values of the Z' mass, $M_{Z'} = 1.4$ and 2.1 TeV, and suitable g'_1 coupling. The heavier the Z' boson, the higher the cross sections, until kinematical limitations occur. In fact, the cross sections for $M_{Z'} = 2.1$ TeV are always above those for $M_{Z'} = 1.4$ TeV for scalar masses below 600 GeV, for which the process with the lighter Z' boson overtakes. It is important to note that the behaviour of these processes with the scalar mixing angle is opposite to the previous case. Hence, for h_1 and for

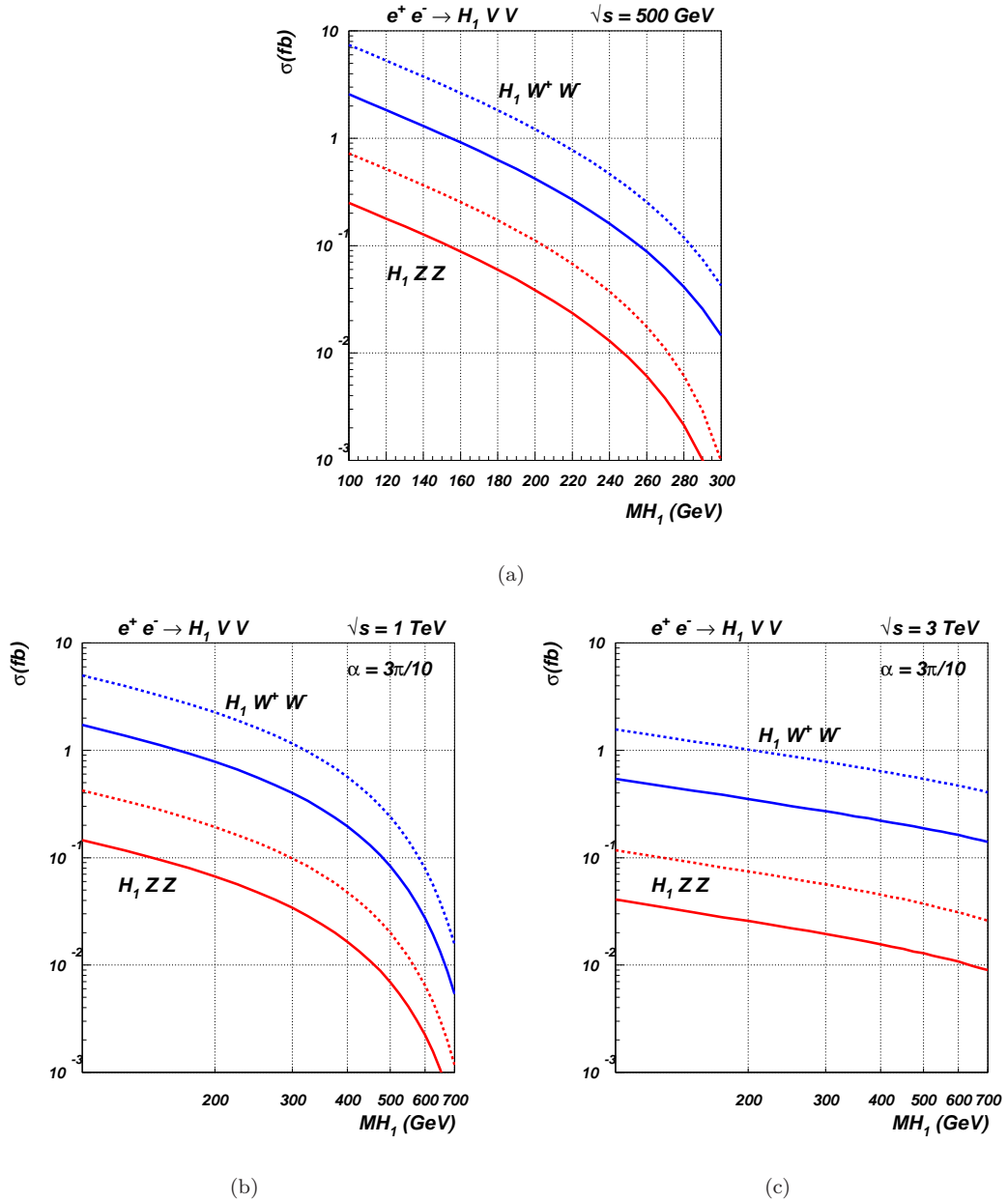


FIGURE 4.16: Cross sections for the light Higgs boson production with two vector bosons ($V = W^\pm, Z$) as a function of the mass at the LC for $\alpha = 3\pi/10$ (4.16(a)) for h_1 at $\sqrt{s} = 500$ GeV, (4.16(b)) for h_1 at $\sqrt{s} = 1$ TeV and (4.16(c)) for h_1 at $\sqrt{s} = 3$ TeV. The dashed lines refer to $\alpha = 0$.

small values of the angle, the associated production with a pair of SM gauge bosons is favoured, while the process with the Z' boson is favoured for big angles. For h_2 it is again the opposite. For intermediate angles, instead, both processes can have small but observable rates, between 0.1 and $\mathcal{O}(1)$ fb, for both Higgs bosons and in the whole range of considered masses.

Finally, notice that the case for $\alpha = 0$ represents the radiative correction to the $Z(Z')$ strahlung of $h_1(h_2)$ for a $Z'(Z)$ boson emission.

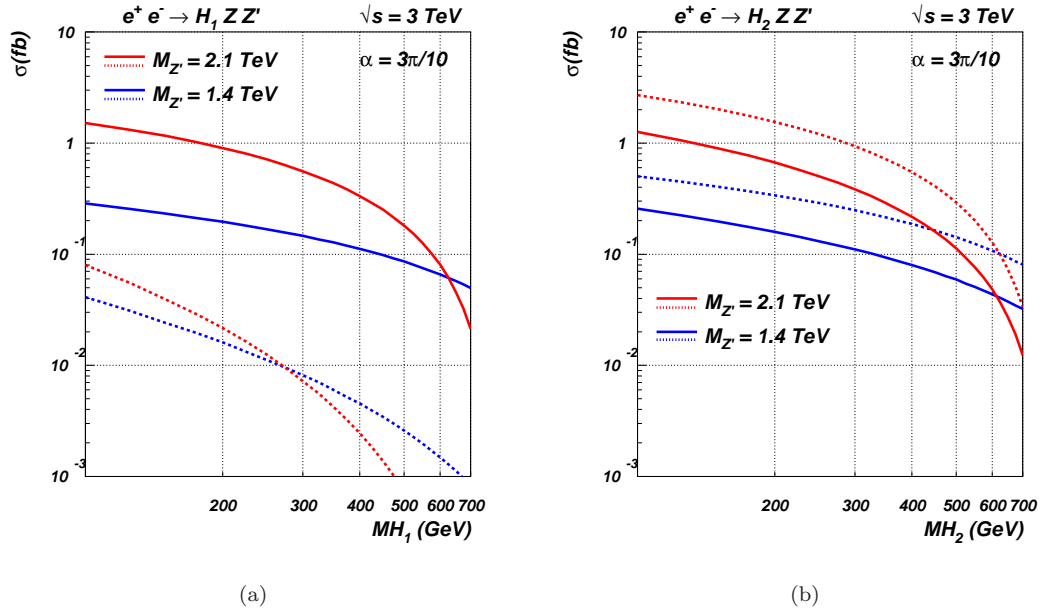


FIGURE 4.17: Cross sections for the Higgs boson production with a Z and a Z' boson as a function of the scalar mass at the LC (4.17(a)) for h_1 and (4.17(b)) for h_2 , at $\sqrt{s} = 3$ TeV. The dashed lines refer to $\alpha = 0$.

4.4.5 Double scalar production mechanisms

The observation of a Higgs boson pair is crucial to measure parameters of the scalar Lagrangian entering directly in the trilinear and quartic self-couplings [87–89], although it requires high statistics and large CM energy. Remarkable in this sense is the possible complementarity between the LHC and LCs, as shown in [90, 91].

In the minimal $B - L$ model, the $h_2 \rightarrow h_1 h_1$ process is also present for a large portion of the parameter space, contrary to the $MSSM$ case, for instance (where it is important only for very low values of $\tan\beta$, region that has been constrained at LEP [92]). On the one side, light Higgs boson pair production is enhanced by this channel, especially when it is resonant. On the other side, also the $h_2 - h_1 - h_1$ coupling is directly testable. Moreover, the Z' boson can give further scope to this, providing an extra mechanism for Higgs pair production, both without and through heavy Higgs boson production.

Figure 4.18 shows the standard production mechanisms of a pair of light Higgs bosons. In the SM case (or when we neglect h_2), they are the same mechanisms discussed in Subsection 4.4.2 when a further Higgs boson is attached. Cross sections for these processes are always below 0.1(1) fb at $\sqrt{s} = 1(3)$ TeV, and above 0.1 fb at $\sqrt{s} = 3$ TeV only for the W -fusion process and for $M_{h_1} \lesssim 350$ GeV, as clear from figures 4.18(a) and 4.18(c), respectively.

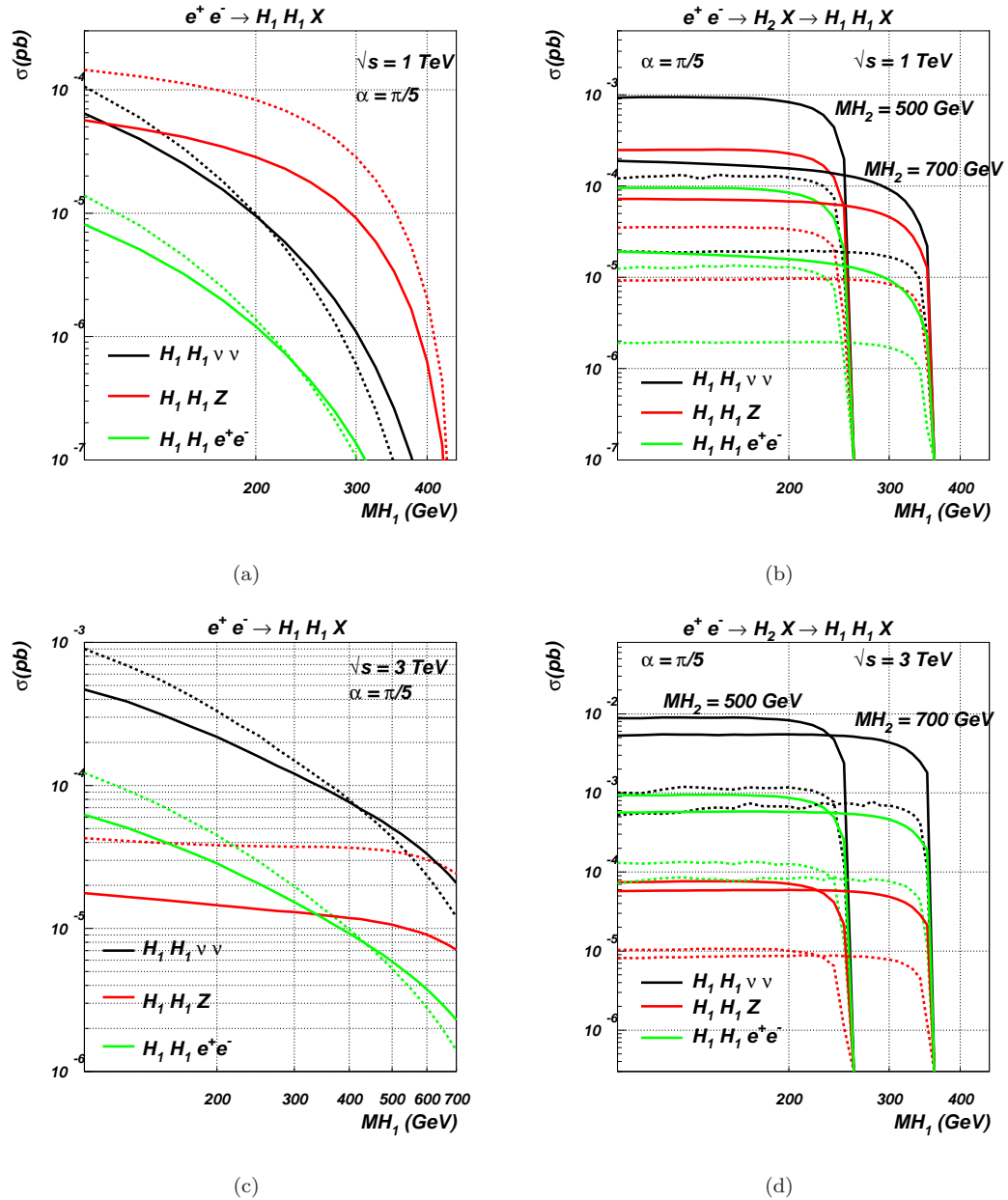


FIGURE 4.18: Cross sections for the double light Higgs boson production at the LC (4.18(a)) alone and (4.18(b)) via h_2 , for $\sqrt{s} = 1 \text{ TeV}$ and (4.18(c)) alone and (4.18(d)) via h_2 , for $\sqrt{s} = 3 \text{ TeV}$. The dashed lines in figures 4.18(a) and 4.18(c) refer to $\alpha = 0$, while in figures 4.18(b) and 4.18(d) refer to $\alpha = \pi/20$.

When instead the light Higgs boson pair is originated by the decay of the heavy Higgs boson, cross sections can be of $\mathcal{O}(1) - \mathcal{O}(10) \text{ fb}$ at $\sqrt{s} = 1 - 3 \text{ TeV}$, in the W -fusion channel (at most, when the mixing is maximal, i.e., $\alpha \approx \pi/4$, and we chose $M_{h_2} = 500 \text{ GeV}$). If we choose a higher value for M_{h_2} , a more massive h_1 boson can be pair produced, but with a sensibly lower cross sections: for $M_{h_2} = 700 \text{ GeV}$, they are roughly a factor 5(2) smaller than for $M_{h_2} = 500 \text{ GeV}$ at $\sqrt{s} = 1(3) \text{ TeV}$. Notice that the cross sections are constant with M_{h_1} as long as the $h_2 \rightarrow h_1 h_1$ decay is allowed. This is a consequence of having chosen a specific value for M_{h_2} and that $BR(h_2 \rightarrow h_1 h_1) \approx 20\%$

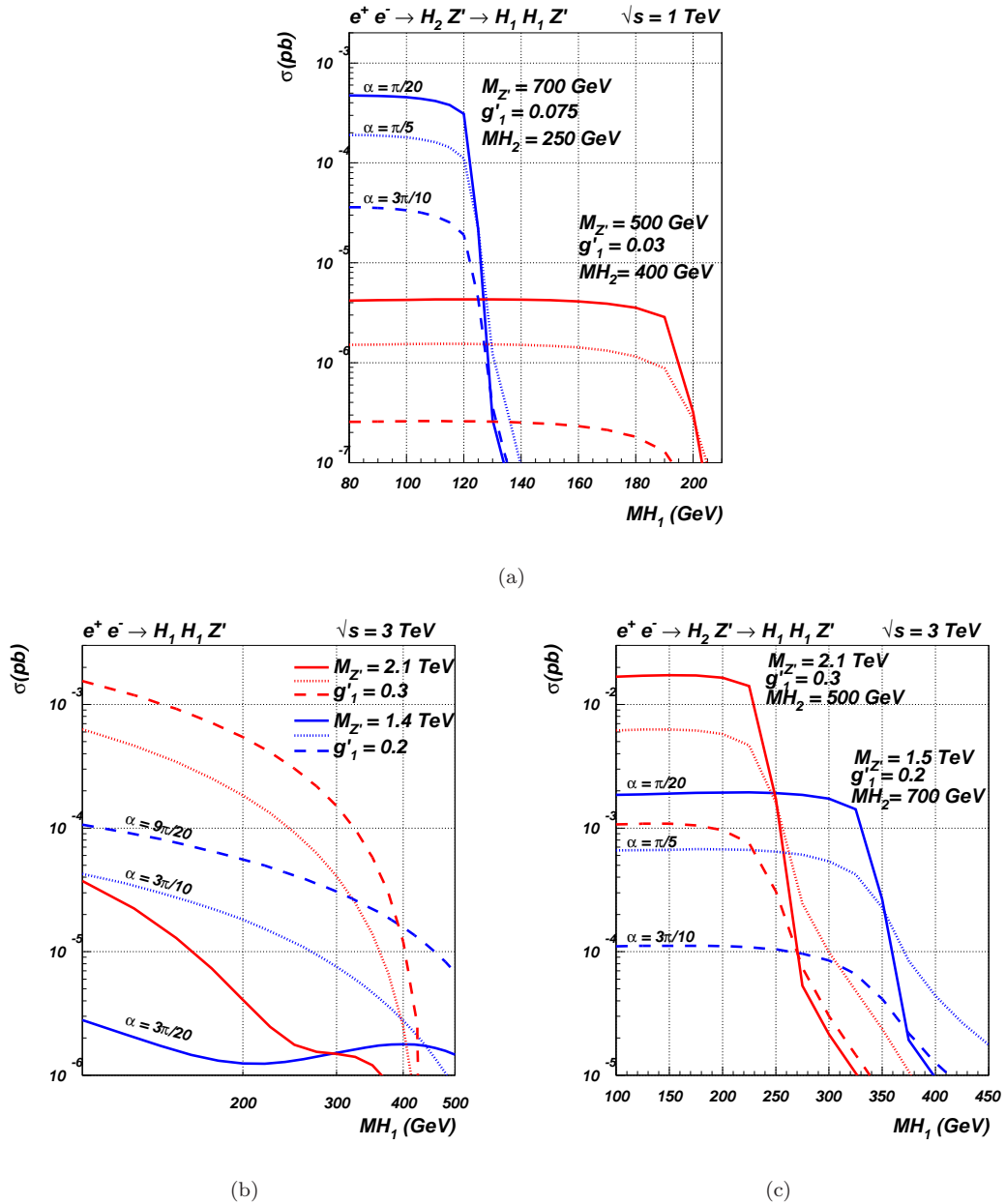


FIGURE 4.19: Cross sections for the process $e^+e^- \rightarrow H_2 Z' \rightarrow H_1 H_1 Z'$ (4.19(a)) for $\sqrt{s} = 1$ TeV and (4.19(c)) for $\sqrt{s} = 3$ TeV, for suitable values of M_{H_2} and for the process $e^+e^- \rightarrow H_1 H_1 Z'$ (4.19(b)) at $\sqrt{s} = 3$ TeV, several values of the angle and of $M_{Z'}$.

is approximately constant for $M_{h_1} > M_W, M_Z$ [24]. Other channels give smaller cross sections: the Z -fusion channel is always an order of magnitude below the W -fusion one, while the strahlung from the Z boson channel gives at most $\sim 0.2(0.08)$ fb for $M_{h_2} = 500$ GeV and $\sim 0.08(0.06)$ fb for $M_{h_2} = 700$ GeV at $\sqrt{s} = 1(3)$ TeV, respectively.

As anticipated, the Z' boson in the minimal $B - L$ model can give further scope to produce also a pair of light Higgs bosons at a LC, both directly (without or through h_2) and indirectly (pair producing heavy neutrinos).

Figure 4.19 shows double Higgs strahlung from the Z' boson (for $\sqrt{s} = 3$ TeV only) and the case in which h_2 is radiated from the Z' boson and it subsequently decays into a light Higgs boson pair. The double Higgs-strahlung from the Z' boson at $\sqrt{s} = 1$ TeV has negligible cross sections, below 10^{-3} fb, especially because of kinematic limitations, and therefore we neglect it here. The cross sections for double Higgs-strahlung at $\sqrt{s} = 3$ TeV are presented in figure 4.19(b), where we see that, for $M_{Z'} = 2.1$ TeV (and $g'_1 = 0.3$), a pair of light Higgs bosons can be produced with cross section $\gtrsim 0.1$ fb for $m_{h_1} \lesssim 300$ GeV and for big values of the scalar mixing angle (roughly bigger than $\pi/4$). The situation improves if we consider the Higgs-strahlung of h_2 from the Z' boson and its subsequent decay into h_1 pairs. Notice that this channel reduces⁴ as we increase the value of the mixing angle, vanishing in the decoupling regimes (both for $\alpha \equiv 0$ and $\pi/2$). At $\sqrt{s} = 1$ TeV this process is still limited by the kinematics: the higher the Z' boson mass the higher the cross sections and the smaller the producible h_2 mass. For $M_{Z'} = 700$ GeV (and suitable values for the g'_1 coupling), the light Higgs boson can be pair produced through h_2 with cross sections bigger than 0.1 fb (for $\alpha < \pi/4$, up to 4 fb) through a heavy Higgs boson of 250 GeV, hence for h_1 masses up to 120 GeV only. To extend the range in M_{h_1} , a higher mass for the heavy Higgs boson has to be considered, needing a smaller Z' boson mass: the cross sections in this case become unobservable, below 10^{-2} fb. If the collider CM energy is increased though, heavier h_1 's can be pair produced through the heavy Higgs boson, in association with a much heavier Z' boson, with bigger cross sections. Figure 4.19(c) shows that, for $M_{Z'} = 2.1$ TeV, a heavy Higgs boson with 500 GeV mass can pair produce the light Higgs boson with cross sections well above the fb level up to $M_{h_1} = 200$ GeV, reaching $\mathcal{O}(10)$ fb for small (but not negligible) values of the mixing angle (i.e., $\pi/20 < \alpha < \pi/5$). If a Z' boson of 1.5 TeV mass is considered, there are no more kinematical limitations for the producible h_2 boson and, in the case of $M_{h_2} = 700$ GeV, an even heavier h_1 can be pair produced, up to masses of 350 GeV with cross sections bigger than 0.1 fb and $\mathcal{O}(1)$ fb for small (but not negligible) values of the mixing angle (i.e., for the same values of the previous case).

The high cross sections of figure 4.14 (and the fact that $BR(\nu_h \rightarrow h_1 \nu_l) \approx 20\%$) allows one to consider the case in which both heavy neutrinos decay into a light Higgs boson each. In figure 4.20 we show this case. Once again, the possibility of tuning the CM energy of the LC to sit at the Z' boson peak is crucial to test this mechanism. Without it, the cross sections would be about $0.1 \div 1$ fb for small values of the scalar mixing angle only: for instance, for $\alpha = 6\pi/20$, light Higgs boson pair production through heavy neutrino pair production (via the Z' boson, one generation only) are above 0.1 fb

⁴This is true when both the Z' boson and the heavy Higgs boson are on-shell. When h_2 is an off-shell intermediate state, the cross sections for light Higgs pair production via h_2 increases as we increase the value of the mixing angle.

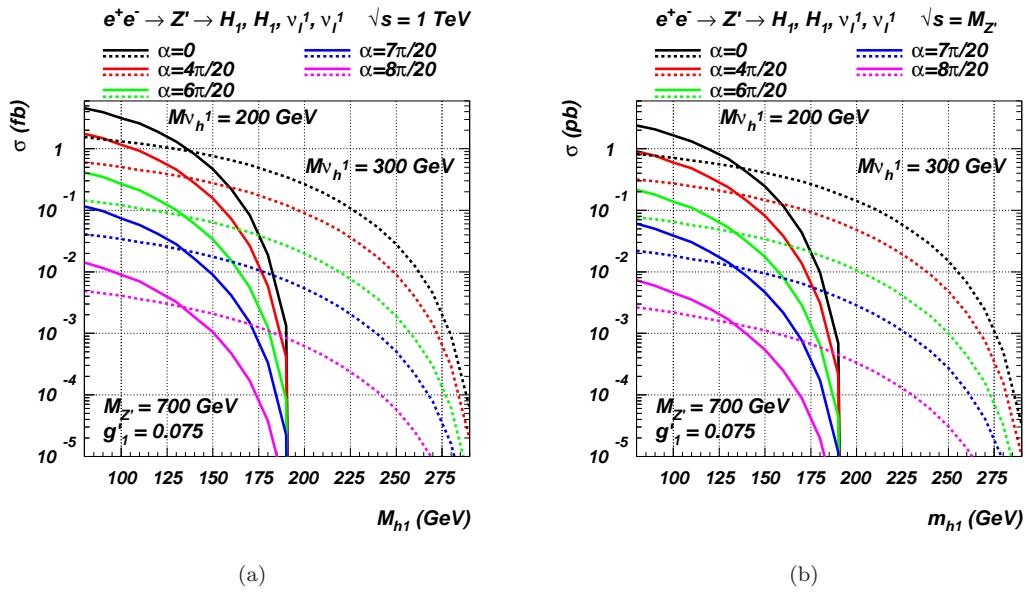


FIGURE 4.20: Cross sections for the associated production of two light Higgs bosons and two light first generation neutrinos (via $Z' \rightarrow \nu_h \nu_h$) at the LC (4.20(a)) for $\sqrt{s} = 1$ TeV and (4.20(b)) for $\sqrt{s} \equiv M_{Z'}$.

for $M_{h_1} < 125$ GeV, for both heavy neutrino masses chosen. When instead the CM is tuned to the Z' boson peak, the cross sections are enhanced and well above the fb level whatever the value for the mixing angle, for h_1 masses kinematically allowed, reaching a few pb (or fractions of pb) for small mixing angles and M_{h_1} values.

Finally, the two Higgs bosons could be produced together, as shown in figure 4.21. Although subleading, this mechanism is peculiar for several reasons: it requires both Higgs bosons to be (simultaneously) significantly coupled to the gauge bosons, it has a very complicated dependence upon α , due to the trilinear and quartic scalar self-couplings, that makes it not invariant under $\alpha \rightarrow \frac{\pi}{2} - \alpha$ (being α the scalar mixing angle)⁵ and it is maximum when the mixing is maximal, i.e., for $\alpha = \pi/4$. These processes could be important to reconstruct the scalar potential and the whole set of self-interaction couplings, together with the $h_2 \rightarrow h_1 h_1$ decay.

If at $\sqrt{s} = 1$ TeV the cross sections for this process are always below 0.1 fb, at $\sqrt{s} = 3$ TeV the W -fusion channel can produce the two Higgs bosons with cross sections of fractions of fb, up to $0.08(0.02) \div 0.2(0.3)$ fb, for $M_{h_1} < M_{h_2} = 300(500)$ GeV. The double Higgs-strahlung from a Z' boson of 2.1 TeV mass (and $g'_1 = 0.3$) has also comparable cross sections, of $\mathcal{O}(0.1)$ fb for $M_{h_1} < M_{h_2} = 300$ GeV only, for values of the mixing angle close to maximal. Notice that the cross sections for this process scale approximately

⁵The behaviour of the trilinear and quartic self-interaction couplings with the scalar mixing angle is not a simple trigonometric function, as one can verify by checking the Feynman rules listed in Appendix B.

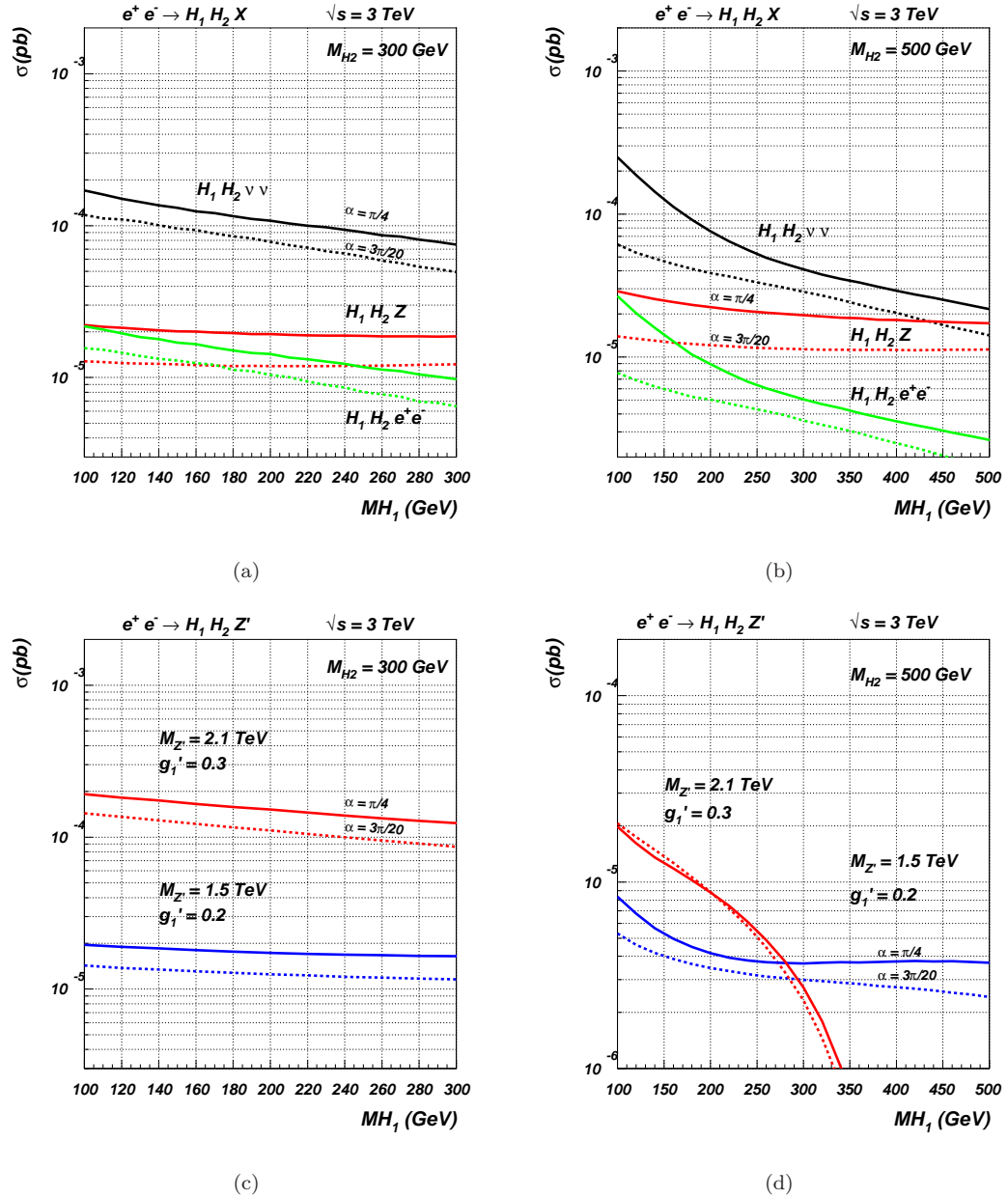


FIGURE 4.21: Cross sections for the associated production of the two higgs bosons at the LC through the standard production mechanisms (4.21(a)) for $M_{h_2} = 300$ GeV and (4.21(b)) for $M_{h_2} = 500$ GeV, for $\sqrt{s} = 3$ TeV, and in association with a Z' boson (4.21(c)) for $M_{h_2} = 300$ GeV and (4.21(d)) for $M_{h_2} = 500$ GeV, for $\sqrt{s} = 3$ TeV and several Z' masses.

with $\sin 2\alpha$, whatever production mechanism is considered. The mixing angle can be measured from other processes and used as an input for these channels, provided that also both scalar masses have been measured elsewhere. If so, the deviation of the cross sections from the naive ones (when the two Higgs bosons are produced independently, i.e., neglecting the self-interactions, that would be exactly proportional to $\sin 2\alpha$) will give further indications about the self-interaction couplings. Very high statistics is required for such a study, barely within the potentiality of the next generation of LCs.

Chapter 5

Conclusions

In this Thesis we have investigated the phenomenology of the Higgs sector of the minimal $B - L$ model at present and future colliders.

The model is realised by mean of a minimal extension of the SM , i.e., by gauging the broken¹ $U(1)_{B-L}$ symmetry in addition to the SM gauge symmetry², hence realising the following symmetry pattern:

$$SU(3)_C \times SU(2)_L \times U(1)_Y \times U(1)_{B-L}. \quad (5.1)$$

This extension is triple-minimal: in the gauge boson sector (adding one gauge boson, Z'), in the Higgs sector (adding one scalar boson, h_2) and in the fermion sector (adding one heavy right-handed neutrino per generation).

In Chapter 1 we have presented the main motivations that call for the $U(1)_{B-L}$ extension, in particular the phenomenological necessity of giving mass to the light neutrinos (via the “see-saw” mechanism) through a TeV-scale symmetry breaking. We have also established two possible experimental environments in which this extension could be studied: the LHC (a currently operative collider) and the ILC/CLIC (two future linear collider proposal).

In Chapter 2 we have presented the formal aspects of the minimal $B - L$ model, focusing on the details that are needed to implement the model Lagrangian in any of the public softwares that are devoted to Feynman Rules generation (such as LanHEP, FeynRules, etc.).

¹At the TeV energy scale.

²Assuming no-mixing between the two gauge groups at tree-level.

In Chapter 3 (based on the results appeared in [21–23]) we have presented a detailed study of the Higgs sector parameter space. In particular, we have focused on the analysis of the parameter space, with emphasis on the experimental and theoretical exclusion methods, in order to set the basis for the phenomenological analysis of the Higgs sector at colliders.

As for the theoretical methods, we have presented a full analysis on unitarity bounds in the Higgs sector of the minimal $B - L$ model. Using the equivalence theorem, we have evaluated the spherical partial wave amplitude of all possible two-to-two scatterings in the scalar Lagrangian at an infinite energy, identifying the $zz \rightarrow zz$ and $z'z' \rightarrow z'z'$ processes as the most relevant scattering channels for this analysis ($z^{(\prime)}$ is the would-be Goldstone boson of the $Z^{(\prime)}$ vector boson). Then, we have shown that these two channels impose an upper bound on the two Higgs masses: the light one cannot exceed the SM bound while the limit on the heavy one is established by the singlet Higgs VEV , whose value is presently constrained by LEP and could shortly be extracted by experiment following a possible discovery of a Z' . We also studied how the discovery of a light Higgs boson at the LHC could impact on the heavy Higgs mass bounds in the minimal $B - L$ model and we discovered that the lighter the h_1 mass the more loose is the bound on M_{h_2} , except in the low-mixing region ($\alpha \rightarrow 0$) of the Higgs parameter space, in which the knowledge of the x VEV is again fundamental.

Then, we have investigated the triviality and vacuum stability conditions of the minimal $B - L$ model with a particular view to define the phenomenologically viable regions of the parameter space of the scalar sector, by computing all relevant $RGEs$ at the one-loop level in presence of all available experimental constraints. The RGE dependence on the Higgs masses and couplings (including mixings) has been studied in detail for discrete choices of the singlet Higgs field VEV , in order to make a fruitful comparison with the unitarity case.

Thereafter, we have shown that, by combining perturbative unitarity and RGE methods, one can significantly constrain the g'_1 coupling of the minimal $B - L$ extension of the SM , by imposing limits on its upper value that are more stringent than standard triviality bounds.

Finally, we have made an illustrative study of the “fine-tuning” induced by the quantum one-loop corrections of the Higgs boson masses, giving the correct solution for the Veltman conjecture in the minimal $B - L$ context.

In Chapter 4 (based on the results appeared in [24, 25]), we have studied in detail the phenomenology of the Higgs sector of the minimal $B - L$ model at colliders.

After a short discussion about the implementation of the model in CalcHEP, we have presented the Higgs bosons branching ratios and total widths for some interesting points of the parameter space.

Then, we have investigated both the foreseen energy stages of the LHC (and corresponding luminosities). While virtually all relevant production and decay processes of the two Higgs states of the model have been investigated, we have eventually paid particular attention to those that are peculiar to the described $B-L$ scenario. The phenomenological analysis has been carried out in presence of all available theoretical and experimental constraints and by exploiting numerical programs at the parton level. While many Higgs signatures already existing in the SM could be replicated in the case of its $B-L$ version, in either of the two Higgs states of the latter (depending on their mixing), it is more important to notice that several novel Higgs processes could act as hallmarks of the minimal $B-L$ model. These include Higgs production via gluon-gluon fusion, in either the light or heavy Higgs state, the former produced at the lower energy stage of the CERN collider and decaying in two heavy neutrinos and the latter produced at the higher energy stage of such a machine and decaying not only in heavy neutrino pairs but also in Z' and light Higgs ones. For each of these signatures we have in fact found parameter space regions where the event rates are sizable and potentially amenable to discovery. Our results have laid the basis for the phenomenological exploitation of the Higgs sector of the minimal $B-L$ model at the LHC.

Finally, we have studied the potential of future LCs in establishing the structure of the Higgs sector of the minimal $B-L$ model. We have considered both an ILC and CLIC. The scope of either machine in this respect is substantial as a large variety of Higgs production processes are accessible. The latter include both single and double Higgs boson channels, at times produced in association with heavy particles, both SM (W and Z bosons and t (anti)quarks) and $B-L$ ones (Z' boson and ν_h neutrinos), thus eventually yielding very peculiar signatures at detector level. This variety of accessible Higgs production processes potentially allows future LCs to accurately pin down the structure of the $B-L$ Higgs sector, including not only the masses and couplings of both Higgs states pertaining to this scenario, but also trilinear and quartic self-couplings between the two scalar bosons themselves. On this score, the interplay and complementarity of measures at the LHC and at LCs is fundamental. The extension in the gauge sector, with a Z' boson dominantly coupled to leptons, is fundamental to distinguish this model from the classic scalar extensions of the SM . Although the scalar Lagrangian is rather a simple one, we showed that the new signatures and production mechanisms led by the Z' are quite peculiar and not shared with any extension of the SM that keeps its gauge content minimal. Finally, the fermion sector can also have very important consequences for the

$B-L$ scalar sector discovery and identification, allowing for peculiar Higgs bosons decay patterns.

In conclusion, we firmly believe that the analysis that we have presented in this Thesis could lay the basis for the phenomenological exploitation of the Higgs sector of the minimal $B-L$ model at present and future colliders, representing a “today’s challenge” for the former’s working schedule and a pressing motivation for the latter’s approval.

For the sake of completeness, it is of fundamental importance to point out the fact that a significative number of open issues is still under investigation: in the first place, one of the next step of our research is to study the phenomenology of the minimal $B-L$ at future photon-photon colliders. Secondly, a whole set of next-to-leading-order corrections should be evaluated both at the LHC and LCs. Thereafter, it should be important to investigate the impact of the mixing between the two $U(1)$ groups, realising the non-minimal $B-L$ model. Finally, one of the most important open issues lies in the supersymmetrisation of the model, for the purpose of making another step of our bottom-up approach, toward the inclusion of the minimal $B-L$ model in a bigger theoretical grand unification picture.

Appendix A

The scalar potential

In this Appendix, we rewrite the interaction part of equation (2.10) in terms of mass eigenstates, separating four-point and three-point functions and classifying them by the nature of the involved fields.

The part of the interacting potential that contains four-point functions involving only would-be Goldstone bosons is:

$$\begin{aligned} V_{4,g} = & \\ - & \frac{\pi\alpha_W (M_{h_1}^2 \cos^2 \alpha + M_{h_2}^2 \sin^2 \alpha)}{8M_W^2} (w^+ w^- + z^2)^2 \\ - & \frac{(g_1')^2 (M_{h_1}^2 \sin^2 \alpha + M_{h_2}^2 \cos^2 \alpha)}{2M_{Z'}^2} (z')^4 \\ - & \frac{\sqrt{\pi\alpha_W} g_1' (M_{h_2}^2 - M_{h_1}^2) \sin(2\alpha)}{4M_W M_{Z'}} (w^+ w^- + z^2)(z')^2. \end{aligned} \tag{A.1}$$

The part of the interacting potential that contains four-point functions involving both would-be Goldstone and Higgs bosons is:

$$\begin{aligned}
V_{4,hg} = & \\
& - \frac{\sqrt{\pi\alpha_W} \cos \alpha}{4M_W^2 M_{Z'}} [2g'_1 (M_{h_2}^2 - M_{h_1}^2) M_W \sin^3 \alpha \\
& + \sqrt{\pi\alpha_W} (M_{h_1}^2 \cos^2 \alpha + M_{h_2}^2 \sin^2 \alpha) M_{Z'} \cos \alpha] h_1^2 (w^+ w^- + z^2) \\
& - \frac{\sqrt{\pi\alpha_W} \sin \alpha}{4M_W^2 M_{Z'}} [2g'_1 (M_{h_2}^2 - M_{h_1}^2) M_W \cos^3 \alpha \\
& + \sqrt{\pi\alpha_W} (M_{h_1}^2 \cos^2 \alpha + M_{h_2}^2 \sin^2 \alpha) M_{Z'} \sin \alpha] h_2^2 (w^+ w^- + z^2) \\
& - \frac{\sqrt{\pi\alpha_W} \sin(2\alpha)}{4M_W^2 M_{Z'}} [g'_1 (M_{h_2}^2 - M_{h_1}^2) M_W \sin(2\alpha) \\
& + \sqrt{\pi\alpha_W} (M_{h_1}^2 \cos^2 \alpha + M_{h_2}^2 \sin^2 \alpha) M_{Z'}] h_1 h_2 (w^+ w^- + z^2) \\
& - \frac{g'_1 \sin \alpha}{2M_W M_{Z'}^2} [-\sqrt{\pi\alpha_W} (M_{h_2}^2 - M_{h_1}^2) M_{Z'} \cos^3 \alpha \\
& + 2g'_1 (M_{h_1}^2 \sin^2 \alpha + M_{h_2}^2 \cos^2 \alpha) M_W \sin \alpha] h_1^2 (z')^2 \\
& - \frac{g'_1 \cos \alpha}{2M_W M_{Z'}^2} [-\sqrt{\pi\alpha_W} (M_{h_2}^2 - M_{h_1}^2) M_{Z'} \sin^3 \alpha \\
& + 2g'_1 (M_{h_1}^2 \sin^2 \alpha + M_{h_2}^2 \cos^2 \alpha) M_W \cos \alpha] h_2^2 (z')^2 \\
& - \frac{g'_1 \sin(2\alpha)}{4M_W M_{Z'}^2} [\sqrt{\pi\alpha_W} (M_{h_2}^2 - M_{h_1}^2) M_{Z'} \sin(2\alpha) \\
& - 4g'_1 (M_{h_1}^2 \sin^2 \alpha + M_{h_2}^2 \cos^2 \alpha) M_W] h_1 h_2 (z')^2. \tag{A.2}
\end{aligned}$$

The part of the interacting potential that contains four-point functions involving only Higgs bosons is:

$$\begin{aligned}
V_{4,h} = & \\
& - \frac{1}{16} \left[\frac{8(g'_1)^2 (M_{h_1}^2 \sin^2 \alpha + M_{h_2}^2 \cos^2 \alpha) \sin^4 \alpha}{M_{Z'}^2} \right. \\
& + \frac{\sqrt{\pi\alpha_W} g'_1 (M_{h_2}^2 - M_{h_1}^2) \sin^3 (2\alpha)}{M_W M_{Z'}} \\
& + \left. \frac{2\pi\alpha_W (M_{h_1}^2 \cos^2 \alpha + M_{h_2}^2 \sin^2 \alpha) \cos^4 \alpha}{M_W^2} \right] h_1^4 \\
& - \frac{\sin (2\alpha)}{4M_W^2 M_{Z'}^2} (2g'_1 M_W \sin \alpha + \sqrt{\pi\alpha_W} M_{Z'} \cos \alpha) \times \\
& \times \left[-2g'_1 (M_{h_1}^2 \sin^2 \alpha + M_{h_2}^2 \cos^2 \alpha) M_W \sin \alpha \right. \\
& + \left. \sqrt{\pi\alpha_W} (M_{h_1}^2 \cos^2 \alpha + M_{h_2}^2 \sin^2 \alpha) M_{Z'} \cos \alpha \right] h_1^3 h_2 \\
& - \frac{\sin (2\alpha)}{16M_W^2 M_{Z'}^2} \left[12(g'_1)^2 (M_{h_1}^2 \sin^2 \alpha + M_{h_2}^2 \cos^2 \alpha) M_W^2 \sin (2\alpha) \right. \\
& + \left. \sqrt{\pi\alpha_W} g'_1 (M_{h_2}^2 - M_{h_1}^2) M_W M_{Z'} (1 + 3 \cos (4\alpha)) \right. \\
& + \left. 3\pi\alpha_W (M_{h_1}^2 \cos^2 \alpha + M_{h_2}^2 \sin^2 \alpha) M_{Z'}^2 \sin (2\alpha) \right] h_1^2 h_2^2 \\
& - \frac{\sin (2\alpha)}{4M_W^2 M_{Z'}^2} (2g'_1 M_W \cos \alpha + \sqrt{\pi\alpha_W} M_{Z'} \sin \alpha) \times \\
& \times \left[-2g'_1 (M_{h_1}^2 \sin^2 \alpha + M_{h_2}^2 \cos^2 \alpha) M_W \cos \alpha \right. \\
& + \left. \sqrt{\pi\alpha_W} (M_{h_1}^2 \cos^2 \alpha + M_{h_2}^2 \sin^2 \alpha) M_{Z'} \sin \alpha \right] h_1 h_2^3 \\
& - \frac{1}{16} \left[\frac{8(g'_1)^2 (M_{h_1}^2 \sin^2 \alpha + M_{h_2}^2 \cos^2 \alpha) \cos^4 \alpha}{M_{Z'}^2} \right. \\
& + \frac{\sqrt{\pi\alpha_W} g'_1 (M_{h_2}^2 - M_{h_1}^2) \sin^3 (2\alpha)}{M_W M_{Z'}} \\
& + \left. \frac{2\pi\alpha_W (M_{h_1}^2 \cos^2 \alpha + M_{h_2}^2 \sin^2 \alpha) \sin^4 \alpha}{M_W^2} \right] h_2^4. \tag{A.3}
\end{aligned}$$

The part of the interacting potential that contains three-point functions involving both would-be Goldstone and Higgs bosons is:

$$\begin{aligned}
V_{3,hg} = & \\
& - \frac{\sqrt{\pi\alpha_W} M_{h_1}^2 \cos \alpha}{2M_W} h_1 (w^+ w^- + z^2) \\
& - \frac{\sqrt{\pi\alpha_W} M_{h_2}^2 \sin \alpha}{2M_W} h_2 (w^+ w^- + z^2) \\
& + \frac{g'_1 M_{h_1}^2 \sin \alpha}{M_{Z'}} h_1 (z')^2 - \frac{g'_1 M_{h_2}^2 \cos \alpha}{M_{Z'}} h_2 (z')^2.
\end{aligned} \tag{A.4}$$

The part of the interacting potential that contains three-point functions involving only Higgs bosons is:

$$\begin{aligned}
V_{3,h} = & \\
& - \frac{M_{h_1}^2}{2} \left(-\frac{2g'_1 \sin^3 \alpha}{M_{Z'}} + \frac{\sqrt{\pi\alpha_W} \cos^3 \alpha}{M_W} \right) h_1^3 \\
& - \frac{\sin(2\alpha)}{4M_W M_{Z'}} (2M_{h_1}^2 + M_{h_2}^2) (2g'_1 M_W \sin \alpha + \sqrt{\pi\alpha_W} M_{Z'} \cos \alpha) h_1^2 h_2 \\
& - \frac{\sin(2\alpha)}{4M_W M_{Z'}} (M_{h_1}^2 + 2M_{h_2}^2) (-2g'_1 M_W \cos \alpha + \sqrt{\pi\alpha_W} M_{Z'} \sin \alpha) h_1 h_2^2 \\
& - \frac{M_{h_2}^2}{2} \left(\frac{2g'_1 \cos^3 \alpha}{M_{Z'}} + \frac{\sqrt{\pi\alpha_W} \sin^3 \alpha}{M_W} \right) h_2^3.
\end{aligned} \tag{A.5}$$

Appendix B

The minimal $B - L$ Feynman rules

In this Appendix we list the Feynman rules of the minimal $B - L$ model in the Feynman-gauge; the labelling of the fields is straightforward, and follows the notation that has been introduced in Chapter 2.

We remark upon the fact that the following list of Feynman rules has been generated by means of the LanHEP package.

All the vertices must be coupled to a phase “ i ”.

All the momenta appearing in the vertices are incoming.

- e is the electric charge.
- $s_w(c_w) \Rightarrow \sin \theta_W(\cos \theta_W)$.
- $s_\alpha(c_\alpha) \Rightarrow \sin \alpha(\cos \alpha)$.
- V is the CKM matrix (see [93, 94]).
- $s_{\alpha i}(c_{\alpha i})$ is the sinus(cosinus) of the “see-saw” mixing of the i^{th} neutrino generation (no mixing between generations has been considered).

Fields in the vertex	Variational derivative of Lagrangian by fields
$A_\mu \quad W_\nu^+ \quad W_\rho^-$	$-e[(p_2^\rho - p_1^\rho)g^{\mu\nu} - (p_2^\mu - p_3^\mu)g^{\nu\rho} + (p_1^\nu - p_3^\nu)g^{\mu\rho}]$
$A_\mu \quad W_\nu^+ \quad w^-$	$ieM_W g^{\mu\nu}$
$A_\mu \quad w^+ \quad W_\nu^-$	$-ieM_W g^{\mu\nu}$
$A_\mu \quad w^+ \quad w^-$	$e(p_3^\mu - p_2^\mu)$
$\bar{C}^A \quad C^{W^+} \quad W_\mu^-$	$-ep_1^\mu$
$\bar{C}^A \quad C^{W^-} \quad W_\mu^+$	ep_1^μ
$\bar{b}_{ap} \quad b_{bq} \quad A_\mu$	$\frac{1}{3}e\delta_{pq}\gamma_{ac}^\mu\delta_{cb}$
$\bar{b}_{ap} \quad b_{bq} \quad G_{\mu r}$	$g_s\lambda_{pq}^r\gamma_{ab}^\mu$
$\bar{b}_{ap} \quad b_{bq} \quad H_1$	$-\frac{1}{2}\frac{c_\alpha e M_b}{M_W s_w}\delta_{pq}\delta_{ab}$
$\bar{b}_{ap} \quad b_{bq} \quad H_2$	$-\frac{1}{2}\frac{e M_b s_\alpha}{M_W s_w}\delta_{pq}\delta_{ab}$
$\bar{b}_{ap} \quad b_{bq} \quad Z_\mu$	$-\frac{1}{6}\frac{e}{c_w s_w}\delta_{pq}\gamma_{ac}^\mu(2s_w^2\frac{(1+\gamma^5)_{cb}}{2} - (3 - 2s_w^2)\frac{(1-\gamma^5)_{cb}}{2})$
$\bar{b}_{ap} \quad b_{bq} \quad z$	$-\frac{1}{2}\frac{ieM_b}{M_W s_w}\delta_{pq}\gamma_{ab}^5$
$\bar{b}_{ap} \quad b_{bq} \quad Z'_\mu$	$-\frac{1}{3}g'_1\delta_{pq}\gamma_{ac}^\mu\delta_{cb}$
$\bar{b}_{ap} \quad c_{bq} \quad W_\mu^-$	$-\frac{1}{2}\frac{e\sqrt{2}V_{cb}}{s_w}\delta_{pq}\gamma_{ac}^\mu\frac{(1-\gamma^5)_{cb}}{2}$
$\bar{b}_{ap} \quad c_{bq} \quad w^-$	$-\frac{1}{2}\frac{ie\sqrt{2}V_{cb}}{M_W s_w}\delta_{pq}(M_b\frac{(1-\gamma^5)_{ab}}{2} - M_c\frac{(1+\gamma^5)_{ab}}{2})$
$\bar{b}_{ap} \quad t_{bq} \quad W_\mu^-$	$-\frac{1}{2}\frac{e\sqrt{2}V_{tb}}{s_w}\delta_{pq}\gamma_{ac}^\mu\frac{(1-\gamma^5)_{cb}}{2}$
$\bar{b}_{ap} \quad t_{bq} \quad w^-$	$-\frac{1}{2}\frac{ie\sqrt{2}V_{tb}}{M_W s_w}\delta_{pq}(M_b\frac{(1-\gamma^5)_{ab}}{2} - M_t\frac{(1+\gamma^5)_{ab}}{2})$
$\bar{b}_{ap} \quad u_{bq} \quad W_\mu^-$	$-\frac{1}{2}\frac{e\sqrt{2}V_{ub}}{s_w}\delta_{pq}\gamma_{ac}^\mu\frac{(1-\gamma^5)_{cb}}{2}$
$\bar{b}_{ap} \quad u_{bq} \quad w^-$	$-\frac{1}{2}\frac{ieM_b\sqrt{2}V_{ub}}{M_W s_w}\delta_{pq}\frac{(1-\gamma^5)_{ab}}{2}$
$\bar{c}_{ap} \quad b_{bq} \quad W_\mu^+$	$-\frac{1}{2}\frac{e\sqrt{2}V_{cb}}{s_w}\delta_{pq}\gamma_{ac}^\mu\frac{(1-\gamma^5)_{cb}}{2}$
$\bar{c}_{ap} \quad b_{bq} \quad w^+$	$\frac{1}{2}\frac{ie\sqrt{2}V_{cb}}{M_W s_w}\delta_{pq}(M_b\frac{(1+\gamma^5)_{ab}}{2} - M_c\frac{(1-\gamma^5)_{ab}}{2})$
$\bar{c}_{ap} \quad c_{bq} \quad A_\mu$	$-\frac{2}{3}e\delta_{pq}\gamma_{ac}^\mu\delta_{cb}$
$\bar{c}_{ap} \quad c_{bq} \quad G_{\mu r}$	$g_s\lambda_{pq}^r\gamma_{ab}^\mu$
$\bar{c}_{ap} \quad c_{bq} \quad H_1$	$-\frac{1}{2}\frac{c_\alpha e M_c}{M_W s_w}\delta_{pq}\delta_{ab}$
$\bar{c}_{ap} \quad c_{bq} \quad H_2$	$-\frac{1}{2}\frac{e M_c s_\alpha}{M_W s_w}\delta_{pq}\delta_{ab}$

Fields in the vertex	Variational derivative of Lagrangian by fields
$\bar{c}_{ap} \quad c_{bq} \quad Z_\mu$	$-\frac{1}{6} \frac{e}{c_w s_w} \delta_{pq} \gamma_{ac}^\mu \left((3 - 4s_w^2) \frac{(1-\gamma^5)_{cb}}{2} - 4s_w^2 \frac{(1+\gamma^5)_{cb}}{2} \right)$
$\bar{c}_{ap} \quad c_{bq} \quad z$	$\frac{1}{2} \frac{ieM_c}{M_W s_w} \delta_{pq} \gamma_{ab}^5$
$\bar{c}_{ap} \quad c_{bq} \quad Z'_\mu$	$-\frac{1}{3} g'_1 \delta_{pq} \gamma_{ac}^\mu \delta_{cb}$
$\bar{c}_{ap} \quad d_{bq} \quad W_\mu^+$	$-\frac{1}{2} \frac{e\sqrt{2}V_{cd}}{s_w} \delta_{pq} \gamma_{ac}^\mu \frac{(1-\gamma^5)_{cb}}{2}$
$\bar{c}_{ap} \quad d_{bq} \quad w^+$	$-\frac{1}{2} \frac{ieM_c\sqrt{2}V_{cd}}{M_W s_w} \delta_{pq} \frac{(1-\gamma^5)_{ab}}{2}$
$\bar{c}_{ap} \quad s_{bq} \quad W_\mu^+$	$-\frac{1}{2} \frac{e\sqrt{2}V_{cs}}{s_w} \delta_{pq} \gamma_{ac}^\mu \frac{(1-\gamma^5)_{cb}}{2}$
$\bar{c}_{ap} \quad s_{bq} \quad w^+$	$\frac{1}{2} \frac{ie\sqrt{2}V_{cs}}{M_W s_w} \delta_{pq} \left(M_s \frac{(1+\gamma^5)_{ab}}{2} - M_c \frac{(1-\gamma^5)_{ab}}{2} \right)$
$\bar{d}_{ap} \quad c_{bq} \quad W_\mu^-$	$-\frac{1}{2} \frac{e\sqrt{2}V_{cd}}{s_w} \delta_{pq} \gamma_{ac}^\mu \frac{(1-\gamma^5)_{cb}}{2}$
$\bar{d}_{ap} \quad c_{bq} \quad w^-$	$\frac{1}{2} \frac{ieM_c\sqrt{2}V_{cd}}{M_W s_w} \delta_{pq} \frac{(1+\gamma^5)_{ab}}{2}$
$\bar{d}_{ap} \quad d_{bq} \quad A_\mu$	$\frac{1}{3} e \delta_{pq} \gamma_{ac}^\mu \delta_{cb}$
$\bar{d}_{ap} \quad d_{bq} \quad G_{\mu r}$	$g_s \lambda_{pq}^r \gamma_{ab}^\mu$
$\bar{d}_{ap} \quad d_{bq} \quad Z_\mu$	$-\frac{1}{6} \frac{e}{c_w s_w} \delta_{pq} \gamma_{ac}^\mu \left(2s_w^2 \frac{(1+\gamma^5)_{cb}}{2} - (3 - 2s_w^2) \frac{(1-\gamma^5)_{cb}}{2} \right)$
$\bar{d}_{ap} \quad d_{bq} \quad Z'_\mu$	$-\frac{1}{3} g'_1 \delta_{pq} \gamma_{ac}^\mu \delta_{cb}$
$\bar{d}_{ap} \quad t_{bq} \quad W_\mu^-$	$-\frac{1}{2} \frac{e\sqrt{2}V_{td}}{s_w} \delta_{pq} \gamma_{ac}^\mu \frac{(1-\gamma^5)_{cb}}{2}$
$\bar{d}_{ap} \quad t_{bq} \quad w^-$	$\frac{1}{2} \frac{ieM_t\sqrt{2}V_{td}}{M_W s_w} \delta_{pq} \frac{(1+\gamma^5)_{ab}}{2}$
$\bar{d}_{ap} \quad u_{bq} \quad W_\mu^-$	$-\frac{1}{2} \frac{e\sqrt{2}V_{ud}}{s_w} \delta_{pq} \gamma_{ac}^\mu \frac{(1-\gamma^5)_{cb}}{2}$
$\bar{e}_a \quad e_b \quad A_\mu$	$e \gamma_{ac}^\mu \delta_{cb}$
$\bar{e}_a \quad e_b \quad H_1$	$-\frac{1}{2} \frac{c_\alpha e M_e}{M_W s_w} \delta_{ab}$
$\bar{e}_a \quad e_b \quad H_2$	$-\frac{1}{2} \frac{e M_e s_\alpha}{M_W s_w} \delta_{ab}$
$\bar{e}_a \quad e_b \quad Z_\mu$	$\frac{1}{2} \frac{e}{c_w s_w} \gamma_{ac}^\mu \left((1 - 2s_w^2) \frac{(1-\gamma^5)_{cb}}{2} - 2s_w^2 \frac{(1+\gamma^5)_{cb}}{2} \right)$
$\bar{e}_a \quad e_b \quad z$	$-\frac{1}{2} \frac{ieM_e}{M_W s_w} \gamma_{ab}^5$
$\bar{e}_a \quad e_b \quad Z'_\mu$	$g'_1 \gamma_{ac}^\mu \delta_{cb}$
$\bar{e}_a \quad \nu_{b1}^1 \quad W_\mu^-$	$-\frac{1}{2} \frac{c_{a1} e \sqrt{2}}{s_w} \gamma_{ac}^\mu \frac{(1-\gamma^5)_{cb}}{2}$
$\bar{e}_a \quad \nu_{b1}^1 \quad w^-$	$-\frac{1}{2} \frac{i}{M_W s_w} \left(c_{a1} e M_e \sqrt{2} \frac{(1-\gamma^5)_{ab}}{2} + 2s_w s_{a1} M_W y_1^\nu \frac{(1+\gamma^5)_{ab}}{2} \right)$
$\bar{e}_a \quad \nu_{b1}^1 \quad W_\mu^-$	$-\frac{1}{2} \frac{e s_{a1} \sqrt{2}}{s_w} \gamma_{ac}^\mu \frac{(1-\gamma^5)_{cb}}{2}$

Fields in the vertex	Variational derivative of Lagrangian by fields
$\bar{e}_a \quad \nu h_b^1 \quad w^-$	$-\frac{1}{2} \frac{i}{M_W s_w} (s_{a1} e M_e \sqrt{2} \frac{(1-\gamma^5)_{ab}}{2} - 2 s_w c_{a1} M_W y_1^\nu \frac{(1+\gamma^5)_{ab}}{2})$
$G_{\mu p} \quad G_{\nu q} \quad G_{\rho r}$	$g_s f_{pqr} [(p_3^\nu - p_1^\nu) g^{\mu\rho} - (p_3^\mu - p_2^\mu) g^{\nu\rho} + (p_1^\rho - p_2^\rho) g^{\mu\nu}]$
$\bar{C}_p^G \quad C_q^G \quad G_{\mu r}$	$g_s p_2^\mu f_{pqr}$
$H_1 \quad H_1 \quad H_1$	$-3 \frac{1}{e} (4 c_\alpha^3 s_w M_W \lambda_1 - 2 s_\alpha^3 e \lambda_2 x - c_\alpha^2 s_\alpha e \lambda_3 x$ $+ 2 s_w s_\alpha^2 c_\alpha M_W \lambda_3)$
$H_1 \quad H_1 \quad H_2$	$-\frac{1}{e} (12 c_\alpha^2 s_w s_\alpha M_W \lambda_1 + 6 s_\alpha^2 c_\alpha e \lambda_2 x + (1 - 3 s_\alpha^2) c_\alpha e \lambda_3 x$ $- 2(2 - 3 s_\alpha^2) s_w s_\alpha M_W \lambda_3)$
$H_1 \quad H_2 \quad H_2$	$-\frac{1}{e} (12 s_w s_\alpha^2 c_\alpha M_W \lambda_1 - 6 c_\alpha^2 s_\alpha e \lambda_2 x + (2 - 3 s_\alpha^2) s_\alpha e \lambda_3 x$ $+ 2(1 - 3 s_\alpha^2) s_w c_\alpha M_W \lambda_3)$
$H_1 \quad W_\mu^+ \quad W_\nu^-$	$\frac{c_\alpha e M_W}{s_w} g^{\mu\nu}$
$H_1 \quad W_\mu^+ \quad w^-$	$\frac{1}{2} \frac{i c_\alpha e}{s_w} (p_3^\mu - p_1^\mu)$
$H_1 \quad w^+ \quad W_\mu^-$	$-\frac{1}{2} \frac{i c_\alpha e}{s_w} (p_1^\mu - p_2^\mu)$
$H_1 \quad w^+ \quad w^-$	$-\frac{1}{e} (4 s_w c_\alpha M_W \lambda_1 - s_\alpha e \lambda_3 x)$
$H_1 \quad Z_\mu \quad Z_\nu$	$\frac{c_\alpha e M_W}{c_w^2 s_w} g^{\mu\nu}$
$H_1 \quad Z_\mu \quad z$	$\frac{1}{2} \frac{i c_\alpha e}{c_w s_w} (p_3^\mu - p_1^\mu)$
$H_1 \quad z \quad z$	$-\frac{1}{e} (4 s_w c_\alpha M_W \lambda_1 - s_\alpha e \lambda_3 x)$
$H_1 \quad Z'_\mu \quad Z'_\nu$	$-8 s_\alpha g_1'^2 x g^{\mu\nu}$
$H_1 \quad Z'_\mu \quad z'$	$-2 i s_\alpha g_1' (p_1^\mu - p_3^\mu)$
$H_1 \quad z' \quad z'$	$2 \frac{1}{e} (s_\alpha e \lambda_2 x - s_w c_\alpha M_W \lambda_3)$
$H_2 \quad H_2 \quad H_2$	$-3 \frac{1}{e} (4 s_w s_\alpha^3 M_W \lambda_1 + 2 c_\alpha^3 e \lambda_2 x + s_\alpha^2 c_\alpha e \lambda_3 x$ $+ 2 c_\alpha^2 s_w s_\alpha M_W \lambda_3)$
$H_2 \quad W_\mu^+ \quad W_\nu^-$	$\frac{e M_W s_\alpha}{s_w} g^{\mu\nu}$
$H_2 \quad W_\mu^+ \quad w^-$	$\frac{1}{2} \frac{i e s_\alpha}{s_w} (p_3^\mu - p_1^\mu)$
$H_2 \quad w^+ \quad W_\mu^-$	$-\frac{1}{2} \frac{i e s_\alpha}{s_w} (p_1^\mu - p_2^\mu)$
$H_2 \quad w^+ \quad w^-$	$-\frac{1}{e} (4 s_w s_\alpha M_W \lambda_1 + c_\alpha e \lambda_3 x)$

Fields in the vertex	Variational derivative of Lagrangian by fields
$H_2 \quad Z_\mu \quad Z_\nu$	$\frac{eM_W s_\alpha}{c_w^2 s_w} g^{\mu\nu}$
$H_2 \quad Z_\mu \quad z$	$\frac{1}{2} \frac{ies_\alpha}{c_w s_w} (p_3^\mu - p_1^\mu)$
$H_2 \quad z \quad z$	$-\frac{1}{e} (4s_w s_\alpha M_W \lambda_1 + c_\alpha e \lambda_3 x)$
$H_2 \quad Z'_\mu \quad Z'_\nu$	$8c_\alpha g_1'^2 x g^{\mu\nu}$
$H_2 \quad Z'_\mu \quad z'$	$2ic_\alpha g_1' (p_1^\mu - p_3^\mu)$
$H_2 \quad z' \quad z'$	$-2\frac{1}{e} (c_\alpha e \lambda_2 x + s_w s_\alpha M_W \lambda_3)$
$\bar{\tau}_a \quad \tau_b \quad A_\mu$	$e\gamma_{ac}^\mu \delta_{cb}$
$\bar{\tau}_a \quad \tau_b \quad H_1$	$-\frac{1}{2} \frac{c_\alpha e M_\tau}{M_W s_w} \delta_{ab}$
$\bar{\tau}_a \quad \tau_b \quad H_2$	$-\frac{1}{2} \frac{e M_\tau s_\alpha}{M_W s_w} \delta_{ab}$
$\bar{\tau}_a \quad \tau_b \quad Z_\mu$	$\frac{1}{2} \frac{e}{c_w s_w} \gamma_{ac}^\mu \left((1 - 2s_w^2) \frac{(1-\gamma^5)_{cb}}{2} - 2s_w^2 \frac{(1+\gamma^5)_{cb}}{2} \right)$
$\bar{\tau}_a \quad \tau_b \quad z$	$-\frac{1}{2} \frac{ieM_\tau}{M_W s_w} \gamma_{ab}^5$
$\bar{\tau}_a \quad \tau_b \quad Z'_\mu$	$g_1' \gamma_{ac}^\mu \delta_{cb}$
$\bar{\tau}_a \quad \nu l_b^3 \quad W_\mu^-$	$-\frac{1}{2} \frac{c_{a3} e \sqrt{2}}{s_w} \gamma_{ac}^\mu \frac{(1-\gamma^5)_{cb}}{2}$
$\bar{\tau}_a \quad \nu l_b^3 \quad w^-$	$-\frac{1}{2} \frac{i}{M_W s_w} (c_{a3} e M_\tau \sqrt{2} \frac{(1-\gamma^5)_{ab}}{2} + 2s_w s_{a3} M_W y_3^\nu \frac{(1+\gamma^5)_{ab}}{2})$
$\bar{\tau}_a \quad \nu h_b^3 \quad W_\mu^-$	$-\frac{1}{2} \frac{es_{a3} \sqrt{2}}{s_w} \gamma_{ac}^\mu \frac{(1-\gamma^5)_{cb}}{2}$
$\bar{\tau}_a \quad \nu h_b^3 \quad w^-$	$-\frac{1}{2} \frac{i}{M_W s_w} (s_{a3} e M_\tau \sqrt{2} \frac{(1-\gamma^5)_{ab}}{2} - 2s_w c_{a3} M_W y_3^\nu \frac{(1+\gamma^5)_{ab}}{2})$
$\bar{\mu}_a \quad \mu_b \quad A_\mu$	$e\gamma_{ac}^\mu \delta_{cb}$
$\bar{\mu}_a \quad \mu_b \quad H_1$	$-\frac{1}{2} \frac{c_\alpha e M_\mu}{M_W s_w} \delta_{ab}$
$\bar{\mu}_a \quad \mu_b \quad H_2$	$-\frac{1}{2} \frac{e M_\mu s_\alpha}{M_W s_w} \delta_{ab}$
$\bar{\mu}_a \quad \mu_b \quad Z_\mu$	$\frac{1}{2} \frac{e}{c_w s_w} \gamma_{ac}^\mu \left((1 - 2s_w^2) \frac{(1-\gamma^5)_{cb}}{2} - 2s_w^2 \frac{(1+\gamma^5)_{cb}}{2} \right)$
$\bar{\mu}_a \quad \mu_b \quad z$	$-\frac{1}{2} \frac{ieM_\mu}{M_W s_w} \gamma_{ab}^5$
$\bar{\mu}_a \quad \mu_b \quad Z'_\mu$	$g_1' \gamma_{ac}^\mu \delta_{cb}$
$\bar{\mu}_a \quad \nu l_b^2 \quad W_\mu^-$	$-\frac{1}{2} \frac{c_{a2} e \sqrt{2}}{s_w} \gamma_{ac}^\mu \frac{(1-\gamma^5)_{cb}}{2}$
$\bar{\mu}_a \quad \nu l_b^2 \quad w^-$	$-\frac{1}{2} \frac{i}{M_W s_w} (c_{a2} e M_\mu \sqrt{2} \frac{(1-\gamma^5)_{ab}}{2} + 2s_w s_{a2} M_W y_2^\nu \frac{(1+\gamma^5)_{ab}}{2})$
$\bar{\mu}_a \quad \nu h_b^2 \quad W_\mu^-$	$-\frac{1}{2} \frac{es_{a2} \sqrt{2}}{s_w} \gamma_{ac}^\mu \frac{(1-\gamma^5)_{cb}}{2}$

Fields in the vertex	Variational derivative of Lagrangian by fields
$\bar{\mu}_a \quad \nu h_b^2 \quad w^-$	$-\frac{1}{2} \frac{i}{M_W s_w} (s_a e M_\mu \sqrt{2} \frac{(1-\gamma^5)_{ab}}{2} - 2s_w c_a e M_W y_2^\nu \frac{(1+\gamma^5)_{ab}}{2})$
$\bar{s}_{ap} \quad c_{bq} \quad W_\mu^-$	$-\frac{1}{2} \frac{e\sqrt{2}V_{cs}}{s_w} \delta_{pq} \gamma_{ac}^\mu \frac{(1-\gamma^5)_{cb}}{2}$
$\bar{s}_{ap} \quad c_{bq} \quad w^-$	$-\frac{1}{2} \frac{ie\sqrt{2}V_{cs}}{M_W s_w} \delta_{pq} (M_s \frac{(1-\gamma^5)_{ab}}{2} - M_c \frac{(1+\gamma^5)_{ab}}{2})$
$\bar{s}_{ap} \quad s_{bq} \quad A_\mu$	$\frac{1}{3} e \delta_{pq} \gamma_{ac}^\mu \delta_{cb}$
$\bar{s}_{ap} \quad s_{bq} \quad G_{\mu r}$	$g_s \lambda_{pq}^r \gamma_{ab}^\mu$
$\bar{s}_{ap} \quad s_{bq} \quad H_1$	$-\frac{1}{2} \frac{c_\alpha e M_s}{M_W s_w} \delta_{pq} \delta_{ab}$
$\bar{s}_{ap} \quad s_{bq} \quad H_2$	$-\frac{1}{2} \frac{e M_s s_\alpha}{M_W s_w} \delta_{pq} \delta_{ab}$
$\bar{s}_{ap} \quad s_{bq} \quad Z_\mu$	$-\frac{1}{6} \frac{e}{c_w s_w} \delta_{pq} \gamma_{ac}^\mu (2s_w^2 \frac{(1+\gamma^5)_{cb}}{2} - (3 - 2s_w^2) \frac{(1-\gamma^5)_{cb}}{2})$
$\bar{s}_{ap} \quad s_{bq} \quad z$	$-\frac{1}{2} \frac{ieM_s}{M_W s_w} \delta_{pq} \gamma_{ab}^5$
$\bar{s}_{ap} \quad s_{bq} \quad Z'_\mu$	$-\frac{1}{3} g_1' \delta_{pq} \gamma_{ac}^\mu \delta_{cb}$
$\bar{s}_{ap} \quad t_{bq} \quad W_\mu^-$	$-\frac{1}{2} \frac{e\sqrt{2}V_{ts}}{s_w} \delta_{pq} \gamma_{ac}^\mu \frac{(1-\gamma^5)_{cb}}{2}$
$\bar{s}_{ap} \quad t_{bq} \quad w^-$	$-\frac{1}{2} \frac{ie\sqrt{2}V_{ts}}{M_W s_w} \delta_{pq} (M_s \frac{(1-\gamma^5)_{ab}}{2} - M_t \frac{(1+\gamma^5)_{ab}}{2})$
$\bar{s}_{ap} \quad u_{bq} \quad W_\mu^-$	$-\frac{1}{2} \frac{e\sqrt{2}V_{us}}{s_w} \delta_{pq} \gamma_{ac}^\mu \frac{(1-\gamma^5)_{cb}}{2}$
$\bar{s}_{ap} \quad u_{bq} \quad w^-$	$-\frac{1}{2} \frac{ieM_s \sqrt{2}V_{us}}{M_W s_w} \delta_{pq} \frac{(1-\gamma^5)_{ab}}{2}$
$\bar{t}_{ap} \quad b_{bq} \quad W_\mu^+$	$-\frac{1}{2} \frac{e\sqrt{2}V_{tb}}{s_w} \delta_{pq} \gamma_{ac}^\mu \frac{(1-\gamma^5)_{cb}}{2}$
$\bar{t}_{ap} \quad b_{bq} \quad w^+$	$\frac{1}{2} \frac{ie\sqrt{2}V_{tb}}{M_W s_w} \delta_{pq} (M_b \frac{(1+\gamma^5)_{ab}}{2} - M_t \frac{(1-\gamma^5)_{ab}}{2})$
$\bar{t}_{ap} \quad d_{bq} \quad W_\mu^+$	$-\frac{1}{2} \frac{e\sqrt{2}V_{td}}{s_w} \delta_{pq} \gamma_{ac}^\mu \frac{(1-\gamma^5)_{cb}}{2}$
$\bar{t}_{ap} \quad d_{bq} \quad w^+$	$-\frac{1}{2} \frac{ieM_t \sqrt{2}V_{td}}{M_W s_w} \delta_{pq} \frac{(1-\gamma^5)_{ab}}{2}$
$\bar{t}_{ap} \quad s_{bq} \quad W_\mu^+$	$-\frac{1}{2} \frac{e\sqrt{2}V_{ts}}{s_w} \delta_{pq} \gamma_{ac}^\mu \frac{(1-\gamma^5)_{cb}}{2}$
$\bar{t}_{ap} \quad s_{bq} \quad w^+$	$\frac{1}{2} \frac{ie\sqrt{2}V_{ts}}{M_W s_w} \delta_{pq} (M_s \frac{(1+\gamma^5)_{ab}}{2} - M_t \frac{(1-\gamma^5)_{ab}}{2})$
$\bar{t}_{ap} \quad t_{bq} \quad A_\mu$	$-\frac{2}{3} e \delta_{pq} \gamma_{ac}^\mu \delta_{cb}$
$\bar{t}_{ap} \quad t_{bq} \quad G_{\mu r}$	$g_s \lambda_{pq}^r \gamma_{ab}^\mu$
$\bar{t}_{ap} \quad t_{bq} \quad H_1$	$-\frac{1}{2} \frac{c_\alpha e M_t}{M_W s_w} \delta_{pq} \delta_{ab}$
$\bar{t}_{ap} \quad t_{bq} \quad H_2$	$-\frac{1}{2} \frac{e M_t s_\alpha}{M_W s_w} \delta_{pq} \delta_{ab}$
$\bar{t}_{ap} \quad t_{bq} \quad Z_\mu$	$-\frac{1}{6} \frac{e}{c_w s_w} \delta_{pq} \gamma_{ac}^\mu ((3 - 4s_w^2) \frac{(1-\gamma^5)_{cb}}{2} - 4s_w^2 \frac{(1+\gamma^5)_{cb}}{2})$

Fields in the vertex	Variational derivative of Lagrangian by fields
$\bar{t}_{ap} \quad t_{bq} \quad z$	$\frac{1}{2} \frac{ieM_t}{M_W s_w} \delta_{pq} \gamma_{ab}^5$
$\bar{t}_{ap} \quad t_{bq} \quad Z'_\mu$	$-\frac{1}{3} g_1' \delta_{pq} \gamma_{ac}^\mu \delta_{cb}$
$\bar{u}_{ap} \quad b_{bq} \quad W_\mu^+$	$-\frac{1}{2} \frac{e\sqrt{2}V_{ub}}{s_w} \delta_{pq} \gamma_{ac}^\mu \frac{(1-\gamma^5)_{cb}}{2}$
$\bar{u}_{ap} \quad b_{bq} \quad w^+$	$\frac{1}{2} \frac{ieM_b \sqrt{2}V_{ub}}{M_W s_w} \delta_{pq} \frac{(1+\gamma^5)_{ab}}{2}$
$\bar{u}_{ap} \quad d_{bq} \quad W_\mu^+$	$-\frac{1}{2} \frac{e\sqrt{2}V_{ud}}{s_w} \delta_{pq} \gamma_{ac}^\mu \frac{(1-\gamma^5)_{cb}}{2}$
$\bar{u}_{ap} \quad s_{bq} \quad W_\mu^+$	$-\frac{1}{2} \frac{e\sqrt{2}V_{us}}{s_w} \delta_{pq} \gamma_{ac}^\mu \frac{(1-\gamma^5)_{cb}}{2}$
$\bar{u}_{ap} \quad s_{bq} \quad w^+$	$\frac{1}{2} \frac{ieM_s \sqrt{2}V_{us}}{M_W s_w} \delta_{pq} \frac{(1+\gamma^5)_{ab}}{2}$
$\bar{u}_{ap} \quad u_{bq} \quad A_\mu$	$-\frac{2}{3} e \delta_{pq} \gamma_{ac}^\mu \delta_{cb}$
$\bar{u}_{ap} \quad u_{bq} \quad G_{\mu r}$	$g_s \lambda_{pq}^r \gamma_{ab}^\mu$
$\bar{u}_{ap} \quad u_{bq} \quad Z_\mu$	$-\frac{1}{6} \frac{e}{c_w s_w} \delta_{pq} \gamma_{ac}^\mu \left((3 - 4s_w^2) \frac{(1-\gamma^5)_{cb}}{2} - 4s_w^2 \frac{(1+\gamma^5)_{cb}}{2} \right)$
$\bar{u}_{ap} \quad u_{bq} \quad Z'_\mu$	$-\frac{1}{3} g_1' \delta_{pq} \gamma_{ac}^\mu \delta_{cb}$
$W_\mu^+ \quad W_\nu^- \quad Z_\rho$	$-\frac{c_w e}{s_w} [(p_1^\nu - p_3^\nu) g^{\mu\rho} - (p_1^\rho - p_2^\rho) g^{\mu\nu} - (p_2^\mu - p_3^\mu) g^{\nu\rho}]$
$W_\mu^+ \quad w^- \quad Z_\nu$	$-\frac{ieM_W s_w}{c_w} g^{\mu\nu}$
$W_\mu^+ \quad w^- \quad z$	$-\frac{1}{2} \frac{e}{s_w} (p_2^\mu - p_3^\mu)$
$\bar{C}^{W^+} \quad C^Z \quad W_\mu^-$	ep_1^μ
$\bar{C}^{W^+} \quad C^Z \quad w^-$	$-ieM_W$
$\bar{C}^{W^+} \quad C^{W^-} \quad A_\mu$	$-ep_1^\mu$
$\bar{C}^{W^+} \quad C^{W^-} \quad H_1$	$-\frac{1}{2} \frac{c_\alpha e M_W}{s_w}$
$\bar{C}^{W^+} \quad C^{W^-} \quad H_2$	$-\frac{1}{2} \frac{e M_W s_\alpha}{s_w}$
$\bar{C}^{W^+} \quad C^{W^-} \quad Z_\mu$	$-\frac{c_w e}{s_w} p_1^\mu$
$\bar{C}^{W^+} \quad C^{W^-} \quad z$	$\frac{1}{2} \frac{ieM_W}{s_w}$
$\bar{C}^{W^+} \quad C^Z \quad W_\mu^-$	$\frac{c_w e}{s_w} p_1^\mu$
$\bar{C}^{W^+} \quad C^Z \quad w^-$	$-\frac{1}{2} \frac{i(1-2s_w^2)eM_W}{c_w s_w}$
$w^+ \quad W_\mu^- \quad Z_\nu$	$\frac{ieM_W s_w}{c_w} g^{\mu\nu}$
$w^+ \quad W_\mu^- \quad z$	$-\frac{1}{2} \frac{e}{s_w} (p_3^\mu - p_1^\mu)$

Fields in the vertex	Variational derivative of Lagrangian by fields
$w^+ \quad w^- \quad Z_\mu$	$\frac{1}{2} \frac{(1-2s_w^2)e}{c_w s_w} (p_2^\mu - p_1^\mu)$
$\bar{C}^{W^-} \quad C^Z \quad W_\mu^+$	$-ep_1^\mu$
$\bar{C}^{W^-} \quad C^Z \quad w^+$	ieM_W
$\bar{C}^{W^-} \quad C^{W^+} \quad A_\mu$	ep_1^μ
$\bar{C}^{W^-} \quad C^{W^+} \quad H_1$	$-\frac{1}{2} \frac{c_\alpha e M_W}{s_w}$
$\bar{C}^{W^-} \quad C^{W^+} \quad H_2$	$-\frac{1}{2} \frac{e M_W s_\alpha}{s_w}$
$\bar{C}^{W^-} \quad C^{W^+} \quad Z_\mu$	$\frac{c_w e}{s_w} p_1^\mu$
$\bar{C}^{W^-} \quad C^{W^+} \quad z$	$-\frac{1}{2} \frac{ieM_W}{s_w}$
$\bar{C}^{W^-} \quad C^Z \quad W_\mu^+$	$-\frac{c_w e}{s_w} p_1^\mu$
$\bar{C}^{W^-} \quad C^Z \quad w^+$	$\frac{1}{2} \frac{i(1-2s_w^2)eM_W}{c_w s_w}$
$\bar{C}^Z \quad C^{W^+} \quad W_\mu^-$	$-\frac{c_w e}{s_w} p_1^\mu$
$\bar{C}^Z \quad C^{W^+} \quad w^-$	$\frac{1}{2} \frac{ieM_W}{c_w s_w}$
$\bar{C}^Z \quad C^{W^-} \quad W_\mu^+$	$\frac{c_w e}{s_w} p_1^\mu$
$\bar{C}^Z \quad C^{W^-} \quad w^+$	$-\frac{1}{2} \frac{ieM_W}{c_w s_w}$
$\bar{C}^Z \quad C^Z \quad H_1$	$-\frac{1}{2} \frac{c_\alpha e M_W}{c_w^2 s_w}$
$\bar{C}^Z \quad C^Z \quad H_2$	$-\frac{1}{2} \frac{e M_W s_\alpha}{c_w^2 s_w}$
$\bar{C}^{Z'} \quad C^{Z'} \quad H_1$	$2M_{Z_{B-L}} s_\alpha g'_1$
$\bar{C}^{Z'} \quad C^{Z'} \quad H_2$	$-2c_\alpha M_{Z_{B-L}} g'_1$
$e_a^c \quad \nu l_b^1 \quad W_\mu^+$	$\frac{1}{2} \frac{c_{a1} e \sqrt{2}}{s_w} \gamma_{ac}^\mu \frac{(1+\gamma^5)_{cb}}{2}$
$e_a^c \quad \nu l_b^1 \quad w^+$	$\frac{1}{2} \frac{i}{M_W s_w} (c_{a1} e M_e \sqrt{2} \frac{(1+\gamma^5)_{ab}}{2} + 2s_w s_{a1} M_W y_1^\nu \frac{(1-\gamma^5)_{ab}}{2})$
$e_a^c \quad \nu h_b^1 \quad W_\mu^+$	$\frac{1}{2} \frac{e s_{a1} \sqrt{2}}{s_w} \gamma_{ac}^\mu \frac{(1+\gamma^5)_{cb}}{2}$
$e_a^c \quad \nu h_b^1 \quad w^+$	$\frac{1}{2} \frac{i}{M_W s_w} (s_{a1} e M_e \sqrt{2} \frac{(1+\gamma^5)_{ab}}{2} - 2s_w c_{a1} M_W y_1^\nu \frac{(1-\gamma^5)_{ab}}{2})$
$\tau_a^c \quad \nu l_b^3 \quad W_\mu^+$	$\frac{1}{2} \frac{c_{a3} e \sqrt{2}}{s_w} \gamma_{ac}^\mu \frac{(1+\gamma^5)_{cb}}{2}$
$\tau_a^c \quad \nu l_b^3 \quad w^+$	$\frac{1}{2} \frac{i}{M_W s_w} (c_{a3} e M_\tau \sqrt{2} \frac{(1+\gamma^5)_{ab}}{2} + 2s_w s_{a3} M_W y_3^\nu \frac{(1-\gamma^5)_{ab}}{2})$
$\tau_a^c \quad \nu h_b^3 \quad W_\mu^+$	$\frac{1}{2} \frac{e s_{a3} \sqrt{2}}{s_w} \gamma_{ac}^\mu \frac{(1+\gamma^5)_{cb}}{2}$

Fields in the vertex	Variational derivative of Lagrangian by fields
$\tau_a^c \quad \nu h_b^3 \quad w^+$	$\frac{1}{2} \frac{i}{M_W s_w} (s_{a3} e M_\tau \sqrt{2} \frac{(1+\gamma^5)_{ab}}{2} - 2s_w c_{a3} M_W y_3^\nu \frac{(1-\gamma^5)_{ab}}{2})$
$\mu_a^c \quad \nu l_b^2 \quad W_\mu^+$	$\frac{1}{2} \frac{c_{a2} e \sqrt{2}}{s_w} \gamma_{ac}^\mu \frac{(1+\gamma^5)_{cb}}{2}$
$\mu_a^c \quad \nu l_b^2 \quad w^+$	$\frac{1}{2} \frac{i}{M_W s_w} (c_{a2} e M_\mu \sqrt{2} \frac{(1+\gamma^5)_{ab}}{2} + 2s_w s_{a2} M_W y_2^\nu \frac{(1-\gamma^5)_{ab}}{2})$
$\mu_a^c \quad \nu h_b^2 \quad W_\mu^+$	$\frac{1}{2} \frac{e s_{a2} \sqrt{2}}{s_w} \gamma_{ac}^\mu \frac{(1+\gamma^5)_{cb}}{2}$
$\mu_a^c \quad \nu h_b^2 \quad w^+$	$\frac{1}{2} \frac{i}{M_W s_w} (s_{a2} e M_\mu \sqrt{2} \frac{(1+\gamma^5)_{ab}}{2} - 2s_w c_{a2} M_W y_2^\nu \frac{(1-\gamma^5)_{ab}}{2})$
$\nu l_a^1 \quad \nu l_b^1 \quad H_1$	$\frac{s_{a1}}{x} (c_\alpha c_{a1} \sqrt{2} x y_1^\nu \delta_{ab} + s_\alpha s_{a1} M_{\nu_1} \delta_{ab})$
$\nu l_a^1 \quad \nu l_b^1 \quad H_2$	$\frac{s_{a1}}{x} (s_\alpha c_{a1} \sqrt{2} x y_1^\nu \delta_{ab} - s_{a1} c_\alpha M_{\nu_1} \delta_{ab})$
$\nu l_a^1 \quad \nu l_b^1 \quad Z_\mu$	$\frac{1}{2} \frac{c_{a1}^2 e}{c_w s_w} \gamma_{ac}^\mu \gamma_{cb}^5$
$\nu l_a^1 \quad \nu l_b^1 \quad z$	$-i c_{a1} s_{a1} \sqrt{2} y_1^\nu \gamma_{ab}^5$
$\nu l_a^1 \quad \nu l_b^1 \quad Z'_\mu$	$-(1 - 2s_{a1}^2) g_1' \gamma_{ac}^\mu \gamma_{cb}^5$
$\nu l_a^1 \quad \nu l_b^1 \quad z'$	$-\frac{i M_{\nu_1} s_{a1}^2}{x} \gamma_{ab}^5$
$\nu l_a^1 \quad \nu h_b^1 \quad H_1$	$-\frac{1}{2} \frac{1}{x} ((1 - 2s_{a1}^2) c_\alpha \sqrt{2} x y_1^\nu \delta_{ab} + 2s_\alpha s_{a1} c_{a1} M_{\nu_1} \delta_{ab})$
$\nu l_a^1 \quad \nu h_b^1 \quad H_2$	$-\frac{1}{2} \frac{1}{x} ((1 - 2s_{a1}^2) s_\alpha \sqrt{2} x y_1^\nu \delta_{ab} - 2s_{a1} c_\alpha c_{a1} M_{\nu_1} \delta_{ab})$
$\nu l_a^1 \quad \nu h_b^1 \quad Z_\mu$	$\frac{1}{2} \frac{c_{a1} e s_{a1}}{c_w s_w} \gamma_{ac}^\mu \gamma_{cb}^5$
$\nu l_a^1 \quad \nu h_b^1 \quad z$	$\frac{1}{2} i (1 - 2s_{a1}^2) \sqrt{2} y_1^\nu \gamma_{ab}^5$
$\nu l_a^1 \quad \nu h_b^1 \quad Z'_\mu$	$-2c_{a1} s_{a1} g_1' \gamma_{ac}^\mu \gamma_{cb}^5$
$\nu l_a^1 \quad \nu h_b^1 \quad z'$	$\frac{i c_{a1} M_{\nu_1} s_{a1}}{x} \gamma_{ab}^5$
$\nu l_a^2 \quad \nu l_b^2 \quad H_1$	$\frac{s_{a2}}{x} (c_\alpha c_{a2} \sqrt{2} x y_2^\nu \delta_{ab} + s_\alpha s_{a2} M_{\nu_2} \delta_{ab})$
$\nu l_a^2 \quad \nu l_b^2 \quad H_2$	$\frac{s_{a2}}{x} (s_\alpha c_{a2} \sqrt{2} x y_2^\nu \delta_{ab} - s_{a2} c_\alpha M_{\nu_2} \delta_{ab})$
$\nu l_a^2 \quad \nu l_b^2 \quad Z_\mu$	$\frac{1}{2} \frac{c_{a2}^2 e}{c_w s_w} \gamma_{ac}^\mu \gamma_{cb}^5$
$\nu l_a^2 \quad \nu l_b^2 \quad z$	$-i c_{a2} s_{a2} \sqrt{2} y_2^\nu \gamma_{ab}^5$
$\nu l_a^2 \quad \nu l_b^2 \quad Z'_\mu$	$-(1 - 2s_{a2}^2) g_1' \gamma_{ac}^\mu \gamma_{cb}^5$
$\nu l_a^2 \quad \nu l_b^2 \quad z'$	$-\frac{i M_{\nu_2} s_{a2}^2}{x} \gamma_{ab}^5$
$\nu l_a^2 \quad \nu h_b^2 \quad H_1$	$-\frac{1}{2} \frac{1}{x} ((1 - 2s_{a2}^2) c_\alpha \sqrt{2} x y_2^\nu \delta_{ab} + 2s_\alpha s_{a2} c_{a2} M_{\nu_2} \delta_{ab})$
$\nu l_a^2 \quad \nu h_b^2 \quad H_2$	$-\frac{1}{2} \frac{1}{x} ((1 - 2s_{a2}^2) s_\alpha \sqrt{2} x y_2^\nu \delta_{ab} - 2s_{a2} c_\alpha c_{a2} M_{\nu_2} \delta_{ab})$

Fields in the vertex	Variational derivative of Lagrangian by fields
$\nu l_a^2 \nu h_b^2 Z_\mu$	$\frac{1}{2} \frac{c_{a2} e s_{a2}}{c_w s_w} \gamma_{ac}^\mu \gamma_{cb}^5$
$\nu l_a^2 \nu h_b^2 z$	$\frac{1}{2} i (1 - 2s_{a2}^2) \sqrt{2} y_2^\nu \gamma_{ab}^5$
$\nu l_a^2 \nu h_b^2 Z'_\mu$	$-2c_{a2} s_{a2} g_1' \gamma_{ac}^\mu \gamma_{cb}^5$
$\nu l_a^2 \nu h_b^2 z'$	$\frac{i c_{a2} M_{\nu_2} s_{a2}}{x} \gamma_{ab}^5$
$\nu l_a^3 \nu l_b^3 H_1$	$\frac{s_{a3}}{x} (c_\alpha c_{a3} \sqrt{2} x y_3^\nu \delta_{ab} + s_\alpha s_{a3} M_{\nu_3} \delta_{ab})$
$\nu l_a^3 \nu l_b^3 H_2$	$\frac{s_{a3}}{x} (s_\alpha c_{a3} \sqrt{2} x y_3^\nu \delta_{ab} - s_{a3} c_\alpha M_{\nu_3} \delta_{ab})$
$\nu l_a^3 \nu l_b^3 Z_\mu$	$\frac{1}{2} \frac{c_{a3}^2 e}{c_w s_w} \gamma_{ac}^\mu \gamma_{cb}^5$
$\nu l_a^3 \nu l_b^3 z$	$-i c_{a3} s_{a3} \sqrt{2} y_3^\nu \gamma_{ab}^5$
$\nu l_a^3 \nu l_b^3 Z'_\mu$	$-(1 - 2s_{a3}^2) g_1' \gamma_{ac}^\mu \gamma_{cb}^5$
$\nu l_a^3 \nu l_b^3 z'$	$-\frac{i M_{\nu_3} s_{a3}^2}{x} \gamma_{ab}^5$
$\nu l_a^3 \nu h_b^3 H_1$	$-\frac{1}{2} \frac{1}{x} ((1 - 2s_{a3}^2) c_\alpha \sqrt{2} x y_3^\nu \delta_{ab} + 2s_\alpha s_{a3} c_{a3} M_{\nu_3} \delta_{ab})$
$\nu l_a^3 \nu h_b^3 H_2$	$-\frac{1}{2} \frac{1}{x} ((1 - 2s_{a3}^2) s_\alpha \sqrt{2} x y_3^\nu \delta_{ab} - 2s_{a3} c_\alpha c_{a3} M_{\nu_3} \delta_{ab})$
$\nu l_a^3 \nu h_b^3 Z_\mu$	$\frac{1}{2} \frac{c_{a3} e s_{a3}}{c_w s_w} \gamma_{ac}^\mu \gamma_{cb}^5$
$\nu l_a^3 \nu h_b^3 z$	$\frac{1}{2} i (1 - 2s_{a3}^2) \sqrt{2} y_3^\nu \gamma_{ab}^5$
$\nu l_a^3 \nu h_b^3 Z'_\mu$	$-2c_{a3} s_{a3} g_1' \gamma_{ac}^\mu \gamma_{cb}^5$
$\nu l_a^3 \nu h_b^3 z'$	$\frac{i c_{a3} M_{\nu_3} s_{a3}}{x} \gamma_{ab}^5$
$\nu h_a^1 \nu h_b^1 H_1$	$-\frac{c_{a1}}{x} (s_{a1} c_\alpha \sqrt{2} x y_1^\nu \delta_{ab} - s_\alpha c_{a1} M_{\nu_1} \delta_{ab})$
$\nu h_a^1 \nu h_b^1 H_2$	$-\frac{c_{a1}}{x} (s_\alpha s_{a1} \sqrt{2} x y_1^\nu \delta_{ab} + c_\alpha c_{a1} M_{\nu_1} \delta_{ab})$
$\nu h_a^1 \nu h_b^1 Z_\mu$	$\frac{1}{2} \frac{e s_{a1}^2}{c_w s_w} \gamma_{ac}^\mu \gamma_{cb}^5$
$\nu h_a^1 \nu h_b^1 z$	$i c_{a1} s_{a1} \sqrt{2} y_1^\nu \gamma_{ab}^5$
$\nu h_a^1 \nu h_b^1 Z'_\mu$	$(1 - 2s_{a1}^2) g_1' \gamma_{ac}^\mu \gamma_{cb}^5$
$\nu h_a^1 \nu h_b^1 z'$	$-\frac{i c_{a1}^2 M_{\nu_1}}{x} \gamma_{ab}^5$
$\nu h_a^2 \nu h_b^2 H_1$	$-\frac{c_{a2}}{x} (s_{a2} c_\alpha \sqrt{2} x y_2^\nu \delta_{ab} - s_\alpha c_{a2} M_{\nu_2} \delta_{ab})$
$\nu h_a^2 \nu h_b^2 H_2$	$-\frac{c_{a2}}{x} (s_\alpha s_{a2} \sqrt{2} x y_2^\nu \delta_{ab} + c_\alpha c_{a2} M_{\nu_2} \delta_{ab})$
$\nu h_a^2 \nu h_b^2 Z_\mu$	$\frac{1}{2} \frac{e s_{a2}^2}{c_w s_w} \gamma_{ac}^\mu \gamma_{cb}^5$

Fields in the vertex	Variational derivative of Lagrangian by fields
$\nu h_a^2 \quad \nu h_b^2 \quad z$	$ic_{a2}s_{a2}\sqrt{2}y_2^\nu\gamma_{ab}^5$
$\nu h_a^2 \quad \nu h_b^2 \quad Z'_\mu$	$(1 - 2s_{a2}^2)g_1^\mu\gamma_{ac}^5\gamma_{cb}^5$
$\nu h_a^2 \quad \nu h_b^2 \quad z'$	$-\frac{ic_{a2}^2M_{\nu 2}}{x}\gamma_{ab}^5$
$\nu h_a^3 \quad \nu h_b^3 \quad H_1$	$-\frac{c_{a3}}{x}(s_{a3}c_\alpha\sqrt{2}xy_3^\nu\delta_{ab} - s_\alpha c_{a3}M_{\nu 3}\delta_{ab})$
$\nu h_a^3 \quad \nu h_b^3 \quad H_2$	$-\frac{c_{a3}}{x}(s_\alpha s_{a3}\sqrt{2}xy_3^\nu\delta_{ab} + c_\alpha c_{a3}M_{\nu 3}\delta_{ab})$
$\nu h_a^3 \quad \nu h_b^3 \quad Z_\mu$	$\frac{1}{2}\frac{es_{a3}^2}{c_w s_w}\gamma_{ac}^\mu\gamma_{cb}^5$
$\nu h_a^3 \quad \nu h_b^3 \quad z$	$ic_{a3}s_{a3}\sqrt{2}y_3^\nu\gamma_{ab}^5$
$\nu h_a^3 \quad \nu h_b^3 \quad Z'_\mu$	$(1 - 2s_{a3}^2)g_1^\mu\gamma_{ac}^5\gamma_{cb}^5$
$\nu h_a^3 \quad \nu h_b^3 \quad z'$	$-\frac{ic_{a3}^2M_{\nu 3}}{x}\gamma_{ab}^5$
$A_\mu \quad A_\nu \quad W_\rho^+ \quad W_\sigma^-$	$-e^2(2g^{\mu\nu}g^{\rho\sigma} - g^{\mu\rho}g^{\nu\sigma} - g^{\mu\sigma}g^{\nu\rho})$
$A_\mu \quad A_\nu \quad w^+ \quad w^-$	$2e^2g^{\mu\nu}$
$A_\mu \quad H_1 \quad W_\nu^+ \quad w^-$	$\frac{1}{2}\frac{ic_\alpha e^2}{s_w}g^{\mu\nu}$
$A_\mu \quad H_1 \quad w^+ \quad W_\nu^-$	$-\frac{1}{2}\frac{ic_\alpha e^2}{s_w}g^{\mu\nu}$
$A_\mu \quad H_2 \quad W_\nu^+ \quad w^-$	$\frac{1}{2}\frac{ie^2s_\alpha}{s_w}g^{\mu\nu}$
$A_\mu \quad H_2 \quad w^+ \quad W_\nu^-$	$-\frac{1}{2}\frac{ie^2s_\alpha}{s_w}g^{\mu\nu}$
$A_\mu \quad W_\nu^+ \quad W_\rho^- \quad Z_\sigma$	$-\frac{c_w e^2}{s_w}(2g^{\mu\sigma}g^{\nu\rho} - g^{\mu\nu}g^{\rho\sigma} - g^{\mu\rho}g^{\nu\sigma})$
$A_\mu \quad W_\nu^+ \quad w^- \quad z$	$-\frac{1}{2}\frac{e^2}{s_w}g^{\mu\nu}$
$A_\mu \quad w^+ \quad W_\nu^- \quad z$	$-\frac{1}{2}\frac{e^2}{s_w}g^{\mu\nu}$
$A_\mu \quad w^+ \quad w^- \quad Z_\nu$	$\frac{(1-2s_w^2)e^2}{c_w s_w}g^{\mu\nu}$
$G_{\mu p} \quad G_{\nu q} \quad G_{\rho r} \quad G_{\sigma s}$	$g_s^2(g^{\mu\rho}g^{\nu\sigma}f_{pqt}f_{rst} - g^{\mu\sigma}g^{\nu\rho}f_{pqt}f_{rst} + g^{\mu\nu}g^{\rho\sigma}f_{prt}f_{qst}$ $- g^{\mu\sigma}g^{\nu\rho}f_{prt}f_{qst} + g^{\mu\nu}g^{\rho\sigma}f_{pst}f_{qrt} - g^{\mu\rho}g^{\nu\sigma}f_{pst}f_{qrt})$
$H_1 \quad H_1 \quad H_1 \quad H_1$	$-6(c_\alpha^4\lambda_1 + s_\alpha^4\lambda_2 + c_\alpha^2s_\alpha^2\lambda_3)$
$H_1 \quad H_1 \quad H_1 \quad H_1$	$-3c_\alpha s_\alpha(2c_\alpha^2\lambda_1 - 2s_\alpha^2\lambda_2 - (1 - 2s_\alpha^2)\lambda_3)$
$H_1 \quad H_1 \quad H_2 \quad H_2$	$-(6c_\alpha^2s_\alpha^2\lambda_1 + 6c_\alpha^2s_\alpha^2\lambda_2 + (1 - 6c_\alpha^2s_\alpha^2)\lambda_3)$
$H_1 \quad H_1 \quad W_\mu^+ \quad W_\nu^-$	$\frac{1}{2}\frac{c_\alpha^2 e^2}{s_w^2}g^{\mu\nu}$

Fields in the vertex	Variational derivative of Lagrangian by fields
$H_1 \ H_1 \ w^+ \ w^-$	$-(2c_\alpha^2 \lambda_1 + s_\alpha^2 \lambda_3)$
$H_1 \ H_1 \ Z_\mu \ Z_\nu$	$\frac{1}{2} \frac{c_\alpha^2 e^2}{c_w^2 s_w^2} g^{\mu\nu}$
$H_1 \ H_1 \ z \ z$	$-(2c_\alpha^2 \lambda_1 + s_\alpha^2 \lambda_3)$
$H_1 \ H_1 \ Z'_\mu \ Z'_\nu$	$8s_\alpha^2 g_1'^2 g^{\mu\nu}$
$H_1 \ H_1 \ z' \ z'$	$-(2s_\alpha^2 \lambda_2 + c_\alpha^2 \lambda_3)$
$H_1 \ H_2 \ H_2 \ H_2$	$-3c_\alpha s_\alpha (2s_\alpha^2 \lambda_1 - 2c_\alpha^2 \lambda_2 + (1 - 2s_\alpha^2) \lambda_3)$
$H_1 \ H_2 \ W_\mu^+ \ W_\nu^-$	$\frac{1}{2} \frac{c_\alpha e^2 s_\alpha}{s_w^2} g^{\mu\nu}$
$H_1 \ H_2 \ w^+ \ w^-$	$-c_\alpha s_\alpha (2\lambda_1 - \lambda_3)$
$H_1 \ H_2 \ Z_\mu \ Z_\nu$	$\frac{1}{2} \frac{c_\alpha e^2 s_\alpha}{c_w^2 s_w^2} g^{\mu\nu}$
$H_1 \ H_2 \ z \ z$	$-c_\alpha s_\alpha (2\lambda_1 - \lambda_3)$
$H_1 \ H_2 \ Z'_\mu \ Z'_\nu$	$-8c_\alpha s_\alpha g_1'^2 g^{\mu\nu}$
$H_1 \ H_2 \ z' \ z'$	$c_\alpha s_\alpha (2\lambda_2 - \lambda_3)$
$H_1 \ W_\mu^+ \ w^- \ Z_\nu$	$-\frac{1}{2} \frac{ic_\alpha e^2}{c_w} g^{\mu\nu}$
$H_1 \ w^+ \ W_\mu^- \ Z_\nu$	$\frac{1}{2} \frac{ic_\alpha e^2}{c_w} g^{\mu\nu}$
$H_2 \ H_2 \ H_2 \ H_2$	$-6(s_\alpha^4 \lambda_1 + c_\alpha^4 \lambda_2 + c_\alpha^2 s_\alpha^2 \lambda_3)$
$H_2 \ H_2 \ W_\mu^+ \ W_\nu^-$	$\frac{1}{2} \frac{e^2 s_\alpha^2}{s_w^2} g^{\mu\nu}$
$H_2 \ H_2 \ w^+ \ w^-$	$-(2s_\alpha^2 \lambda_1 + c_\alpha^2 \lambda_3)$
$H_2 \ H_2 \ Z_\mu \ Z_\nu$	$\frac{1}{2} \frac{e^2 s_\alpha^2}{c_w^2 s_w^2} g^{\mu\nu}$
$H_2 \ H_2 \ z \ z$	$-(2s_\alpha^2 \lambda_1 + c_\alpha^2 \lambda_3)$
$H_2 \ H_2 \ Z'_\mu \ Z'_\nu$	$8c_\alpha^2 g_1'^2 g^{\mu\nu}$
$H_2 \ H_2 \ z' \ z'$	$-(2c_\alpha^2 \lambda_2 + s_\alpha^2 \lambda_3)$
$H_2 \ W_\mu^+ \ w^- \ Z_\nu$	$-\frac{1}{2} \frac{ie^2 s_\alpha}{c_w} g^{\mu\nu}$
$H_2 \ w^+ \ W_\mu^- \ Z_\nu$	$\frac{1}{2} \frac{ie^2 s_\alpha}{c_w} g^{\mu\nu}$
$W_\mu^+ \ W_\nu^+ \ W_\rho^- \ W_\sigma^-$	$\frac{e^2}{s_w^2} (2g^{\mu\nu} g^{\rho\sigma} - g^{\mu\sigma} g^{\nu\rho} - g^{\mu\rho} g^{\nu\sigma})$
$W_\mu^+ \ w^+ \ W_\nu^- \ w^-$	$\frac{1}{2} \frac{e^2}{s_w^2} g^{\mu\nu}$

Fields in the vertex	Variational derivative of Lagrangian by fields
$W_\mu^+ \quad W_\nu^- \quad Z_\rho \quad Z_\sigma$	$-\frac{c_w^2 e^2}{s_w^2} (2g^{\mu\nu} g^{\rho\sigma} - g^{\mu\rho} g^{\nu\sigma} - g^{\mu\sigma} g^{\nu\rho})$
$W_\mu^+ \quad W_\nu^- \quad z \quad z$	$\frac{1}{2} \frac{e^2}{s_w^2} g^{\mu\nu}$
$W_\mu^+ \quad w^- \quad Z_\nu \quad z$	$\frac{1}{2} \frac{e^2}{c_w} g^{\mu\nu}$
$w^+ \quad w^+ \quad w^- \quad w^-$	$-4\lambda_1$
$w^+ \quad W_\mu^- \quad Z_\nu \quad z$	$\frac{1}{2} \frac{e^2}{c_w} g^{\mu\nu}$
$w^+ \quad w^- \quad Z_\mu \quad Z_\nu$	$\frac{1}{2} \frac{(1-2s_w^2)^2 e^2}{c_w^2 s_w^2} g^{\mu\nu}$
$w^+ \quad w^- \quad z \quad z$	$-2\lambda_1$
$w^+ \quad w^- \quad z' \quad z'$	$-\lambda_3$
$Z_\mu \quad Z_\nu \quad z \quad z$	$\frac{1}{2} \frac{e^2}{c_w^2 s_w^2} g^{\mu\nu}$
$z \quad z \quad z \quad z$	$-6\lambda_1$
$z \quad z \quad z' \quad z'$	$-\lambda_3$
$Z'_\mu \quad Z'_\nu \quad z' \quad z'$	$8g_1'^2 g^{\mu\nu}$
$z' \quad z' \quad z' \quad z'$	$-6\lambda_2$

Bibliography

- [1] M. E. Peskin and D. V. Schroeder, p. 842 (1995), Reading, USA: Addison-Wesley.
- [2] A. Djouadi, Phys. Rept. **457**, 1 (2008), hep-ph/0503172.
- [3] P. W. Higgs, Phys. Rev. Lett. **13**, 508 (1964).
- [4] S. M. Bilenky and S. T. Petcov, Rev. Mod. Phys. **59**, 671 (1987).
- [5] G. Altarelli and F. Feruglio, New J. Phys. **6**, 106 (2004), hep-ph/0405048.
- [6] A. Strumia and F. Vissani, (2006), hep-ph/0606054.
- [7] G. Bertone, D. Hooper, and J. Silk, Phys. Rept. **405**, 279 (2005), hep-ph/0404175.
- [8] E. Gildener and S. Weinberg, Phys. Rev. **D13**, 3333 (1976).
- [9] S. Weinberg, Phys. Lett. **B82**, 387 (1979).
- [10] S. P. Martin, (1997), hep-ph/9709356.
- [11] U. Ellwanger, C. Hugonie, and A. M. Teixeira, Phys. Rept. **496**, 1 (2010), 0910.1785.
- [12] E. E. Jenkins, Phys. Lett. **B192**, 219 (1987).
- [13] W. Buchmuller, C. Greub, and P. Minkowski, Phys. Lett. **B267**, 395 (1991).
- [14] S. Khalil, J. Phys. **G35**, 055001 (2008), hep-ph/0611205.
- [15] W. Emam and S. Khalil, Eur. Phys. J. **C52**, 625 (2007), 0704.1395.
- [16] L. Basso, A. Belyaev, S. Moretti, and C. H. Shepherd-Themistocleous, Phys. Rev. **D80**, 055030 (2009), hep-ph/0812.4313.
- [17] W. Emam and P. Mine, Erratum-ibid. **G36**, 129701 (2009).
- [18] K. Huitu, S. Khalil, H. Okada, and S. K. Rai, Phys. Rev. Lett. **101**, 181802 (2008), 0803.2799.

- [19] L. Basso, A. Belyaev, S. Moretti, and G. M. Pruna, *JHEP* **10**, 006 (2009), 0903.4777.
- [20] L. Basso, A. Belyaev, S. Moretti, G. M. Pruna, and C. H. Shepherd-Themistocleous, (2010), 1002.3586.
- [21] L. Basso, A. Belyaev, S. Moretti, and G. M. Pruna, *Phys. Rev.* **D81**, 095018 (2010), 1002.1939.
- [22] L. Basso, S. Moretti, and G. M. Pruna, *Phys. Rev.* **D82**, 055018 (2010), 1004.3039.
- [23] L. Basso, S. Moretti, and G. M. Pruna, (2010), 1009.4164.
- [24] L. Basso, S. Moretti, and G. M. Pruna, *Phys. Rev.* **D83**, 055014 (2011), 1011.2612.
- [25] L. Basso, S. Moretti, and G. M. Pruna, (2010), 1012.0167.
- [26] P. Minkowski, *Phys. Lett.* **B67**, 421 (1977).
- [27] P. Van Nieuwenhuizen and D. Z. Freedman, p. 341 (1979), Amsterdam, Netherlands: North-Holland.
- [28] T. Yanagida, (1979), In Proceedings of the Workshop on the Baryon Number of the Universe and Unified Theories, Tsukuba, Japan, 13-14 Feb.
- [29] M. Gell-Mann, P. Ramond, and R. Slansky, Print-80-0576 (CERN).
- [30] S.L. Glashow, in *Quarks and Leptons*, eds. M.Lèvy et al. (Plenum, New York 1980), p. 707.
- [31] R. N. Mohapatra and G. Senjanovic, *Phys. Rev. Lett.* **44**, 912 (1980).
- [32] N. Okada and O. Seto, *Phys. Rev.* **D82**, 023507 (2010), 1002.2525.
- [33] S. Khalil, H. Okada, and T. Toma, (2011), 1102.4249.
- [34] A. V. Semenov, (1996), hep-ph/9608488.
- [35] N. D. Christensen and C. Duhr, *Comput. Phys. Commun.* **180**, 1614 (2009), 0806.4194.
- [36] <http://www.ifh.de/~pukhov/calchep.html>.
- [37] A. Pukhov, (2004), hep-ph/0412191.
- [38] J. Alwall *et al.*, *JHEP* **09**, 028 (2007), 0706.2334.
- [39] T. Hahn, *Nucl. Phys. Proc. Suppl.* **89**, 231 (2000), hep-ph/0005029.
- [40] M. S. Chanowitz and M. K. Gaillard, *Nucl. Phys.* **B261**, 379 (1985).

-
- [41] G. L. Fogli, E. Lisi, A. Marrone, and A. Palazzo, *Prog. Part. Nucl. Phys.* **57**, 742 (2006), hep-ph/0506083.
- [42] G. L. Fogli *et al.*, *Phys. Rev.* **D75**, 053001 (2007), hep-ph/0608060.
- [43] B. Pontecorvo, *Sov. Phys. JETP* **6**, 429 (1957).
- [44] B. Pontecorvo, *Sov. Phys. JETP* **7**, 172 (1958).
- [45] Z. Maki, M. Nakagawa, and S. Sakata, *Prog. Theor. Phys.* **28**, 870 (1962).
- [46] B. Pontecorvo, *Sov. Phys. JETP* **26**, 984 (1968).
- [47] M. E. Peskin and T. Takeuchi, *Phys. Rev. Lett.* **65**, 964 (1990).
- [48] M. E. Peskin and T. Takeuchi, *Phys. Rev.* **D46**, 381 (1992).
- [49] S. Dawson and W. Yan, *Phys. Rev.* **D79**, 095002 (2009), 0904.2005.
- [50] ALEPH, D. Buskulic *et al.*, *Phys. Lett.* **B384**, 427 (1996).
- [51] DELPHI, P. Abreu *et al.*, *Nucl. Phys.* **B421**, 3 (1994).
- [52] L3, M. Acciarri *et al.*, *Phys. Lett.* **B385**, 454 (1996).
- [53] OPAL, G. Alexander *et al.*, *Z. Phys.* **C73**, 189 (1997).
- [54] LEP Working Group for Higgs boson searches, R. Barate *et al.*, *Phys. Lett.* **B565**, 61 (2003), hep-ex/0306033.
- [55] G. Cacciapaglia, C. Csaki, G. Marandella, and A. Strumia, *Phys. Rev.* **D74**, 033011 (2006), hep-ph/0604111.
- [56] SLAC E158, P. L. Anthony *et al.*, *Phys. Rev. Lett.* **92**, 181602 (2004), hep-ex/0312035.
- [57] LEP, The ALEPH, DELPHI, L3, OPAL, SLD Collaborations, the LEP Electroweak Working Group, the SLD Electroweak and Heavy Flavour Groups, (2003), hep-ex/0312023.
- [58] CDF and D0 and Tevatron Electroweak Working Group, P. Azzi *et al.*, (2004), hep-ex/0404010.
- [59] SLAC E158, M. Woods, (2004), hep-ex/0403010.
- [60] The ALEPH, DELPHI, L3, OPAL, SLD Collaborations, the LEP Electroweak Working Group, the SLD Electroweak and Heavy Flavour Groups, *Phys. Rept.* **427**, 257 (2006), hep-ex/0509008.

- [61] M. S. Carena, A. Daleo, B. A. Dobrescu, and T. M. P. Tait, Phys. Rev. **D70**, 093009 (2004), hep-ph/0408098.
- [62] CDF, T. Aaltonen *et al.*, Phys. Rev. Lett. **102**, 031801 (2009), 0810.2059.
- [63] CDF, T. Aaltonen *et al.*, Phys. Rev. Lett. **102**, 091805 (2009), 0811.0053.
- [64] G. L. Fogli *et al.*, Phys. Rev. **D78**, 033010 (2008), 0805.2517.
- [65] M. Luscher and P. Weisz, Nucl. Phys. **B300**, 325 (1988).
- [66] B. W. Lee, C. Quigg, and H. B. Thacker, Phys. Rev. **D16**, 1519 (1977).
- [67] G. Cynolter, E. Lendvai, and G. Pocsik, Acta Phys. Polon. **B36**, 827 (2005), hep-ph/0410102.
- [68] J. Maalampi, J. Sirkka, and I. Vilja, Phys. Lett. **B265**, 371 (1991).
- [69] H. Huffel and G. Pocsik, Zeit. Phys. **C8**, 13 (1981).
- [70] R. Casalbuoni, D. Dominici, F. Feruglio, and R. Gatto, Nucl. Phys. **B299**, 117 (1988).
- [71] M. Aoki and S. Kanemura, Phys. Rev. **D77**, 095009 (2008), 0712.4053.
- [72] R. W. Robinett, Phys. Rev. **D34**, 182 (1986).
- [73] L. Basso, A minimal extension of the Standard Model with $B - L$ gauge symmetry, Master's thesis, Università degli Studi di Padova, 2007, http://www.hep.phys.soton.ac.uk/~l.basso/B-L_Master_Thesis.pdf.
- [74] M. J. G. Veltman, Acta Phys. Polon. **B12**, 437 (1981).
- [75] D. Graudenz, M. Spira, and P. M. Zerwas, Phys. Rev. Lett. **70**, 1372 (1993).
- [76] M. Spira, A. Djouadi, D. Graudenz, and P. M. Zerwas, Nucl. Phys. **B453**, 17 (1995), hep-ph/9504378.
- [77] J. F. Gunion, H. E. Haber, G. L. Kane, and S. Dawson, *The Higgs hunter's guide* (Addison Wesley, 1990).
- [78] T. Cuhadar-Donszelmann, M. Karagoz, V. E. Ozcan, S. Sultansoy, and G. Unel, JHEP **10**, 074 (2008), 0806.4003.
- [79] O. Bahat-Treidel, Y. Grossman, and Y. Rozen, JHEP **05**, 022 (2007), hep-ph/0611162.
- [80] V. Barger, P. Langacker, M. McCaskey, M. J. Ramsey-Musolf, and G. Shaughnessy, Phys. Rev. **D77**, 035005 (2008), 0706.4311.

-
- [81] G. Bhattacharyya, G. C. Branco, and S. Nandi, Phys. Rev. **D77**, 117701 (2008), 0712.2693.
- [82] P. Fileviez Perez, T. Han, and T. Li, Phys. Rev. **D80**, 073015 (2009), 0907.4186.
- [83] D. M. Asner *et al.*, (2010), 1004.0535.
- [84] S. Jadach and B. F. L. Ward, Comput. Phys. Commun. **56**, 351 (1990).
- [85] ILC, J. Brau, (Ed.) *et al.*, (2007), 0712.1950.
- [86] H. Baer, S. Dawson, and L. Reina, Phys. Rev. **D61**, 013002 (2000), hep-ph/9906419.
- [87] C. Castanier, P. Gay, P. Lutz, and J. Orloff, (2001), hep-ex/0101028.
- [88] U. Baur, T. Plehn, and D. L. Rainwater, Phys. Rev. Lett. **89**, 151801 (2002), hep-ph/0206024.
- [89] U. Baur, Phys. Rev. **D80**, 013012 (2009), 0906.0028.
- [90] U. Baur, T. Plehn, and D. L. Rainwater, Phys. Rev. **D68**, 033001 (2003), hep-ph/0304015.
- [91] T. Plehn and M. Rauch, Phys. Rev. **D72**, 053008 (2005), hep-ph/0507321.
- [92] ALEPH, S. Schael *et al.*, Eur. Phys. J. **C47**, 547 (2006), hep-ex/0602042.
- [93] N. Cabibbo, Phys. Rev. Lett. **10**, 531 (1963).
- [94] M. Kobayashi and T. Maskawa, Prog. Theor. Phys. **49**, 652 (1973).